CHALMERS

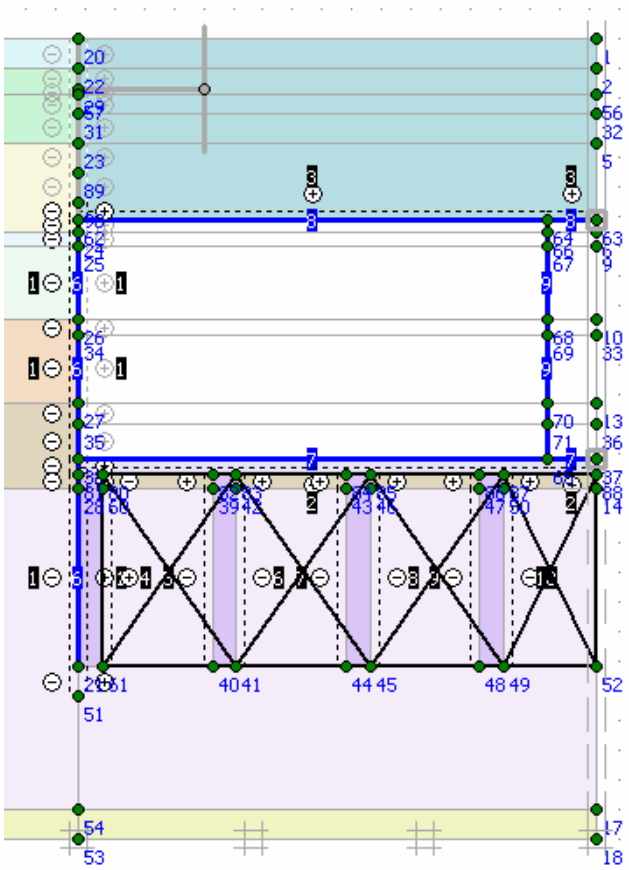

Load Effects on Permanent Diaphragm Walls

Interaction between soil and concrete structure

Master's Thesis in the Master's degree programme Structural Engineering

ANETTE JANSSON

JOHANNA WIKSTRÖM

Department of Civil and Environmental Engineering
Division of Geo Engineering
CHALMERS UNIVERSITY OF TECHNOLOGY
Göteborg, Sweden 2006

Master's Thesis 2006:22

MASTER'S THESIS 2006:22

Load Effects on Permanent Diaphragm Walls

Interaction between soil and concrete structure

Master's Thesis in the Master's degree programme Structural Engineering

ANETTE JANSSON

JOHANNA WIKSTRÖM

Department of Civil and Environmental Engineering
Division of Geo Engineering
CHALMERS UNIVERSITY OF TECHNOLOGY
Göteborg, Sweden 2006

Load effects on Permanent Diaphragm Walls
Interaction between soil and concrete structure
Master's Thesis in the Master's degree programme Structural Engineering
ANETTE JANSSON
JOHANNA WIKSTRÖM

Master's Thesis 2006:22
Department of Civil and Environmental Engineering
Division of Geo Engineering
Chalmers University of Technology
SE-412 96 Göteborg
Sweden
Telephone: + 46 (0)31-772 1000

Cover:
Tunnel section modelled with the FE software PLAXIS, Chapter 6.

Reproservice / Department of Civil and Environmental Engineering
Göteborg, Sweden 2006

Load effects on Permanent Diaphragm Walls
Interaction between soil and concrete structure
Master's Thesis in the Master's degree programme Structural Engineering
ANETTE JANSSON
JOHANNA WIKSTRÖM
Department of Civil and Environmental Engineering
Division of Geo Engineering
Chalmers University of Technology

ABSTRACT

Temporary diaphragm walls are used as support structure for the excavation of the Lilla Bommen part of the Göta Tunnel in Gothenburg. In several other countries, e.g. England and Germany, diaphragm walls have been allowed as part of permanent structures for many years. Finding a way to control durability and accessibility for inspection of the soil-facing side of the wall, which are the two main issues regarding diaphragm walls as permanent structures in Sweden, would make e.g. tunnel construction in especially urban environment more efficient in many ways. The work presented in this thesis is part of a larger project regarding whether diaphragm walls could be allowed as permanent structures in Sweden or not. Durability of concrete structures is closely linked to the control of crack development. For example will wide crack openings allow for a faster chloride penetration, which will initiate earlier corrosion of the reinforcement. Thus, knowledge of expected load effects on a structure is of great importance as a step towards solving the durability problem.

The aim of this thesis is to obtain loads acting on diaphragm walls when, as a tunnel wall, is part of a permanent structure, and to model the interaction between soil- and concrete for an actual section of the Göta Tunnel. The two-dimensional FE-program PLAXIS is used to create a number of models, where the most promising model is used for further analyses. Soil- as well as concrete parameters are evaluated for input in the program and a model simulating the temporary stage of the construction is created and analysed. The results from the first model are compared with measurements of movements on site, where it is seen that similar patterns are obtained even though the magnitudes differ with approximately 5-10 mm for the vertical displacements and 7-20 mm for the horizontal. In the second model an imaginary tunnel is created where, in order to investigate load variations, the stiffness of the concrete is varied for the permanent stage (stiffness values are according to BBK), which refers to long-term analysis. Results from the FE-analyses of the second model are compared with results from hand calculations, and it can be seen that when simulating the prescribed lifetime of the tunnel, the loads from the FE-analyses correspond to the design load according to BRO 2004, the soil pressure "at rest".

Key words: Diaphragm wall, soil/concrete interaction, PLAXIS, the Göta Tunnel.

Lasteffekter på permanenta slitsmurar
Interaktion mellan jord och betong konstruktion
Examensarbete inom Structural Engineering
ANETTE JANSSON & JOHANNA WIKSTRÖM
Institutionen för bygg- och miljöteknik
Avdelningen för Geoteknik
Chalmers tekniska högskola

SAMMANFATTNING

Temporära slitsmurar används som stödkonstruktion vid urschaktningen för Lilla Bommen delen av Götatunneln i Göteborg. I flera andra länder, till exempel England och Tyskland, är slitsmurar tillåtna som permanent del i en konstruktion sedan många år. Genom att finna sätt att kontrollera beständigheten samt möjliggöra besiktning av den sida av muren som vetter mot jord, vilka är de två huvudproblemen angående slitsmurar som permanenta konstruktioner i Sverige, skulle till exempel tunnelbyggande, särskilt i tätbebyggda områden, effektiviseras på många sätt. Arbetet som presenteras i denna rapport är en del av ett större projekt i Sverige angående användande av slitsmur som permanent konstruktion. Att kunna kontrollera sprickutveckling har nära samband med beständighet. Exempelvis kommer stora sprickbredder att tillåta snabbare penetrering av klorider, vilket i sin tur snabbare initierar korrodering av armering. Kunskap om förväntade lasteffekter på konstruktionen är därför av stor vikt som ett steg mot att lösa beständighetsproblemen.

Målet med rapporten är att, utgående från en sektion av Götatunneln, finna laster verkandes på slitsmuren då denna, så som tunnelvägg, är del av en permanent konstruktion, samt att modellera samverkan mellan jord- och betongkonstruktion. Det tvådimensionella FE-programmet PLAXIS används för att skapa ett antal modeller, av vilka den mest lovande är använd för fortsatta analyser. Såväl jord- som betongparametrar utvärderas för att användas som indata i programmet och en modell över det temporära byggskedet skapas och analyseras. Resultaten från FE-analyserna av den första modellen jämförs med fältmätningar där man kan se en differens på 5-10 millimeter för de vertikala förskjutningarna och 7-20 millimeter för de horisontella, men med liknande rörelsemönster. I en andra modell skapas en imaginär tunnel, där betongstyvheten varieras för att kunna undersöka olika laster för permanentstadiet (olika styvheter erhålls från BBK), vilket motsvarar långtidsanalys. Resultat från FE-analyserna av den andra modellen jämförs med handberäkningar, där man kan se att lasterna från FE-analyserna vid simulering över tunnelns förväntade livslängd svarar mot vilojordtryck, vilket är dimensioneringslasten enligt BRO 2004.

Nyckelord: Slitsmur, jord/betong samverkan, PLAXIS, Götatunneln.

Contents

Appendices

Preface

The work in this thesis is focused on loads acting on diaphragm walls when they are part of a permanent structure. This thesis is part of a larger project where it is investigated whether diaphragm walls could be allowed as permanent structures in Sweden or not. The method used is two-dimensional FE-modelling combined with hand calculations. This study has been carried out from September 2005 until January 2006, mainly at NCC Teknik in Gothenburg and partly at the Department of Civil and Environmental Engineering, Division of Geo Engineering at Chalmers University of Technology in Gothenburg.

Firstly we would like to thank Thomas Järphag at NCC Teknik for the opportunity to carry out our work on their premises. A great support during the whole project has been Anders Kullingsjö at the Division of Geo Engineering, who has patiently answered all our questions and showed interest in our project. We would also like to thank our supervisor Jonas Magnusson at NCC Teknik and our examiner Claes Alén at the Division of Geo Engineering for their support and good advice during this project. Other people we would like to thank are Martin Laninge and Daniel Svärd at Vägverket, Tara Wood at NCC Teknik, Niklas Davidsson at LBT, Kjell Karlsrud/Lars Andresen at NGI, as well as Maria Sandberg and Cecilia Edmark.

Göteborg January 2006

Anette Jansson and Johanna Wikström

Notations

Roman letters

E	Young's modulus (soil)
E_c	Young's modulus (concrete)
E_s	Young's modulus (steel)
E_{ref}	Reference stiffness
EI	Flexural rigidity
EA	Flexural stiffness
GWL	Ground water level
I	Moment of inertia
K_0	Lateral soil pressure coefficient at rest
K_0^{nc}	Lateral soil coefficient for virgin compression
$L_{spacing}$	Center distance between elements
M	Modulus of compression (soil)
M_{cr}	Critical moment (concrete)
M_0	Modulus of compression for pressure below pre-consolidation pressure
M_{field}	Field moment (concrete)
M_A , M_B	Support moment (concrete)
N	Axial force (concrete)
OCR	Over consolidation ratio
Q	Shear force
$R_{\text{int}er}$	Friction value
S_t	Sensitivity
b	Width (concrete)
c_{uk}	Characteristic undrained shear strength, cohesion
$c_k^{'}$	Effective cohesion
c_{ref}	Reference shear strength (soil)
f_{ct}	Tensile strength (concrete)
h	Height of cross section
k	Permeability (geo engineering)
k	Coefficient at critical moment (structural engineering)
u	Pore water pressure
w_L	Water content
w	Weight
y_{ref}	Reference depth for E_{ref}
z	Depth below reference ground level (geo engineering)
z	Distance from neutral axis (structural engineering)
z	Direction out of the plane (FEM modelling)

Greek letters

γ_{xz} , γ_{yz}	Strain out of the plane (FEM modelling)
γ_k	Bulk unit weight (clay)
$\gamma_{k,dry}$	Bulk unit weight above GWL (friction soil)
$\gamma_{k,sat}$	Bulk unit weight below GWL (friction soil)
$\gamma_k^{'}$	Effective bulk unit weight (clay, friction soil)
ε	Strain
ν	Poisson's ratio
σ	Total soil pressure
σ'	Effective soil pressure
σ_v	Vertical soil pressure
σ_h	Horizontal soil pressure
σ_1	Largest principal soil pressure
σ_3	Smallest principal soil pressure
σ_m	Tensile stress from bending moment
σ_n	Stress from axial force
τ	Shear stress
τ_{fuk}	Characteristic undrained shear strength
$\tau_{fu}^{passive}$	Undrained shear strength from passive tri-axial test
ζ	Safety factor
ϕ	Friction angle
φ_{ef}	Effective creep factor
ψ	Dilatancy angle

PLAXIS commands used for this thesis

PLATE	For concrete elements.
Cluster	An area designated by geometry lines drawn in between nodes. Used for soil. With concrete properties also used for concrete.
INTERFACE	To model the surface where two different materials coincide.
NODE TO NODE ANCHOR	Used to model the cross wall as a truss.
FIXED END ANCHOR	Used to model the prop in the Verification Model.
ROTATION FIXITY	Used to lock the rotations of the PLATE elements at the symmetry line.
STANDARD FIXITIES	Restricts vertical and horizontal movements along the horizontal model boundaries and restricts horizontal movements along vertical boundaries of the model.

For a closer description of commands, see the PLAXIS manual, reference [6]

1 Introduction

1.1 General

Diaphragm walls are used for underground structures, e.g. tunnels, often produced with the "cut and cover method", which will be dealt with in this report. This method is used to construct tunnels by installing two parallel diaphragm walls and then excavate the area in between. After that the floor- and the roof slabs are cast and finally the volume on top of the roof is refilled. Other fields of application are construction of deep groundwater barriers and underground garages. One advantage with diaphragm walls is that they can be installed in close proximity to existing structures, with minimal loss of support to existing foundations along with a minimum of environmental disturbance, such as noise. Also, no subsidence is associated with this method due to no required dewatering. Sometimes the walls are used as permanent foundation walls, especially in European countries such as Germany and England. The technique used in Europe today has its origin from the USA in the 1940's, and is named the slurry trench technique. Sweden has not yet adopted the use of this method for permanent structures since today's methods cannot fulfil the requirements of durability stated by the Swedish Road Administration and by the Swedish Railroad administration. If the present questions concerning the durability of diaphragm walls could be solved, the construction of for instance a tunnel could be more cost efficient and more time effective. [1], [5]

1.2 Aim and Purpose

The aim of this thesis is to obtain loads acting on diaphragm walls as part of a permanent structure, and to model the interaction between soil and concrete for an actual section of the Göta Tunnel. Durability of concrete structures is closely linked to the control of crack development. For example will wide crack openings allow for a faster chloride penetration, which will initiate earlier corrosion of the reinforcement. Thus, knowledge of possible expected loads on a structure is of great importance as a step towards solving the durability problem.

1.3 Method

Conventional design methods for stiff underground structures in Sweden today are to determine the soil pressure "at rest" and apply this on the structure, according to BRO 2004. In this thesis a two-dimensional FE-program is used to create a number of models, where the most promising model is used for further analyses. Soil- as well as concrete parameters are evaluated for input in the program and a model simulating the temporary stage of the construction is created and analysed. The results are compared with measurements of movements on site.

The model representing the temporary stage is further developed into an imaginary tunnel structure, with diaphragm walls used as permanent tunnel walls. In order to

investigate load variations, the stiffness of the concrete is varied. Results from the FE-analyses are compared with results from hand calculations according to BRO 2004.

1.4 Limitations

In this project only the type of clay found underneath the city of Gothenburg is considered for the analyses. The type of diaphragm wall is the one produced with the slurry trench technique, commonly used in tunnel projects. Loads acting on the diaphragm wall are obtained from gravity acting on, and possible movement within, the clay. Loads from the backfill on top of the roof slab might cause a deflection of the wall in an outward direction relative the shaft, and this also will be regarded in the analyses.

Since only the behaviour of the finished wall is of interest, the installation phase will not be studied. This will be described in the thesis as the diaphragm walls are "wished in place". However, the excavation phase is considered since the work order on site affects the loads acting on the wall. Thus, this thesis contains short-term as well as long-term analyses.

The effects of the shrinkage as well as effects from differences in temperature will not be considered in this thesis.

2 Literature study

2.1 Installation

Definitions of the geometry of a diaphragm wall can be viewed in Figure 2.1. Broadly the slurry-trench method can be explained in a few steps, see Figure 2.2. Firstly a narrow trench, a panel, is excavated and filled with a bentonite- or polymer-slurry to prevent the trench walls to collapse. Secondly a reinforcement cage is lowered in to the centre of the panel, see Figure 2.3. Starting from the bottom, concrete is then poured continuously through one or more tremie pipes, which are extracted as the concrete rises. As the concrete is poured into the panel the slurry and the concrete do not mix, since the slurry has a lower density than concrete. The replaced slurry is taken care of and is reused for the next panel. To take care of the lateral movement, the panels may require props. In some cases, the panels act as a cantilever if there is no support. The geometry of the panels can vary from 2.4 m to 7.0 m in width and from 0.5 m to 1.5 m in thickness. After a support structure is installed, construction of the actual structure can start. All types of soil can be considered for slurry trench excavation; even construction below the ground water table is practicable. Depths of up to 50 m and more are possible. [1]

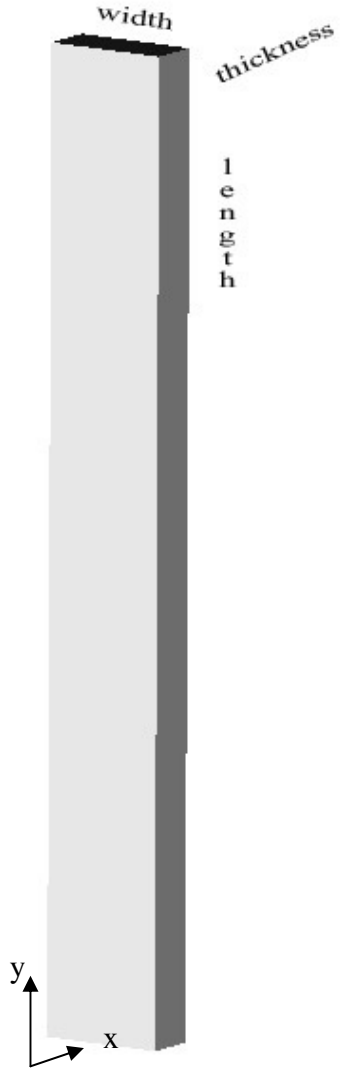

Figure 2.1 *Definitions of the wall geometry.*

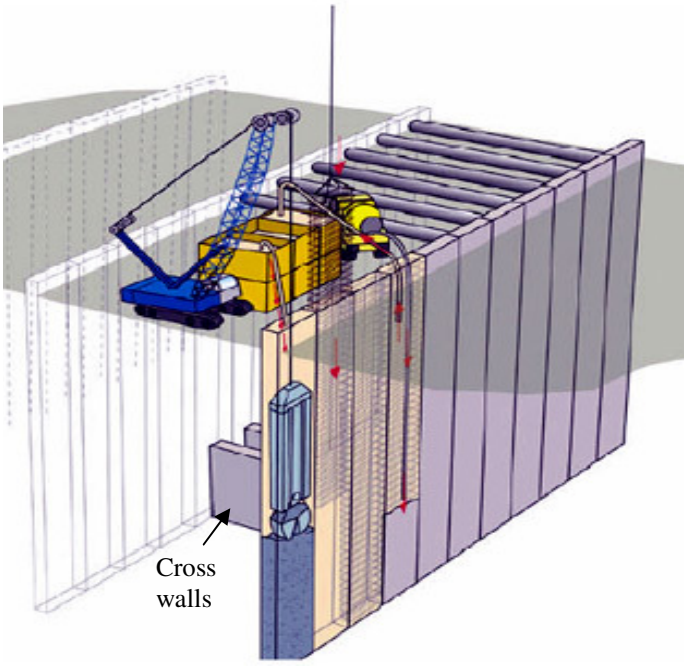

Figure 2.2 *Installation of diaphragm walls with the slurry trench technique.* [19]

Figure 2.3 Lowering reinforcement cage into trench. [27]

2.2 Geotechnique

2.2.1 Gothenburg clay

In general, clay that is found in Gothenburg is very soft, see Figure 2.4. It has a bulk unit weight, γ, of about $16 kN/m^3$. The undrained shear strength, τ_{fuk}, is approximately 20 kN/m^2 from ground to 3 m below. Depths below 3 m have an increment variation of the shear strength in between 0.6-1.0 kN/m^2 per meter till 18 m depth. The pore water pressure, u, is close to hydrostatic and the ground water level is located at approximately +10 m. [3], [4]

Figure 2.4 Excavation in Gothenburg clay. [27]

2.2.2 Modulus of stiffness

Deformation properties of clay are usually determined from incrementally loaded oedometer tests and/or from tri-axial tests. Young's modulus, *E*, is defined as the ratio between the stress increment in one direction and the strain increment in the same direction, see Figure 2.5a, while deformations in the other two principal directions are unrestricted. For calculations of settlement caused by for instance distributed load, the modulus of compression, *M*, is commonly used. It is defined as the relationship between loading in one direction and the deformation in the same direction; see Figure 2.5b, while deformations in the other two principal stress directions are restricted. [9]

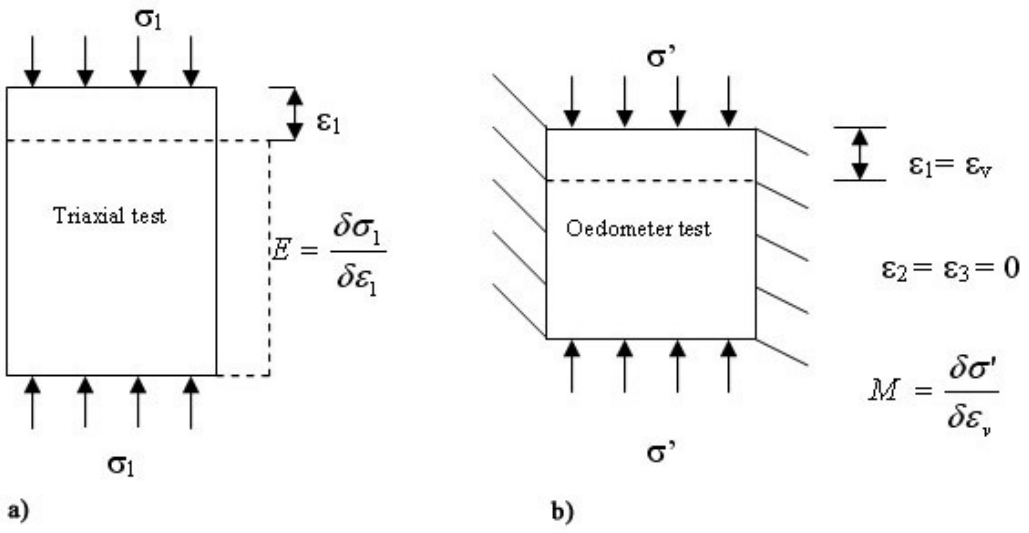

Figure 2.5 *Derivation of Young's modulus, E, and the compression modulus, M.* [9]

2.3 Loads

When installing structures, e.g. tunnel structures with cross walls, there are different types of loads to consider in the ground. Different pressures act on the structure, see Figure 2.6 and Figure 2.7, where the vertical pressure, σ_v, and the horizontal pressure, σ_h, on a diaphragm wall after excavation is shown.

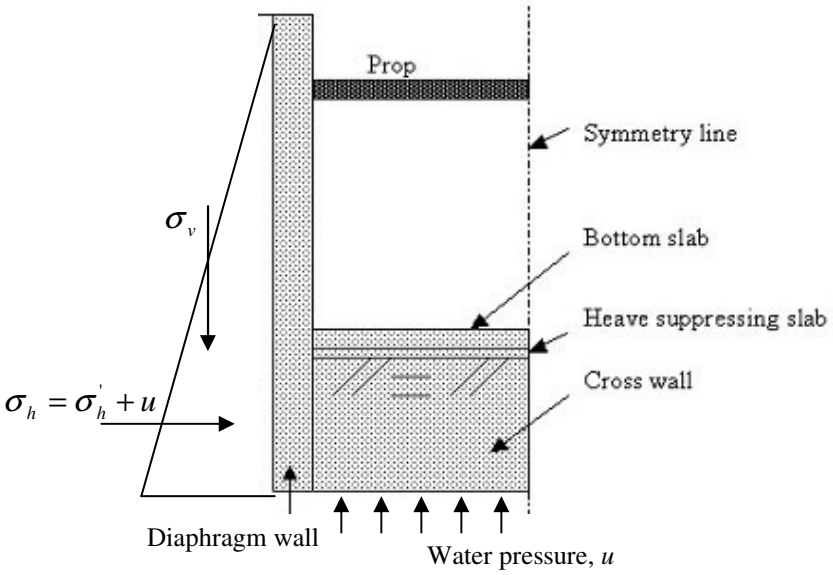

Figure 2.6 *Loads on diaphragm wall.*

Weight from remaining soil outside the excavation along with swelling of clay underneath the excavation cause uplift forces on the bottom of the shaft. This heave effect is restricted by weight of concrete slabs, cohesion (shear strength) between clay and cross walls and friction between cross walls and longitudinal diaphragm walls, see Figure 2.7.

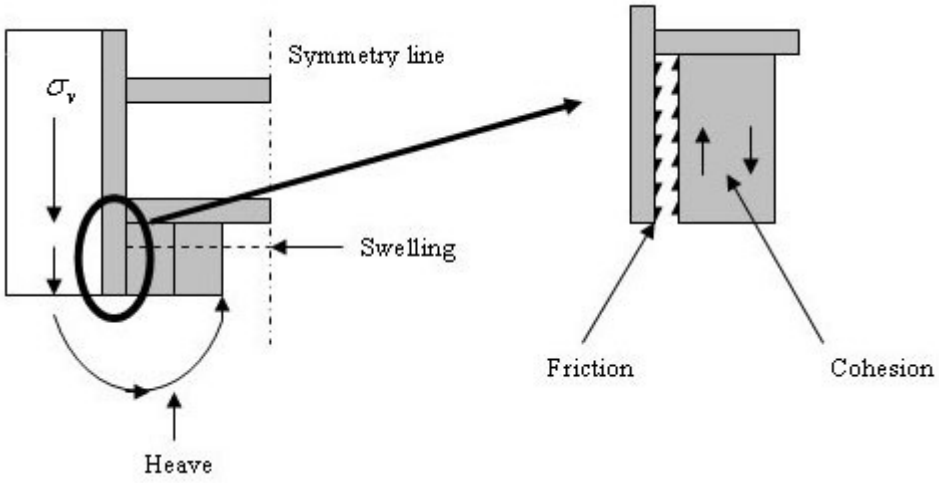

Figure 2.7 Schematic view of bottom heave and soil swelling.

In a complete tunnel structure, besides earth and water pressure on the outsides, there are additional loads from soil that is refilled on top of the tunnel roof, pressure on the bottom of the floor slab from the clay underneath and also from self weight of the structure, see Figure 2.8. Long-term loads can be defined as additional soil pressures, which due to negative excess pore pressures resulting from the excavation develop during time. [7]

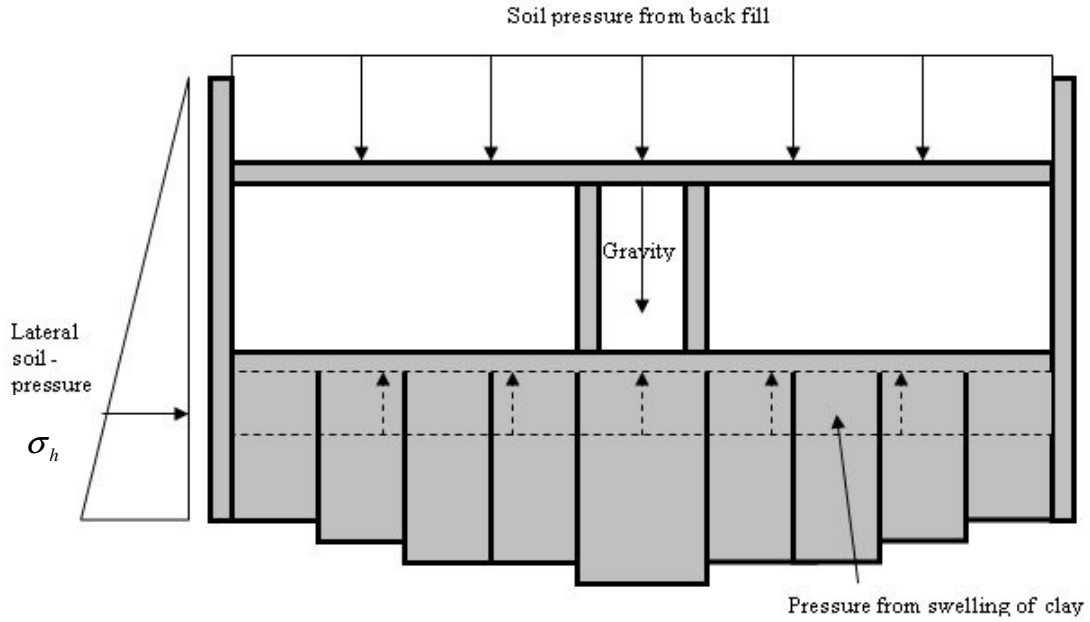

Figure 2.8 Schematic view of loads acting on tunnel structure.

2.3.1 Loads on underground structures

When designing diaphragm walls as permanent, the horizontal load to apply at dimensioning is the soil pressure "at rest", obtained by equation (2.1) according to BRO 2004, see Chapter 3.1.6 for a closer explanation of K_0. [25]

$$\sigma_h = K_0 \cdot \sigma_v^{'} + u \tag{2.1}$$

2.4 Concrete structure

In order to obtain maximum values for load distributions on the diaphragm walls, analyses are performed when assuming different concrete stiffness. How these stiffness combinations are used is described closer in Chapter 6 where the tunnel is analysed. This sub-chapter gives an introduction to concrete behaviour and describes what stiffness to be used in the analyses.

2.4.1 General

Only linear elastic models are used in this thesis for the modelling of concrete, although non-linear analyses are possible with the finite element method when using programs for structural engineering. Since PLAXIS is a FE-program developed for soil modelling, the possibility to model concrete as a non-linear material is restricted.

2.4.2 Stiffness and cracking

Numerous loading tests on reinforced simply supported concrete beams have been carried out trough the years. The general concrete behaviour resulting from these tests is illustrated in Figure 2.9. The first part of the load-deflection diagram corresponds to when the load acting on the concrete cross section results in a moment, which does not exceed the cracking moment, i.e. the concrete is uncracked. This condition is referred to as State I. For a description of cracking moment, see Chapter 2.4.3. As soon as the cross section is subjected to a moment that exceeds the cracking moment, the concrete is cracked, and the condition of the section is referred to as State II.

When concrete cracks the stiffness of the cross-section decreases rapidly, and the reinforcement plays an important role for the equilibrium. The last part of the diagram corresponds to when the reinforcement yields i.e. the behaviour of the beam is plastic. This part of the diagram also refers to when plasticity of the concrete starts. Finally, the beam reaches its ultimate state which means that the concrete crushes in the compressive zone. [15]

Also, when looking at Figure 2.10 where the curvature is described, it can be seen that the stiffness changes rapidly from EI_I to EI_{II} when the concrete cracks. [14]

State I and State II are used in this thesis in order to describe uncracked and cracked concrete members.

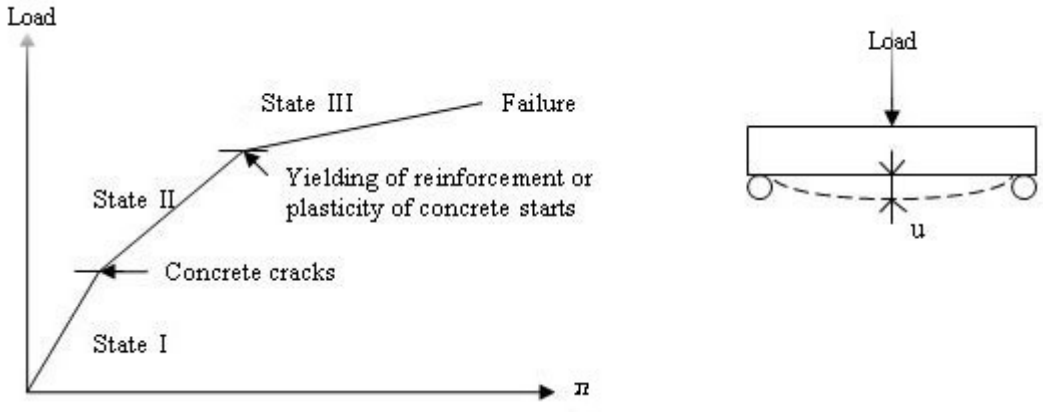

Figure 2.9 Relationship between load and deflection for a simply supported reinforced concrete beam. [15]

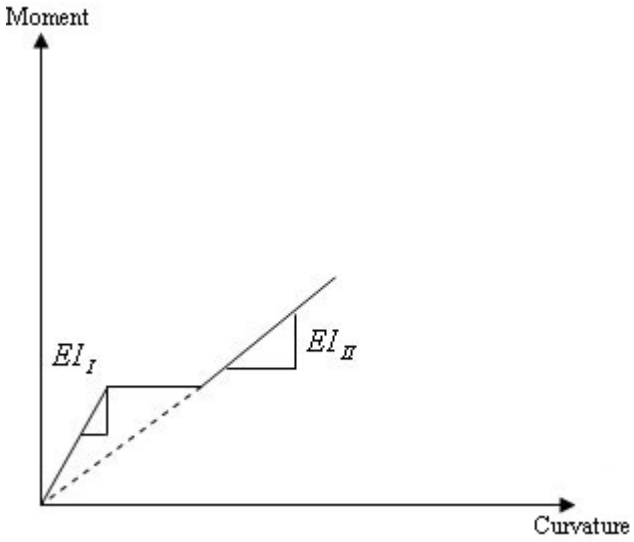

Figure 2.10 Change of curvature: state I to state II. [14]

2.4.3 Cracking conditions

To estimate whether a section is cracked or not, a cracking condition is used. A section that is loaded in either pure bending or bending with a tensile axial force is assumed to be uncracked if condition (2.2) is fulfilled. [29] In structural engineering the distance, z, from the neutral axis is defined as positive in a downward direction, see Figure 2.11.

$$k \cdot \sigma_n + \sigma_m \leq k \frac{f_{ct}}{\zeta} \tag{2.2}$$

A section loaded in bending besides a compressive axial force, is uncracked if condition (2.3) is fulfilled.

$$\sigma_n + \sigma_m \leq \frac{k \cdot f_{ct}}{\zeta} \tag{2.3}$$

where f_{ct} = tensile strength

ζ = safety factor at cracking

$$k = 0.6 + \frac{0.4}{\sqrt[4]{h}}, \quad \text{where } 1.0 \leq k \leq 1.45 \tag{2.4}$$

$\sigma_n = \frac{N}{A}$ = stress from axial force

$\sigma_m = \frac{M}{I} z$ = tensile stress from bending moment

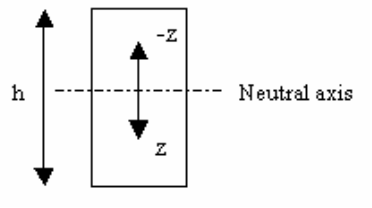

Figure 2.11 Definition of distance, z, from the neutral axis.

Normally the safety factor, ζ, is set to 1 since this corresponds to realistic cracking. A higher value can be chosen if damage to the structure can occur, or if the behaviour of the structure will drop.

The analyses performed in this thesis contain element stiffness corresponding State I and State II in different element combinations of the tunnel (more closely described in Chapter 6). These expressions can be seen in equations (2.5)-(2.8). In this thesis equation (2.2) and equation (2.3) are used for the analyses in order to investigate if the actual cross-sections are cracked or not with the stiffness assumed.

The flexural rigidity referring to State I is calculated according to equation (2.5), whereas for the flexural rigidity used in State II, the equation that yields the lowest value of the equations (2.7)-(2.8) is used. [29]

$$EI = \frac{0.8 \cdot E_c \cdot I_c}{1 + \varphi_{ef}} \tag{2.5}$$

The effective creep factor, φ_{ef}, is obtained by expression (2.6). For a tunnel located under ground, permanent loads as well as a rather damp environment is assumed. [29]

$$\varphi_{ef} = \varphi = 1 \tag{2.6}$$

$$EI = \frac{0.4 \cdot E_c \cdot I_c}{1 + \varphi_{ef}} \tag{2.7}$$

$$EI = E_s \cdot I_s + \frac{0.2 \cdot E_c \cdot I_c}{1 + \varphi_{ef}} \tag{2.8}$$

When evaluating whether a structural member belongs to State I or State II, the critical moment, M_{cr}, is obtained as M from equations (2.2) and (2.3).

2.4.4 Concrete quality

During construction of temporary diaphragm walls, since the durability requirements here are lower, most often a low strength concrete is used, whereas for diaphragm walls used as permanent structures, there is a need for a concrete with higher quality.

Due to the slurry trench technique used when casting diaphragm walls there is an upper limit on the concrete quality that can be used. The higher cement content in a high strength concrete makes it more viscous than one with low strength. Since the tremie pipes are rather long and have a limited diameter there can be difficulties pouring the concrete if it is too viscous and also the risk for mixture segregation increases the higher the cement content. This has to be regarded in the design of a diaphragm wall.

2.5 Interaction of materials

In calculations including different materials interacting with each other, estimation has to be done of the friction value in between the adjoining material surfaces. According to the Swedish code of practice, BRO 2004, values exceeding 0.5 are not approved. [25]

2.6 PLAXIS

In this chapter, a short introduction to the two-dimensional finite element program PLAXIS is given. Also, two soil models are presented which require different kinds of input, Hooke and Mohr-Coulomb.

2.6.1 General

PLAXIS is a finite element program that has been developed for analysis of deformations and stability in geotechnical engineering projects. It is available in a 2D version as well as in the 3D version PLAXIS 3D Tunnel. [6]

The development of PLAXIS started in 1973, and it was introduced in 1990 on the public market. In 1998, the first Windows based software was developed and has since then been used as a practical design tool. [2]

In this thesis PLAXIS version 8 is used for all analyses. The software is divided into four sub programs: Input, Calculations, Output and Curves.

2.6.2 Input

In the Input program of PLAXIS the geometry is given by entering different soil layers, structural parts, and external loads etc. A choice between five available material models: Hooke, Mohr-Coulomb, Hardening Soil, Soft Soil and Modified Soft Soil, is made at the input for each material. The material is given relevant material properties, such as stiffness and density, which are assigned to elements together with appropriate boundary conditions. Also the model in whole is assigned boundary conditions, *STANDARD FIXITIES*. When the model is complete a mesh is generated

and initial stresses and pore water pressures are initiated before moving on to the Calculation program.

2.6.3 Calculation

Choices between different ways of analysing the actual problem are made in the Calculation program. Depending on the nature of the studied problem, the permeability of the soils and the time span considered, *CONSOLIDATION* or *PLASTIC* may be chosen, which considers long-term or short-term analysis. Varying time spans can be considered by choosing *CONSOLIDATION* and then enter the desired number of days. If full consolidation analysis is wanted, *MINIMUM PORE PRESSURE* should be selected, where all excess pore pressures are reduced. If a safety factor for the studied case is wanted, *PHI/C REDUCTION* should be selected. The mode *STAGED CONSTRUCTION* allows for simulation of a complete working sequence.

Different calculation phases are defined, where each phase represents an additional construction phase. Thus, an analysis can contain several calculation phases, where for instance in a first phase an excavation has been performed and in a second phase props have been installed etc.

2.6.4 Output

When the calculations are complete the results can be viewed in the Output program. Stresses, pore pressures and displacements are outputs for soils, whereas outputs for *PLATE* elements (used for e.g. diaphragm walls) are stresses and displacements along with structural forces such as bending moments and shear forces.

2.6.5 Curves

In the Calculation program there is an option to select points of interest in the model. If such a point is selected, the displacement or the pore pressure of the point for each iteration, step or time can be viewed in the sub program Curves. The results can be viewed in either a table or as a graphic curve.

2.6.6 Hooke

Hooke's law, isotropic linear elastic behaviour, is the simplest material model in PLAXIS, and can be used for both soils and solid elements. An elastic model does not have a yield surface, and therefore the behaviour is elastic and the strains are reversible, see Figure 2.12. [6]

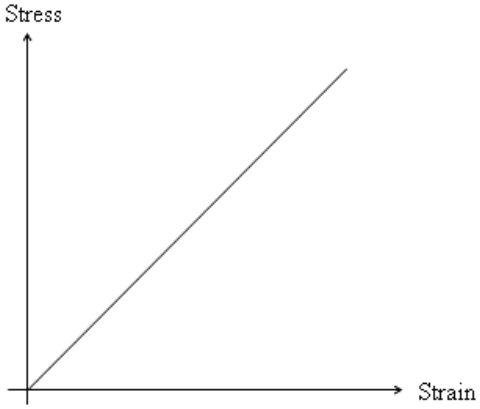

Figure 2.12 Stress as a function of the deformation according to Hooke. All strains are reversible. [2]

Since soil has a non-linear behaviour, the linear-elastic model by Hooke is of limited value. The model though, is of interest when wanting to simulate structural behaviour such as thick concrete walls or plates, which have higher strength properties compared to those of soil. Deformations in diaphragm walls are small, and therefore modelling with Hooke is usable. The model is also applicable for an initial approximate estimation of soil behaviour.

2.6.7 Mohr-Coulomb

The ideal-elastic-plastic model according to Mohr-Coulomb is a development of the elastic Hooke model. For Mohr-Coulomb, which is the most used model in geotechnics, both elastic and plastic parameters are used. Plastic deformations are developed as stresses exceed the elastic stress interval. Irreversible strains are associated with plasticity, see Figure 2.13. In reality the soil stiffness is dependant on the soil stresses, which is not considered in the PLAXIS Mohr-Coulomb model. Instead the stiffness has to be regarded empirically and a linear increment with depth is assumed, which is described closer in Chapter 4.2.3. [2], [6]

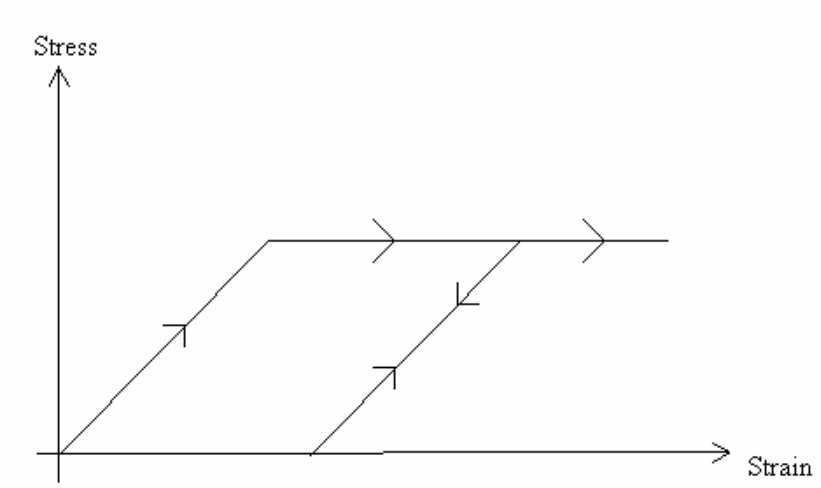

Figure 2.13 Stress as a function of the deformation according to Mohr-Coulomb. Both elastic and plastic strains. [6]

Six yield functions are associated with the Mohr-Coulomb yield condition, which define the appearance of the yield surface; a hexagonal cross-section in the principal stress space, see Figure 2.14. Also, in order to describe the plastic deformations that are established when a material is exposed to stresses above its elastic stress field, plastic potential functions are required. See the PLAXIS manual for formulations of these equations. [2], [6]

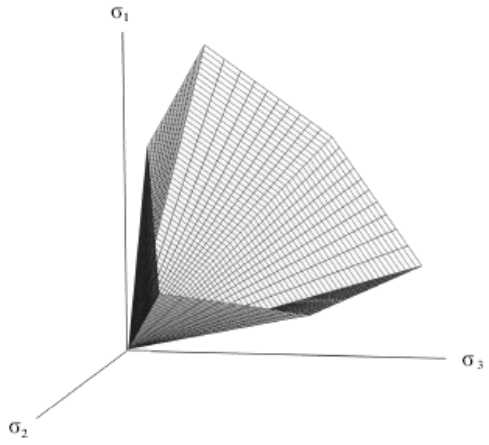

Figure 2.14 Yield surface in principal stress space according to Mohr-Coulomb. [6]

For a Mohr-Coulomb analysis in PLAXIS a total of five parameters are needed; Young's modulus, E, Poisson's ratio, ν, the friction angle, ϕ, the cohesion, c, and the dilatancy angle, ψ. [6]

3 Case study – The Göta Tunnel

The Göta Tunnel is an ongoing project in Gothenburg and this chapter describes a section of the tunnel, which all analyses in this thesis are based upon. First, a description of the location of the tunnel is shown. Thereafter the actual soil layers for the chosen section are presented, and finally the tunnel structure as it is built today is described. Figure 3.1 shows where the tunnel project is located.

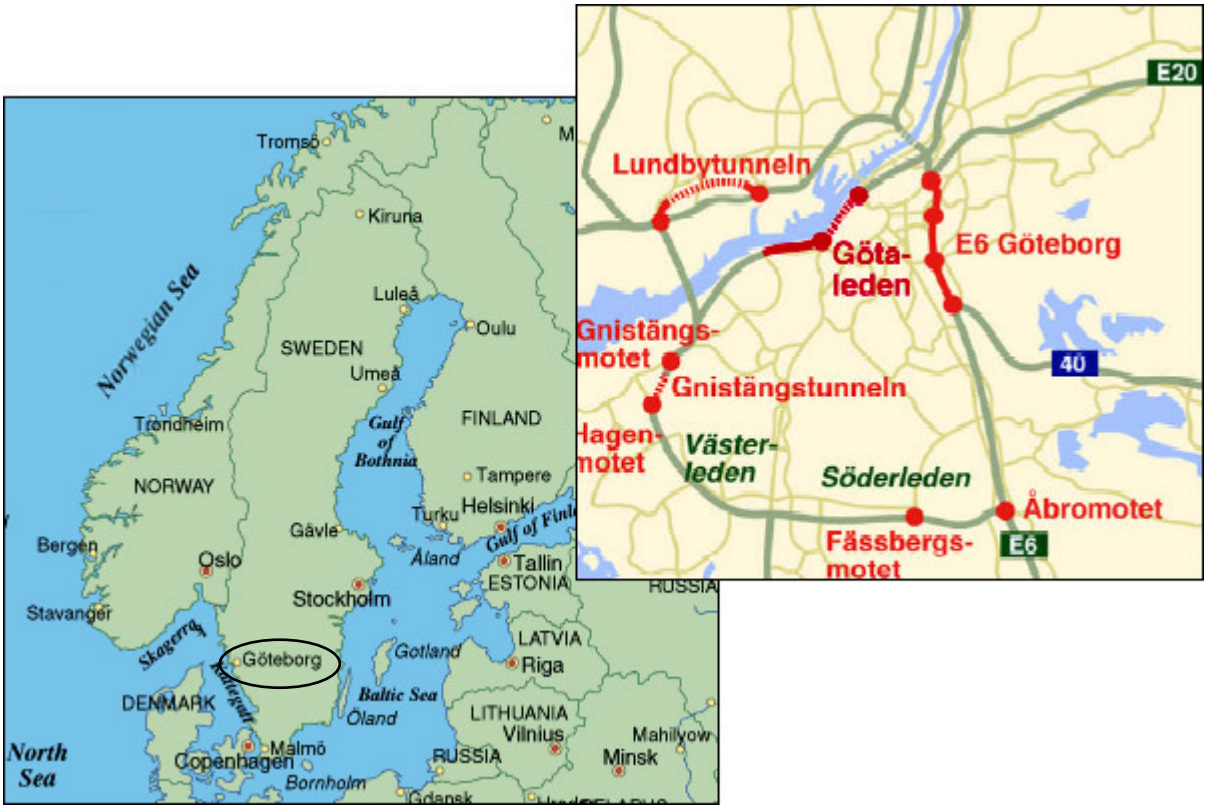

Figure 3.1. Location of the Göta Tunnel project (here: Götaleden) in Gothenburg. [20], [30]

3.1 Soil parameters

In order to perform analyses based upon a specific section along the Göta Tunnel, a number of soil parameters are evaluated. In this thesis, section 2/717, which is situated in the A1-pit, is chosen, see Figures 3.2 and 3.3. The soil profile for the studied section can be viewed in Figure 3.4, where the ground surface is located at +12 m and bedrock at -10 m.

Generally when investigating a realistic behaviour, it is preferred to use mean values of material parameters. For soil, such parameters would be obtained by conducting tests on several soil samples from the area of interest and then determine the mean values of the results. These values will be the best estimation for material properties and in geotechnics these values are the same as the characteristic values. In structural

engineering though, the characteristic value refers to the $5\% - fraction$, i.e. 5 % of the measured test values are lower than the characteristic value. Material parameters obtained from tests on the soil samples taken on the site will represent the characteristic parameters for the analyses in this thesis. Also for realistic/true behaviour, there are no partial factors used .

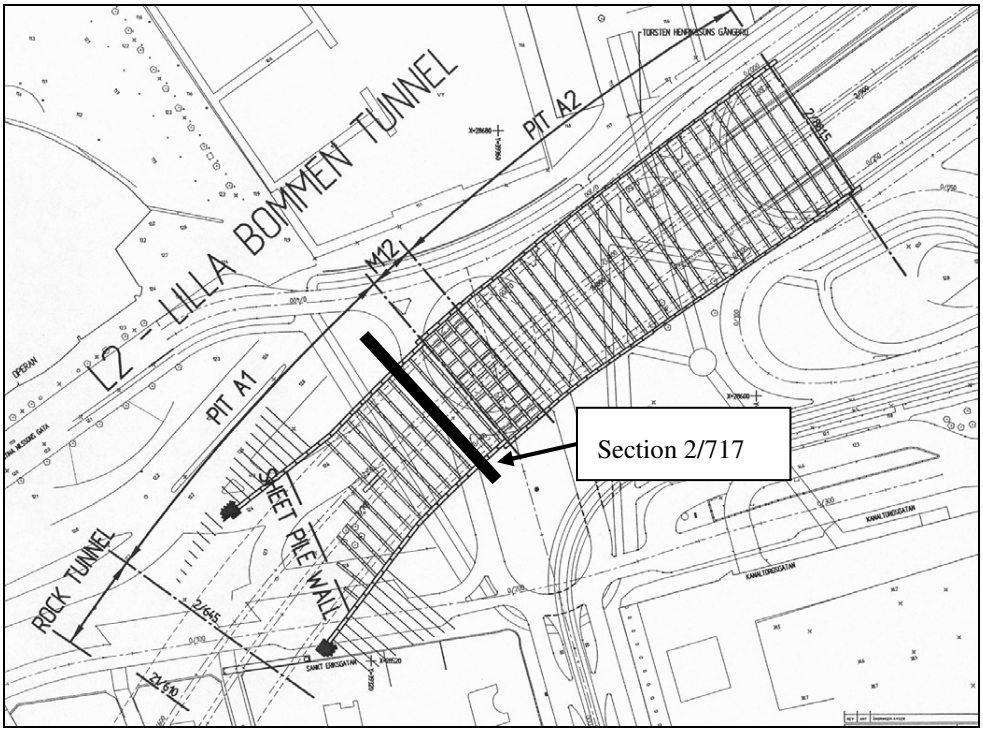

Figure 3.2 Plan view of the Göta Tunnel. The chosen section is situated in pit A1. [4]

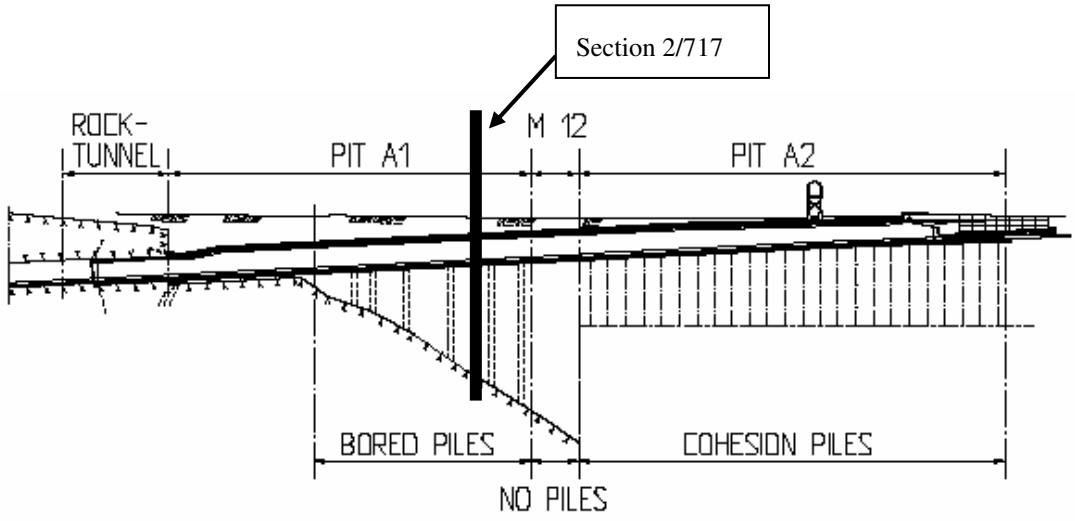

Figure 3.3 Side view of the Göta Tunnel. [22]

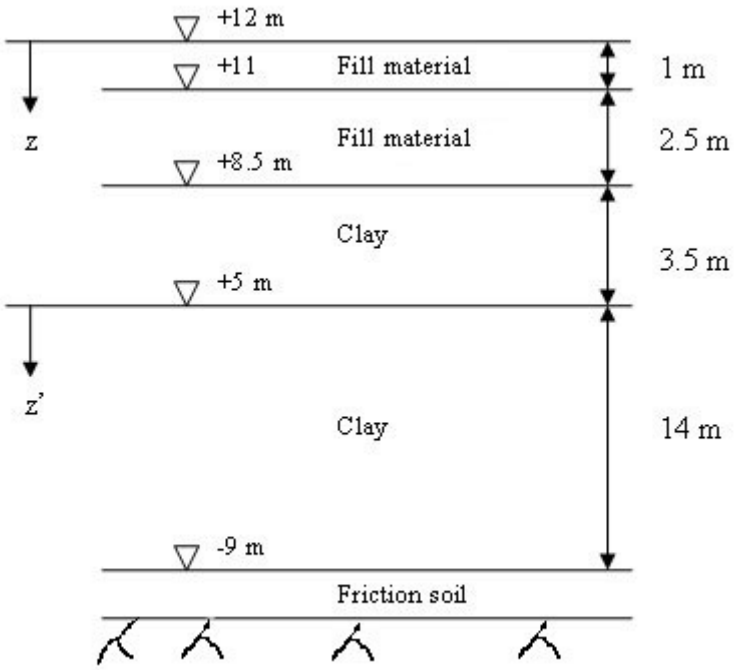

Figure 3.4 Soil profile of the studied section. [4]

3.1.1 Bulk unit weight

Looking at the different soil layers from top down, the top 3.5 m consist of two types of fill material resting on a 17.5 m thick layer of clay. Underneath the clay there is a thin layer of friction soil followed by bedrock. [4]

3.1.1.1 Fill material

The fill material down to one meter below the ground surface consists of a mixture of fill material used for the over ground structures with the approximate characteristic- and effective unit weight as given by expression (3.1). [4]

$$\begin{aligned} \gamma_{k,dry} &= 19\ kN/m^3 \qquad 0\ m \geq z \geq 1\ m \\ \gamma_{k,sat} &= 21\ kN/m^3 \qquad 0\ m \geq z \geq 1\ m \\ \gamma'_k &= 11\ kN/m^3 \qquad 0\ m \geq z \geq 1\ m \end{aligned} \tag{3.1}$$

Underneath the top layer there is a layer of weathered clay and gravely materials together with fractions of miscellaneous rubble materials from torn down buildings. This layer is assigned the same unit weight as the fill layer on top, also with values according to expression (3.1). [4]

3.1.1.2 Clay

The clay is divided into two layers with separate unit weights according to expression (3.2) and expression (3.3). [4]

$$\begin{aligned} \gamma_k &= 16\ kN/m^3 \qquad 3.5\ m \geq z \geq 7\ m \\ \gamma'_k &= 6\ kN/m^3 \qquad 3.5\ m \geq z \geq 7\ m \end{aligned} \tag{3.2}$$

$$\begin{aligned} \gamma_k &= 17\ kN/m^3 \qquad 0\ m \geq z' \geq 14\ m \\ \gamma'_k &= 7\ kN/m^3 \qquad 0\ m \geq z' \geq 14\ m \end{aligned} \tag{3.3}$$

3.1.2 Shear strength

The undrained shear strength of the clay in the studied section was evaluated by use of vane apparatus. The drained shear strength is expressed by equation (3.4). Values for drained cohesion can be obtained by multiplying the undrained values by 0.1, see equation (3.5). The shear strength follows the same division of the soil layers as the unit weight, with a constant value in the upper layer and with an approximate linear increase in the lower layer, see Appendix H, Figure H.1. [4]

$$\tau'_k = c'_k + \sigma \cdot \tan\phi' \tag{3.4}$$

$$c'_k = 0.1 \cdot c_{uk} \tag{3.5}$$

For soils with horizontal ground surfaces, the principal stresses are vertical and horizontal. Based on principal stresses, circles are constructed in a coordinate system with shear stress on the vertical axis and principal stress on the horizontal axis. The angle of friction, ϕ', is found as the angle of the strength envelope line.

For drained conditions the relationship in Figure 3.5 applies where $\phi' \neq 0$, whereas for undrained conditions the soil volume is constant and a vertical stress increase gives a horizontal stress increase, this due to the excess pore pressures established. The friction angle is then zero, and with $\tau = c$ the relationship looks like in Figure 3.6.

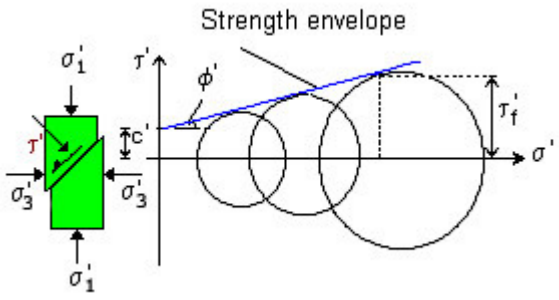

Figure 3.5 Mohr-Coulomb failure criterion at drained conditions. [10]

For the chosen section in this thesis, the drained values for shear strength demand cohesion according to equation (3.6). [4]

$$\begin{aligned} c'_k &= 1.6\ kPa && 3.5\ m \geq z \geq 7\ m \\ c'_k &= 1.6 + 0.14z'\ kPa && 0\ m \geq z' \geq 9\ m \end{aligned} \tag{3.6}$$

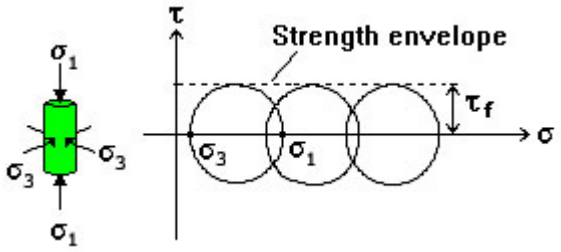

Figure 3.6 Mohr-Coulomb failure criterion at undrained conditions. [10]

The cohesion for use as undrained input is according to equation (3.7). [4]

$$\begin{aligned} c_{uk} &= 16\ kPa && 3.5\ m \geq z \geq 7\ m \\ c_{uk} &= 16 + 1.4z'\ kPa && 0\ m \geq z' \geq 9\ m \end{aligned} \tag{3.7}$$

Clay is a material with low permeability and one can in many cases assume undrained conditions for short term analysis, i.e. $\phi = 0°$. In this thesis short-term as well as long-term analyses are performed, therefore drained conditions are also considered. In this case the friction angle is estimated to: $\phi' = 35°$ in combination with E from tri-axial test results performed in an earlier Master's thesis, see Reference [16], and as $\phi' = 30°$ when $E = 650 \cdot c_{uk}$, see Reference [22].

3.1.3 Ground water level

The Göta tunnel is located in Gothenburg, close to the river Göta Älv. Thus, the ground water level is to be found at approximately the level in the river, at +10.1 m. [4]

3.1.4 Over consolidation ratio

The over consolidation ratio, OCR, describes the loading history of the soil. It is defined as the ratio between the pre-consolidation pressure, σ'_c, and the current effective stress, σ'_0, see equation (3.8). The pre-consolidation pressure is the pressure the soil is able to withstand before its behaviour changes remarkably. If σ'_c exceeds σ'_0 the soil is denoted over consolidated. Loads not exceeding σ'_c will generate only small deformations. In this thesis the OCR is equal to 1.2. [4]

$$OCR = \frac{\sigma'_c}{\sigma'_0} \tag{3.8}$$

3.1.5 Lateral soil coefficient for virgin compression

The lateral soil coefficient for virgin compression, K_0^{nc}, where nc means normally consolidated, can be described as the ratio between horizontal- and vertical soil stresses at normally consolidated conditions. It can be estimated by equation (3.9). [8]

$$K_0^{nc} = 0.31 + 0.71(w_L - 0.2) \tag{3.9}$$

In this thesis the lateral soil coefficient for virgin compression is set to 0.6, which is a common value for Gothenburg clay.

3.1.6 Lateral earth coefficient "at rest"

One important input for a finite element analysis is the ratio of the horizontal to vertical effective stress, K_0, see equation (3.10). The geological process that the soil has been subjected to determines this parameter. For normally consolidated soils it varies between 0.6 and 0.8 and for over consolidated soils it can be higher than 1.0. Based on the theory of elasticity, K_0 can be obtained with equation (3.11). [11], [6]

$$K_0 = \frac{\sigma'_h}{\sigma'_v} = \frac{\nu}{(1-\nu)} \tag{3.10}$$

In this thesis K_0 is equal to K_0^{oc} according to equation 3.11. [13]

$$K_0 = K_0^{oc} = K_0^{nc} \cdot OCR^{\sin(\phi')} \tag{3.11}$$

When using equation (3.11), K_0 for the clay layers is determined to 0.66. The two fill layers as well as the sand layer are assigned 0.5 for K_0 according to earlier written material, see Reference [16].

3.1.7 Poisson's ratio

From a triaxial test, Poisson's ratio can be determined as the ratio between horizontal and vertical strain, equation (3.12). [8]

$$\nu = \frac{\Delta\varepsilon_h}{\Delta\varepsilon_v} \tag{3.12}$$

At undrained conditions, the soil volume is constant, and ν has a value of approximately 0.5. For drained conditions Poisson's ratio is often assumed as 0.33, even though it varies depending on the stress- and loading conditions. At unloading Poisson's ratio ranges from 0.1 to 0.2 and in this thesis ν is chosen to 0.2. For gravel material not previously loaded, ν is set to 0.33. [8], [7]

3.1.8 Angle of dilatation

The angle of dilatation, Ψ, is defined by the ratio between the rate of volumetric strain, and the rate of shear strain. For clay this parameter is most commonly chosen to zero. [6]

3.1.9 Permeability

Since the permeability varies with depth a refined soil division is made, see Figure 3.7. The values for the permeability are listed in Appendix A, Table A.1 and Table A.2.

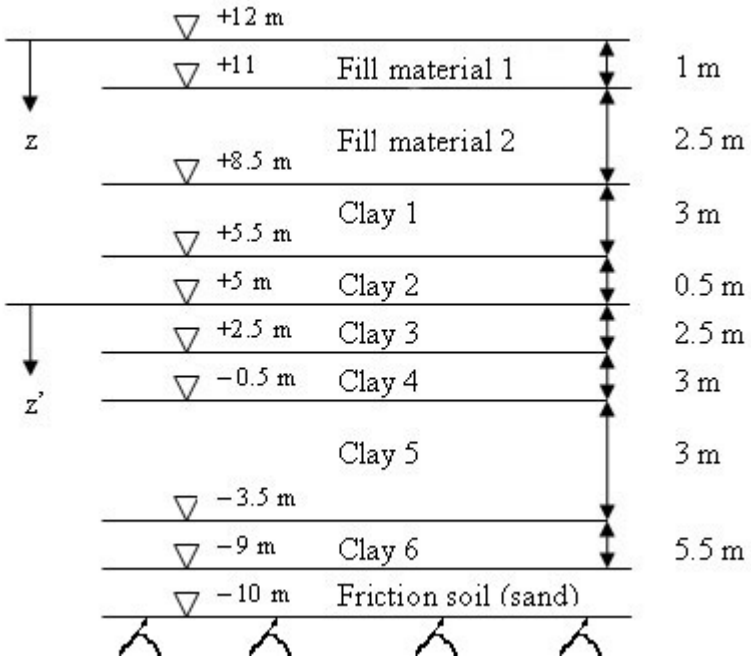

Figure 3.7 Refined soil division according to the permeability used for finite element analyses.

3.2 Tunnel structure

The Göta Tunnel consists of a mid-tunnel cut through rock, connected to a concrete tunnel on each side, see Figure 3.8. It is located underneath the centre of Gothenburg,

where a variety of buildings, representing a wide range of age shape and foundation, can be found. The concrete tunnels are founded in mostly soft clay, leading to a demand for extensive foundation work.

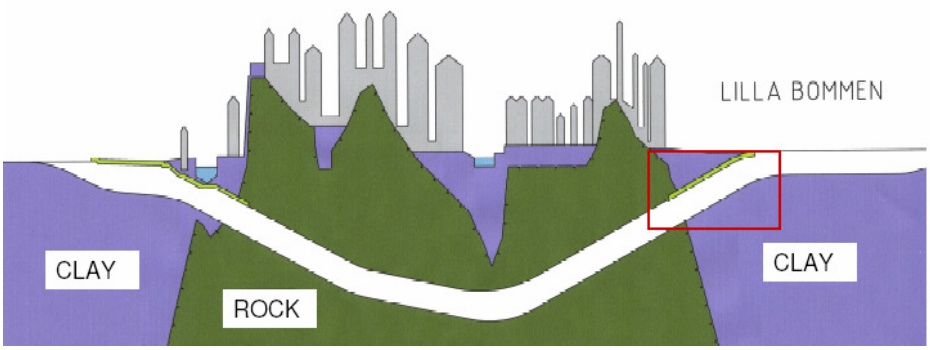

Figure 3.8 Longitudinal view of the Göta Tunnel. [27]

In Figure 3.9, a side view of section 2/717, the section studied in this thesis, is visualized. In order to minimize deformations and disturbing noises, the contractor at the east tunnel opening, at Lilla Bommen, chose to support the excavation shaft with temporary diaphragm walls. Cross walls, which are transversal diaphragm walls, were cast from ground level, which were required to prevent bottom heave during excavation, see Figure 2.2. [1] The support structure includes diaphragm walls prevented from inward movement by props and cross walls. The props are supported at half their length by vertical braces, see Figure 3.10.

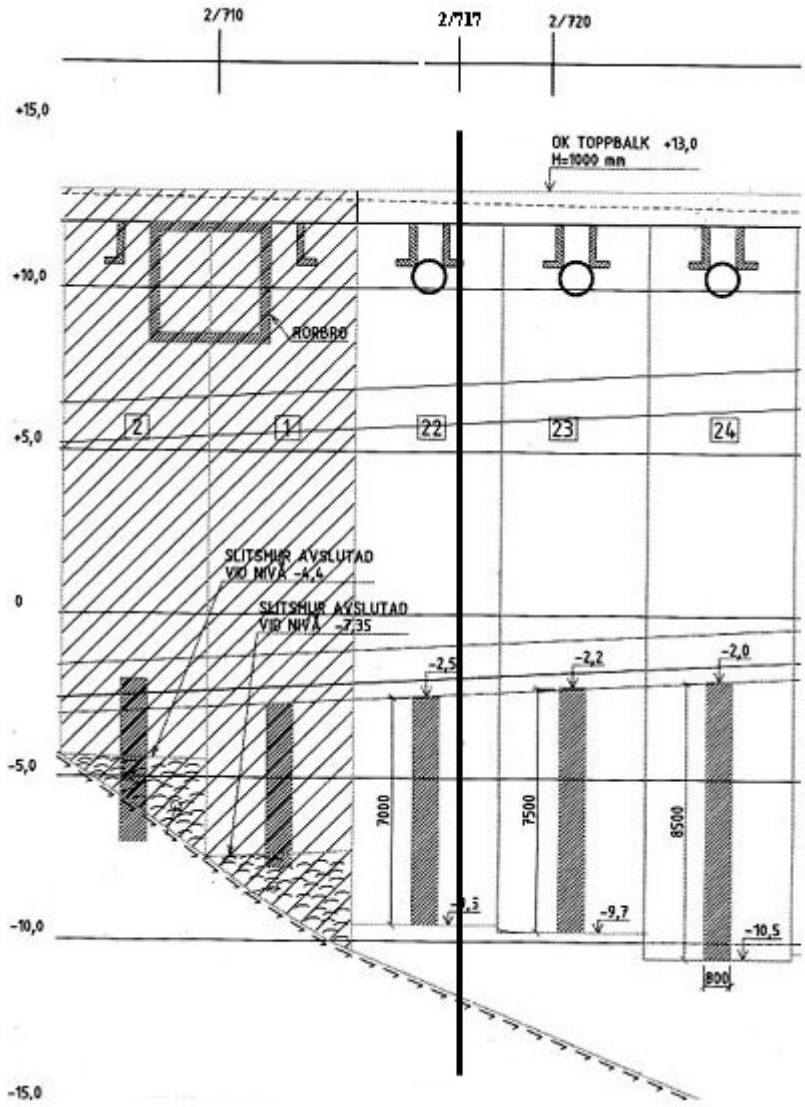

Figure 3.9 Longitudinal view of the studied section 2/717. [4]

Figure 3.10 Props with vertical braces. [27]

A view of the Göta Tunnel where the excavation phases are finished can be seen in Figure 3.11. The floor slab is not in place though. The width of each cross wall element is 5.3 m. [4], [5]

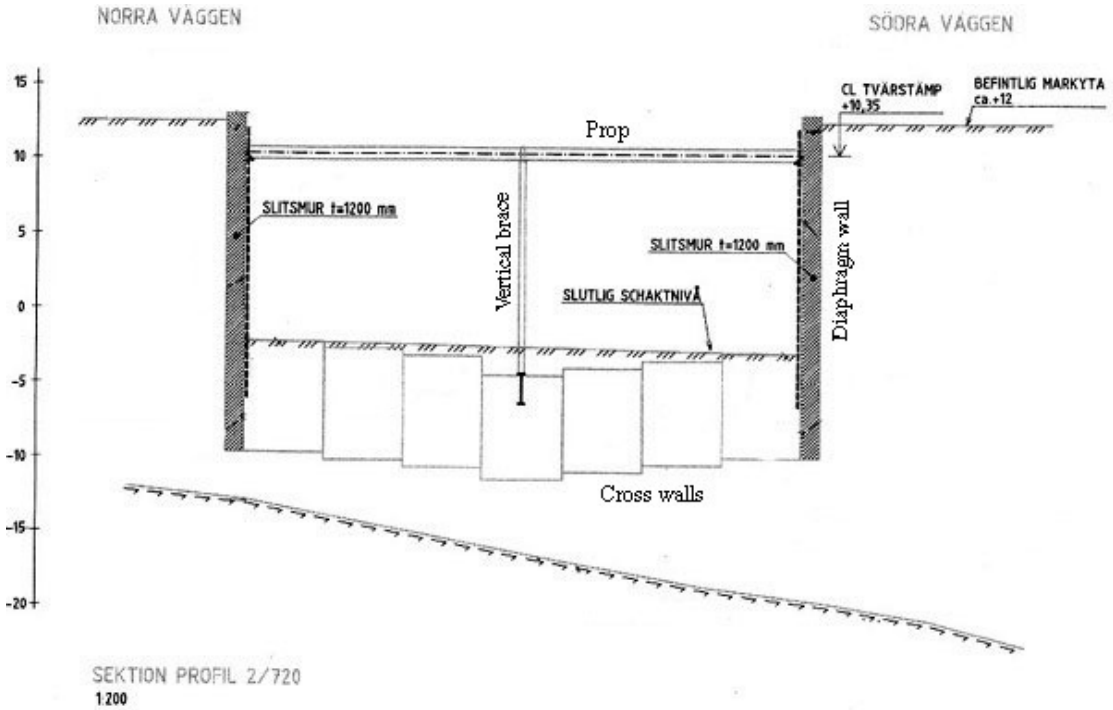

Figure 3.11 Finished excavation of shaft. [5]

In the first step of the tunnel construction, the floor slab is cast followed by the tunnel walls and finally the roof slab. The props are removed before the soil is filled back on top of the tunnel roof. In Figure 3.12, the tunnel section is seen. Also, this figure shows that tunnel walls are cast inside of the temporary diaphragm walls. The thickness of the diaphragm walls varies between 0.8 m and 1.2 m along the length of the tunnel. The thickness of the tunnel walls as well as for the floor slab in the studied section is 1.2 m, and the two inner walls have a thickness of 0.5 m. The concrete quality used in the Göta Tunnel is K40, which is assigned to all elements in the analyses in this thesis. The concrete weight is $24\ kN/m^3$. [5]

Due to the ongoing secondary consolidation caused by refill on top of the clay in the A1-pit and the rather short distance to bedrock, bored piles are used to steady the structure vertically. This means that the heave effect will be of less significance in this area. The piles, which are anchored in bedrock and in the tunnel walls with a spacing of 9 m along the outsides and 22.5 m under the mid walls, prevent vertical movement of the tunnel structure. Since the piles are anchored through the floor of the Göta Tunnel and the floor does not interact with the diaphragm walls, the piles are omitted in the Verification Model. Also, since the Evaluation Model simulates the behaviour of an imaginary tunnel, the piles will be omitted here as well.

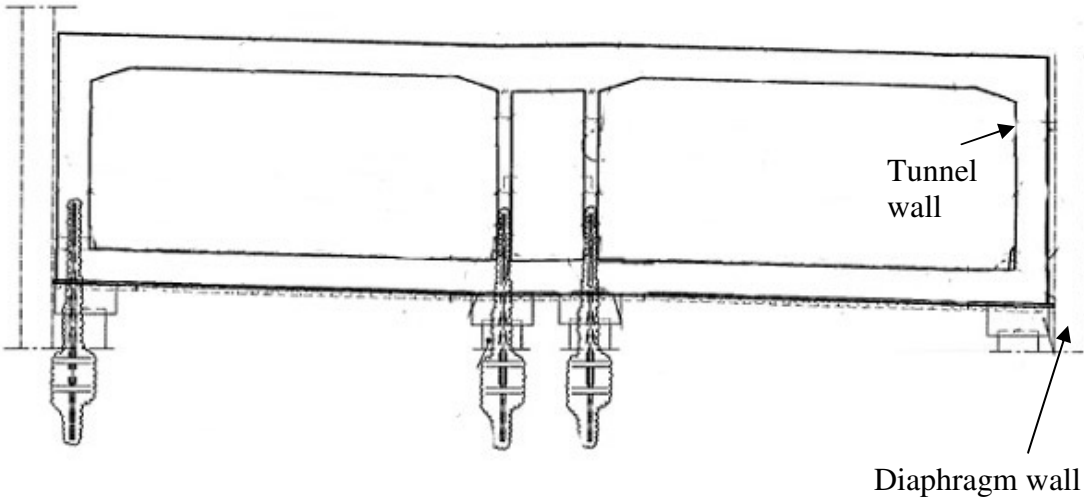

Figure 3.12 Geometry of section 2/717. [4]

3.3 Site measurements

During the time of construction, the movements of the propped diaphragm walls at the Göta Tunnel were monitored. During this time the piles were installed, the area was excavated, and the floor slab was cast. In the attempt to find a representative computer model, results from the model are compared with the displacement measurements from the site. The placing of the measuring equipment, which includes inclinometers to measure horizontal displacements, and point gauges to measure vertical displacements, is shown in Figure 3.13. It should be noted that measures from the inclinometer inside of the diaphragm walls are not used. Instead, in this thesis

measures from inclinometers placed at a small distance outside the wall are used. This is also illustrated in Figure 3.13. In Figure 3.14, it is shown where the inclinometers are placed along the studied section. [24]

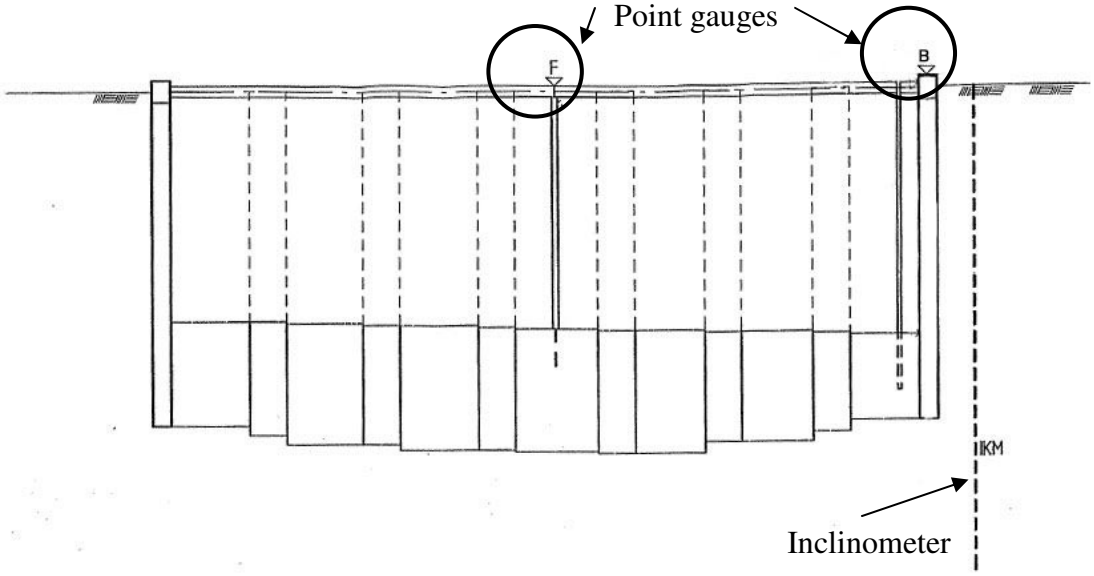

Figure 3.13 Placing of in situ measuring equipment, i.e. inclinometers and point-gauges, at the studied section. [24]

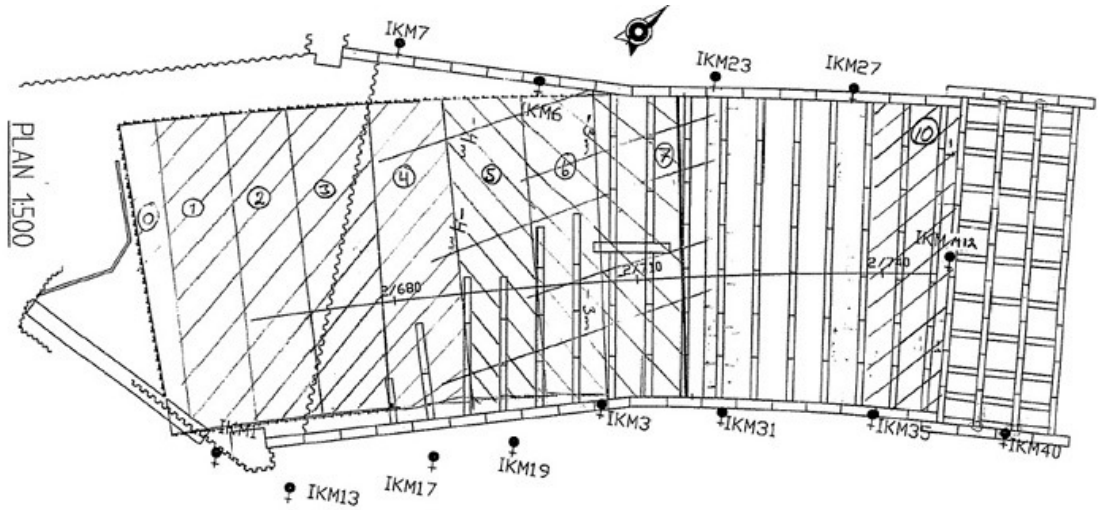

Figure 3.14 Plan view of tunnel. Inclinometers marked as IKM. [24]

The comparison between in situ measurements and the results from modelling gives an opportunity to verify the model. The measuring equipment was broken some time into the construction phase, where new equipment was installed. The deformations, which had occurred up to this point of time, were lost, meaning that later measurements start from a new reference measuring. Due to this, the applicability of the comparison with these measurements should be considered approximately. [24]

4 Modelling

This chapter presents general information about FE modelling as well as describes assumptions and simplifications for modelling of the Göta Tunnel. Also, some problems connected with the modelling of concrete are discussed.

4.1 General

It is important to select appropriate constitutive models for analysis. Simplified methods for analysis or empirical methods have traditionally been used for the design of retaining walls. Since these methods are simplified, engineers can only obtain approximate values of the desired information, i.e. they only get limited information about soil movements, soil pressures, section forces as well as no information about the interaction with adjacent structures. Over the years, progress has been made in attempting to model the behaviour of retaining structures and to investigate the mechanism of soil/structure interaction. [13]

4.1.1 Sources of ground movements

At the installation of the diaphragm walls there will be movements in the soil leading to changes of the in situ stresses. Beside the installation effects, there are several sources of ground movements such as:

- Excavation in front of the wall, where the ground movements are influenced by:
    - Stress changes due to the excavation.
    - Soil strength and soil stiffness.
    - Changes in ground water conditions.
    - Stiffness of the wall and its support system.
    - Shape and dimension of the excavation.
    - Other effects such as site preparation works.
    - Quality of construction workmanship.
- Flow of water causing loss of ground and consolidation caused by changes in water pressures due to seepage through and/or around the wall.

Where ground movements cannot be predicted accurately they are possible to estimate, either with an empirical approach based on field measurements or with analytical methods based on numerical models calibrated against comparable experience.

The first five of the above mentioned factors that affect the modelling, can be handled by evaluating proper material parameters and making choices of site conditions which are interpreted into model properties. Regarding the last two, they are difficult to comprise in the modelling, but one would presume they will not affect the work.

4.1.2 2D / 3D

Geotechnical problems that involve retaining structures are always three-dimensional. Therefore a three dimensional analysis that fully represents the geometry of the structure, the loading and ground conditions together with appropriate boundary conditions, would be preferred. There are three-dimensional finite element programs available, but those use very simple constitutive models and coarse meshes since very large computer resources are needed. For that reason, it is questionable how reliable the results from the three-dimensional programs are. The most common analysis models used are instead the two-dimensional plane strain and axi-symmetric strain. This simplification of the system makes it necessary to make some assumptions, which are explained closer in the following chapter. [13]

4.1.3 Plane strain / Axi-symmetric analysis

For plane strain- and axi-symmetric strain analyses, the model can be reduced to half its original size by use of symmetry about an axis along the centre line, thus saving time as well as work by reducing the model mesh. One must be careful though, since very rarely there are absolutely symmetrical conditions on site and if there are, it is still not likely that the construction work will be carried out in a symmetrical manner. [13]

4.1.4 Models

When choosing input parameters for the different soil models, it is of importance to identify what type of problem to be analysed since the deformation properties of the soil depend on the current- and previous stress levels, as well as on the stress paths. [7]

Some parameters are well known from both field- and laboratory tests, for instance shear strength, c_{uk} and c_k', while others are more difficult to determine like for instance the stiffness modulus, *M*.

For soils, the use of linear elastic analyses, using either isotropic or anisotropic constitutive models, is in general not to recommend since in a majority of cases it is can be misleading. The reason for this is that there are no restrictions of the magnitude of the maximum soil pressures, nor the tensile stresses that can develop within the soil. Instead, using a linear-elastic perfectly plastic model, limits the tensile stresses in the soil as well as the active and passive pressures that can occur. [13]

4.1.5 Undrained / drained behaviour of soils

Depending on the soil permeability and the time span considered, a choice of drainage conditions has to be made. Undrained behaviour is preferred when taking short-term loading into account. Long-term loading is used for consolidation analyses where drained behaviour is adopted. As described earlier in the PLAXIS chapter, long-term analysis or short-term analysis is obtained by choosing either *CONSOLIDATION* or *PLASTIC* in the Calculations program. For instance, short-term analysis can be used for excavation phases whereas *CONSOLIDATION* can be used together with a number of entered days in order to simulate a specific time span, i.e. a combination of calculation phases.

4.1.6 Size of geometry

A soil model large enough to make certain that whatever actions are performed on the tunnel structure do not affect the properties at the model boundaries, must be used. This means that no deformations of the soil, or any change of the groundwater level is accepted. Approximately three to four times the height of the soil model should be used for the width.

4.1.7 Boundary conditions

The command *STANDARD FIXITIES* in PLAXIS is used for describing the general boundary conditions of the model, which sets the horizontal displacement, n_x, equal to zero on the vertical geometry lines, and sets both the horizontal displacement, n_x, and the vertical displacement, n_y, equal to zero on the horizontal geometry line. See Figure 4.1 where these *STANDARD FIXITIES* are applied on a soil model with horizontal soil layers. [6]

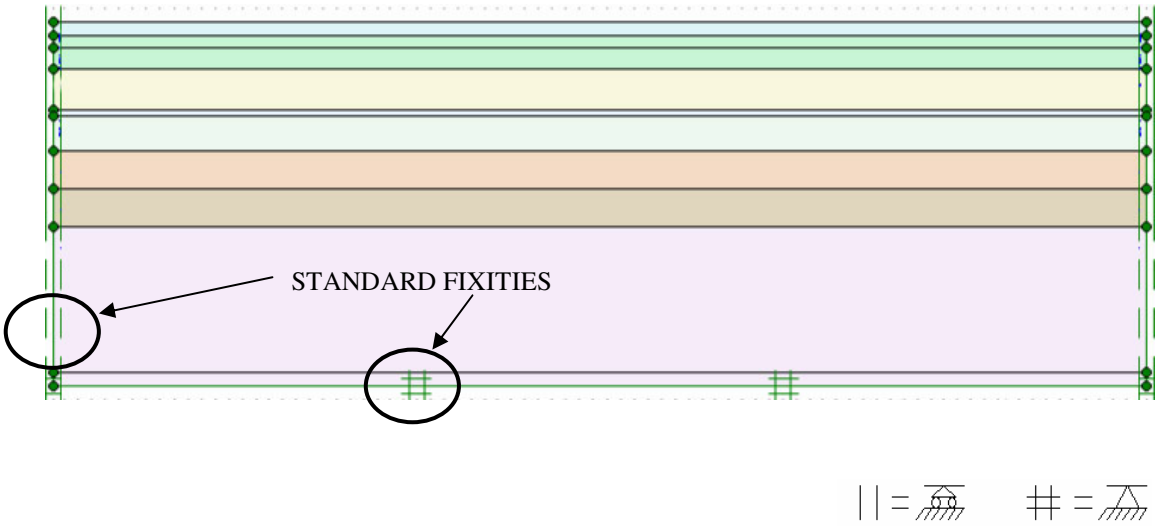

Figure 4.1 Boundary conditions, STANDARD FIXITIES.

4.1.8 Mesh

It is sensible to experiment with mesh sizes. Obvious is that a coarse mesh will not yield as exact results as a fine mesh would. Though, to use a fine mesh over the whole model is not to recommend, since it increases the calculation time and increases the demands on the computer resources. Instead, a refinement of the mesh in the section of most interest is to prefer.

When using FE-programs such as PLAXIS, one must be aware that there might be problems when creating the mesh if placing nodes too close to another node. As a result, modifications of the soil model must sometimes be made in order for the model to work.

If wanting to change in the material properties without changing in the geometry, this is possible to do without extra measures by returning to the Input program. If instead wanting to change in the geometry, this is also possible when returning to the Input program, but then a regeneration of the mesh is necessary as well as a redefinement of the phases.

4.2 The Göta Tunnel – Modelling issuses

In this chapter modelling issues regarding the actual tunnel are described and discussed.

4.2.1 Assumptions

When creating a soil/concrete model some general assumptions and simplifications have to be made:

- The soil surface of each layer is considered horizontal.
- The ground water level is considered constant in undrained analysis.
- Each soil layer is considered homogeneous with distinct borders.
- The fill materials are assumed cohesion less, but are given a small c since PLAXIS does not accept a cohesion equal to zero.
- The influence of concrete shrinkage is neglected.
- "Wished in place" diaphragm walls are used, as mentioned in Chapter 1.4.
- The structural members are added instantly in their respective calculation phase.
- The excavation phase is modelled in three instant steps, contrary to the continuous procedure in reality.
- The bored piles are omitted.

.

4.2.2 Plane strain

Plane strain is used for the FE-analyses in this thesis according to relation (4.1), where z is the direction out of the 2D-plane contrary to the z used to define the depth in the soil model. [13]

$$\gamma_{xz} = \gamma_{yz} = \varepsilon_z = 0 \tag{4.1}$$

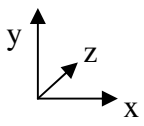

4.2.3 Material modelling

Some input values for the PLAXIS models need to be specially evaluated from laboratory tests, but since this thesis does not contain such tests, the parameters used are verified in earlier written thesis for the same soil, see reference [2] and [16]. Input for concrete parameters is taken from the Tender Document of the Göta Tunnel.

The analyses in this thesis start with an elastic model, theory according to Hooke, for the soil as well as for the concrete, developing into a model with theory according to Mohr-Coulomb for the soil. The reason for choosing elastic relationships for the diaphragm wall throughout the analyses in this thesis is due to that small deformations are expected.

A Hooke model can be used for analysis in PLAXIS if choosing elastic behaviour for the soil layers in the Input program. This model is used in this thesis in order to

compare results from varied input since the calculations most often are faster than with the Mohr-Coulomb model.

In the Input program in PLAXIS, the material behaviour is set to undrained for clay layers, and the entered parameters are effective. The reason for this is that if undrained parameters were to be entered, the behaviour would be locked in the undrained mode, and possible drainage occurring during the calculation would not be accounted for. Even though undrained behaviour is not coupled with effective parameters, it is possible to tick *IGNORE UNDRAINED BEHAVIOUR* in the calculation program when performing calculations with *PLASTIC* in order to obtain drained behaviour. For more information about calculation options, see the PLAXIS manual. [7]

Since the relationship between the soil stiffness and the soil stress is not accounted for in the Hooke model and Mohr-Coulomb model in PLAXIS, as mentioned earlier in Chapter 2.6.7, reference inputs have to be entered for each soil layer. These inputs are the reference stiffness, E_{ref}, and the reference depth, y_{ref}. The stiffness increment by the depth can be considered by assuming that the increase is proportionate to the shear strength, as can be seen in Figure 4.2; it shows how the modulus is constant down to approximately +5 m and thereafter increases. In the Tender Document of the Göta Tunnel, the stiffness modulus, M_0, is estimated according to equation (4.2a). In order though to be able to complete a full analysis in the Calculation program in PLAXIS, M_0 according to NGI (the Norweigan Geotechnical Institute) is used in this thesis, see equation (4.2b). [4], [22], [16]

$$M_0 = 250 \cdot c_{uk} \tag{4.2a}$$

$$M_0 = 650 \cdot c_{uk} \tag{4.2b}$$

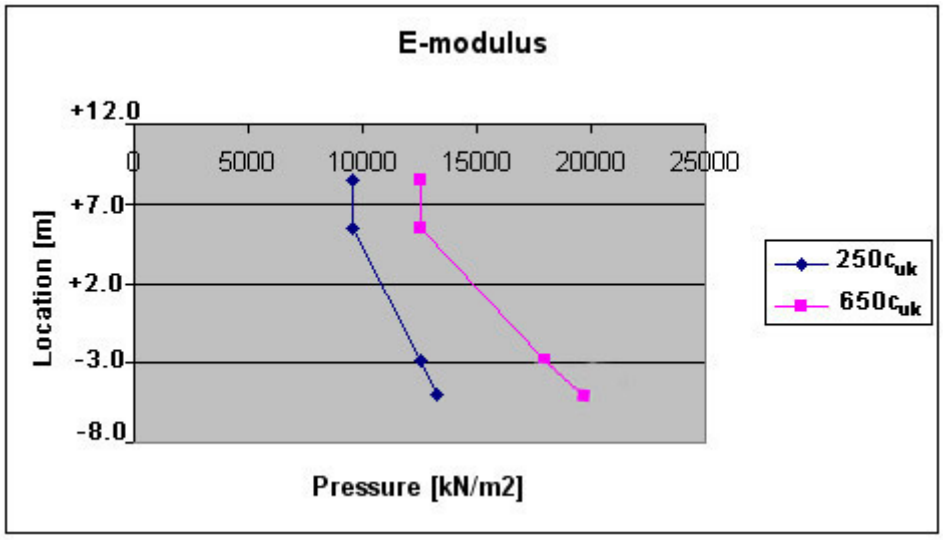

Figure 4.2 E-modulus based on equations (4.2). [16], [22], [4]

4.2.4 Working procedure in reality: Phases in PLAXIS

One important issue in numerical analyses is the simulation of the work procedure, which is considered by creating different calculation phases in PLAXIS, which each corresponds to a working stage. All actions executed on the soil, e.g. installation of diaphragm walls, introduce stresses. Installation effects are difficult to model within the program. However, since this thesis is focused on the behaviour of the finished structure, installation- as well as excavation effects are dealt with in a simplified way by use of "wished in place" diaphragm walls.

The procedure is to add and/or remove structural members or soil in different steps by activating/deactivating. Depending on when and where the props during excavation are placed on the diaphragm wall, there are different moment distributions.

The working phases in this thesis are two-dimensional, while in reality they are three-dimensional. To make use of the weight of the soil, and thereby avoid bottom heave, the excavation on site is performed in a stepwise manner. To simulate this in the model an extra excavation level is included in the phases. Also, instead of excavating to the bottom of the heave-suppressing slab in one separate phase and activating the slab in the phase after, these two actions are performed simultaneously in one combined phase. The calculation phases for the tunnel are more closely described in Chapter 6.3. A general view of an excavation site can be seen in Figure 4.3.

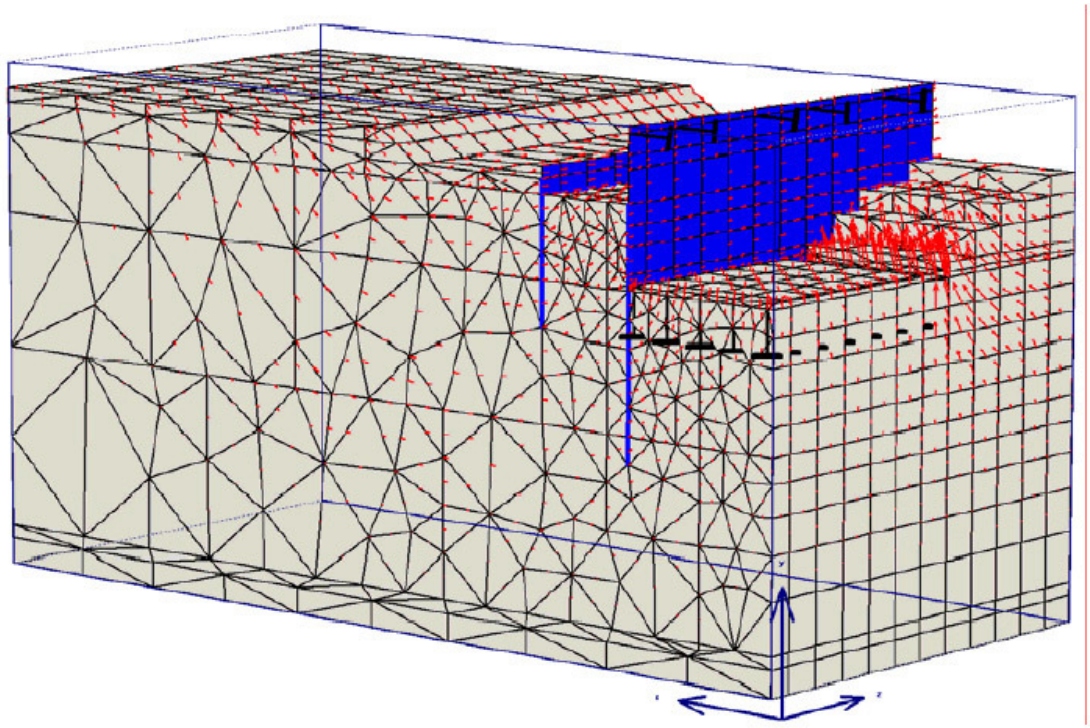

Figure 4.3 Schematic view of three-dimensional-effects of excavation. [26]

4.2.5 Interfaces between soil and concrete

Another important issue in the analyses is how to handle friction between concrete and soil as well as between different soil layers. To achieve appropriate friction values in the PLAXIS model, *INTERFACE* elements are used in the modelling of the Göta Tunnel. The friction value is set to 0.4 for clay layers and 0.5 for fill/sand. These *INTERFACEs* also function as closed water boundaries. For the modelling in this thesis, *INTERFACE* elements are adopted on the concrete elements, i.e. on the diaphragm wall, the equivalent cross walls and the concrete slabs. The *INTERFACE* elements representing e.g. the interface between the diaphragm wall and soil, will adopt the friction values that are assigned to the actual soil layer they run through. [13]

4.2.6 Size of geometry

The geometry of the model is shown in Figure 4.4. The tunnel section in this thesis is modelled in half its size around a vertical symmetry axis. It is possible though to model it in whole, but that would be time consuming as well as would require large computer resources.

Since only horizontal soil layers are used for the PLAXIS models, a modification of the thickness of the bottom soil layers is made. See Figure 3.11, where the slope of the bedrock is shown.

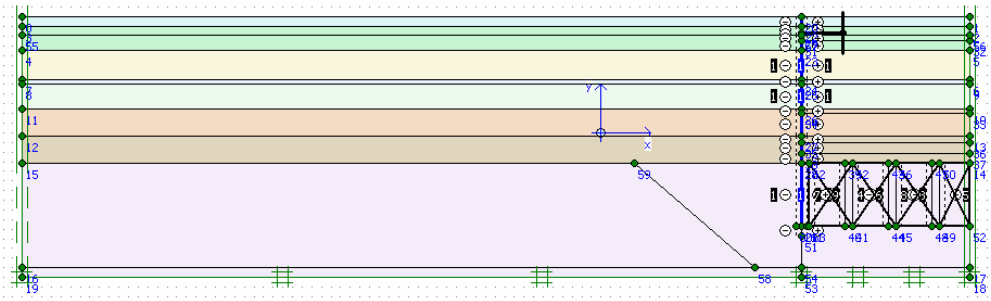

Figure 4.4 Geometry of soil model.

4.2.7 Boundary conditions

It is important to decide what boundary conditions to use. Since props and anchors etc. have enormous influence on the distribution of the bending moments, forces and displacements, it is of great importance to handle these boundary conditions in a correct manner. Table 4.1 shows the properties and what element type to be used as input in PLAXIS for the prop in this thesis. A choice can be made in the program between elastic or elasto-plastic behaviour, and for all steel material used for the work in this thesis, elastic is chosen since small deformations are expected. The input

$L_{spacing}$ refers to the spacing of the props, which are circular steel pipes with a diameter of 1016 mm and a thickness of 8.8 mm. [13], [5]

Table 4.1 Properties used for prop during excavation. [5]

Input	***Prop CHS 1016 x 8.8*** *(FIXED END ANCHOR)*
Type	Elastic
$L_{spacing}$ $[m]$	4.5
EA $[kN/m]$	2.94E6

To model the ground water flow, there are restrictions for water movement through the boundaries placed along the outer limits of the model, see Figure 4.5. At consolidation it is not likely that the water would escape sideways, since the clay layers cover very large areas. Instead the water will be rearranged within the model at increased pressure due to loading. These conditions are set in the Input program in PLAXIS.

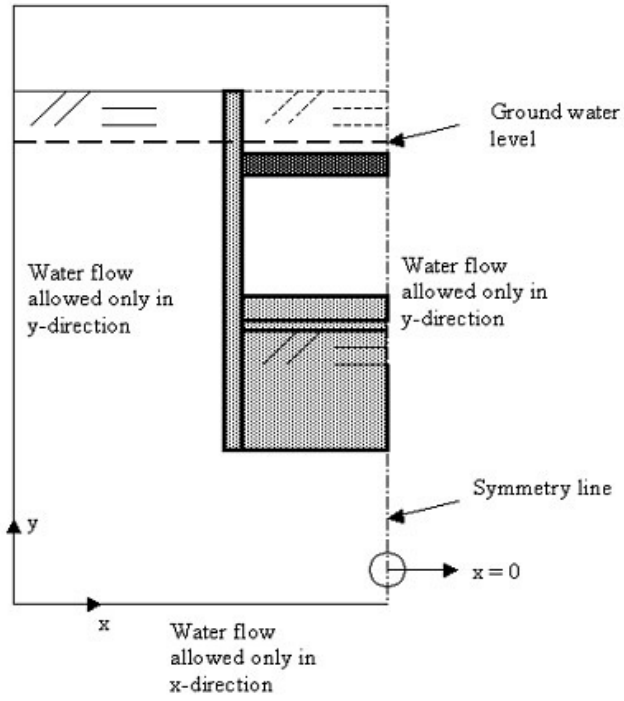

Figure 4.5 Boundary conditions for modelling around a vertical symmetry axis.

4.2.8 Modelling of concrete

Since PLAXIS is a two-dimensional FE-program used for soils, it might not be the best tool for concrete analyses. Some of the issues with modelling concrete are presented in the following sub-chapter, as well as suggestions to overcome them.

4.2.8.1 Out-of-plane concrete

The calculations in PLAXIS are performed on the particular cross section drawn in the model, without regarding that the cross section might change out of the plane. Changes in the structural geometry can be accounted for by use of a transformed cross section. In a transformed cross-section an additional part e.g. a cross wall is not physically present in the model, but instead the stiffness provided by the additional part is accounted for by adding some extra stiffness to, in this case, the cross-section of the diaphragm wall.

The default calculations in the FE-program are based on a thickness of 1 m out of the plane. By this the moment of inertia is calculated according to equation (4.3). The area for this calculation can be seen in Figure 4.6. (The area is rotated 90° for the roof and the floor.)

$$I = \frac{bh^3}{12}, \text{ where b is 1 m and h is the actual element thickness.} \qquad (4.3)$$

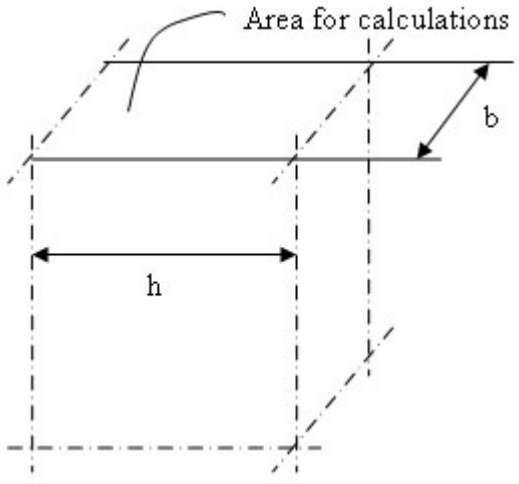

Figure 4.6 Area of diaphragm wall used for FE-analysis.

4.2.8.2 Longitudinal diaphragm walls

For the longitudinal diaphragm walls, there are two options for modelling concrete in PLAXIS.

In the first option a *PLATE* element can be used where input parameters are the flexural rigidity, EI , the flexural stiffness, EA , as well as the weight, w. To confirm that realistic inputs have been used for EI and EA , PLAXIS automatically calculates the corresponding equivalent thickness, d, for the concrete element, which should be equal to the actual thickness of the element.

Alternatively, the concrete can be modeled in the same manner as the soil layers, i.e. the *LINE* command is used to create areas, so called clusters, that can be assigned properties corresponding to concrete. By doing this, the same input as for a soil layer is required. Since the only known parameters for the concrete within the cluster command are EI , EA and w, the remaining required parameters will be an estimation, and therefore this might not be the best option for modelling of concrete. Also, results such as stresses and forces in the Output program in PLAXIS are not as accessible as in the *PLATE*-alternative.

In both options though, the friction between the wall and the adjacent material can be accounted for in the calculations.

If the cross walls are modelled according to either of these two suggestions, the program will acknowledge them as continuous out of the plane and the resistance against heave, created by the adhesion between clay and concrete, will be lost. This effect is of great importance for the stability against heave before the heave-suppressing slab is cast, which is discussed in Chapter 4.2.8.4 below. [21]

4.2.8.3 Concrete plates

A concrete plate can be modelled using the same options as discussed above in Chapter 4.2.8.2. For the simulation of two concrete slabs on top of each other (in this thesis: floor slab and heave-suppressing slab), it is not possible to use two plate elements. The *PLATE* elements are only lines in the geometry with two nodes. If placing them apart considering their actual thickness a problem arises, namely how to handle the area in between. Although a thickness for the plate can be given, this is only a number and nothing that can be visualized in the model. To overcome this problem, two soil layers, which can be given concrete properties, can be created on top of each other. Another option is to model one of the slabs with a *PLATE* element and the second slab as a soil layer with concrete properties. Which option to choose depends on the interaction properties required between the slab and the vertical element to which they are connected. Full interaction requires a *PLATE* to *PLATE* connection, see Figure 4.7 for both options.

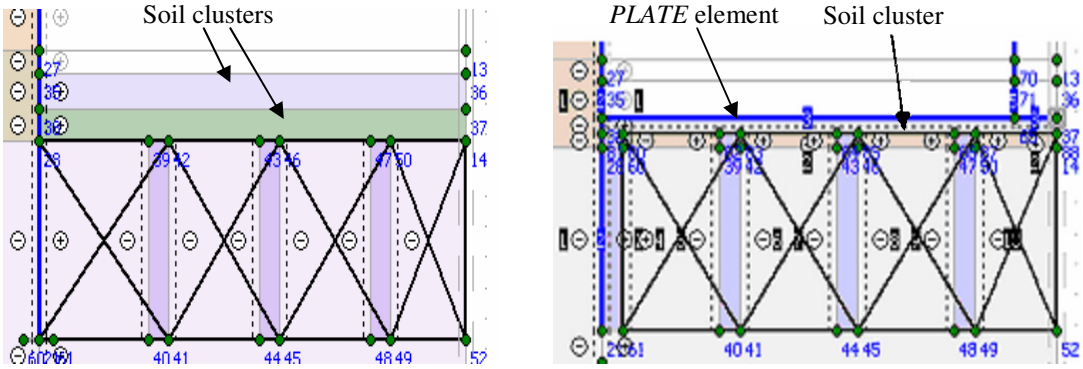

Figure 4.7 *View of the options for modelling two concrete slabs on top of each other.*

4.2.8.4 Cross walls

Cross walls are transversal diaphragm walls, placed every 4.5 m along the longitudinal diaphragm wall. They are used in the Göta Tunnel for two reasons. Firstly, they prevent horizontal movement of the longitudinal diaphragm walls in the inward direction. Secondly, they prevent bottom heave during excavation before the heave-suppressing slab of the tunnel is cast.

For modelling of the cross walls, the options are restricted by the two dimensions available in the used PLAXIS version.

If the stiffness provided by the cross walls are accounted for by the use of a transformed cross section, as described in Chapter 4.2.8.1 as well as in 4.2.8.3, only the problem with the concrete being continuous out of the plane is overcome. Also, a transformed concrete section will create difficulties when wanting to compare calculated displacements with the site measurements, since then the PLAXIS model represents an average section of the tunnel, whereas the site measurements are taken from one specific section.

Norwegian engineers have performed FE-analyses on the Göta Tunnel, and therefore their solution for cross walls is looked upon and used in this thesis, as described in the following text. One must be aware though, that they focused on different matters than the ones studied for this thesis.

To be able to account for the heave suppressing effect mentioned above, the cross walls are replaced with internal walls in the longitudinal direction, called equivalent cross walls. The equivalent cross walls have the same height, thickness and spacing as the real cross walls and will therefore, with a well balanced choice of friction value between concrete and soil, provide the same resistance against bottom heave. To account for the horizontal stiffness, the equivalent cross walls are connected to the longitudinal walls through an imaginary steel truss with the same axial- and bending stiffness across the excavation as the real cross walls. According to Lars Andresen at NGI, this is achieved by dividing EA for the real cross walls by 6. The PLAXIS input for the cross walls can be seen in Table 4.2 and Table 4.3. The truss is modelled with

NODE TO NODE ANCHORs and the soil clusters, representing the concrete in the equivalent cross walls, are given a friction value, R_{int}, equal to 0.4. [22], [19], [5]

In order to investigate the influence of varying stiffness for the truss elements, several analyses were performed with lower values than proposed by Andresen. Only the horizontal displacements in the diaphragm wall were considered. Since the differences were so small, 1 to 2 mm, they are not presented here and the Norwegian proposal is accepted.

Table 4.2. Properties used for the concrete in the equivalent cross walls. [5]

Input	***Equivalent cross walls*** *(cluster)*
Type	Non-porous
$\gamma\,[kN/m^3]$	24
$E_{ref}\,[kN/m^2]$	3.2E7
$\nu\,[-]$	0.2
$c_{ref}\,[kN/m^2]$	2.85E4
$R_{int}\,[-]$	0.4

Table 4.3 Properties used for the truss in the cross walls. [19]

Input	***Truss*** *(NODE TO NODE ANCHOR)*
Type	Elastic
$L_{spacing}\,[m]$	4.5
$EA\,[kN/m]$	4.27 E 6

4.3 Procedure

The diaphragm walls in the Göta Tunnel are today only used in the temporary stage of construction, whereas the work in this thesis treats the diaphragm walls as permanent. When the excavation for the Göta Tunnel is finished, the actual tunnel was built in between the temporary diaphragm walls. The capacity of the diaphragm walls were

not regarded when designing the tunnel capacity. For this thesis the diaphragm walls are used as support structure at the excavation stage as well as for permanent walls in the tunnel.

Two different models are treated, each with a specific purpose. Firstly a model, which represents the open shaft for the actual chosen section of the Göta Tunnel before the tunnel construction starts, is created. It is denoted the Verification Model and is used for verification by comparing the displacements obtained from the FE-analyses with measurements made on site in the studied section of the Göta Tunnel. Secondly a model of an imaginary tunnel is created, denoted the Evaluation Model. Contrary to the real Göta Tunnel, in the Evaluation Model the diaphragm walls are used as permanent tunnel walls. The Evaluation Model is used for evaluation of load effects, where results from the FE-analyses are compared with results from hand calculations.

For all analyses on the Verification Model the stiffness of each concrete element refers to uncracked concrete i.e. the elements belong to State I. For the Evaluation Model variations of the concrete stiffness yield different loads and elements belonging to both State I and to State II are used. For advanced analyses it is possible to divide the elements in smaller parts, which each can be assigned a different stiffness. When investigating the moment distribution in each element in the model by simple analyses, according to equation (2.2) and equation (2.3), it is seen that the critical moment is exceeded at the same time along the whole element length. Therefore it is decided not to divide the elements.

For the Evaluation Model two extreme cases are analysed, namely where the whole tunnel structure belongs to either State I or to State II throughout the analysis. Also a model simulating an estimated real behaviour is analysed, where the concrete stiffness assigned to each structural member depends on whether the critical bending moment is exceeded or not.

In Figure 4.8 a sign rule is shown, which provides understanding for which side of the diaphragm wall that is subjected to tension in the moment diagrams in the following chapters. A negative sign indicates tension on the outside.

Figure 4.8 Schematic view of the tunnel structure with sign rule for the diaphragm wall.

5 Temporary Stage with Results

In this chapter, a Verification Model is created that simulates the early stage of the construction of the Göta Tunnel, where diaphragm walls are used only temporarily. In order to verify that the model yields reasonable results, results from FE-analyses are compared with field measurements. In the search for an acceptable soil model, also the cross walls are investigated. It should be noted that contrary to the information from the beginning of this project that the tunnel includes a heave-suppressing-slab as shown in Figure 2.6 in section 2/717, it later appeared that there is no heave-suppressing slab but only a layer of gravel. Due to the time limit of this project it is decided to continue with FE-models including a concrete heave-suppressing slab. This should be regarded when reading the following sub-chapters.

5.1 Mesh

The mesh used for the Verification Model is shown in Figure 5.1. A refinement of the element mesh surrounding the shaft is made.

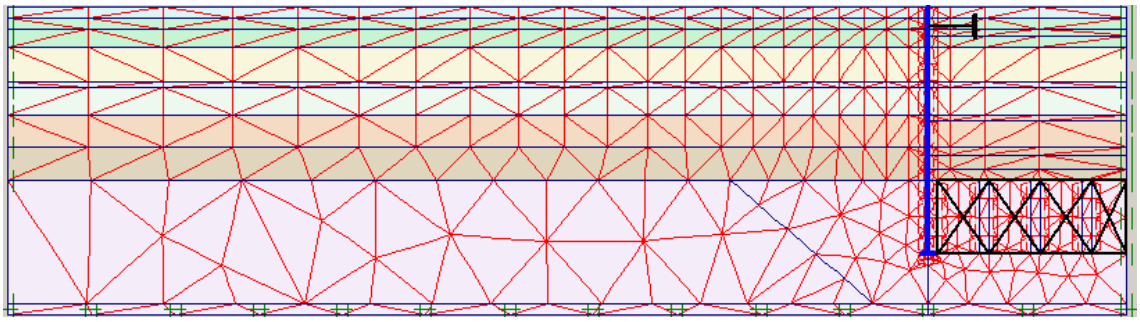

Figure 5.1 Mesh used for Verification Model.

5.2 Calculation phases

In the last phase of the excavation, according to Table 5.1, all considered actions have been accounted for in the Calculations program. This table also describes the calculation phases adopted, and what procedures they contain.

When analysing the effects of the excavation, mainly plastic phases are used. For phase 4 and 7-9 though, in order to be able to compare FE-results with on site measurements, consolidation phases are used. During construction the shaft has been left open for some time at different levels of excavation and this governs the time used for consolidation in the analyses.

Table 5.1 Calculation phases used for Verification Model.

Phase no	*Calculation*	*Actions*	*Time [days]*
1	*PLASTIC*	Activate diaphragm wall and cross wall	-
2	*PLASTIC*	Excavate down to prop level, +9.5 m	-
3	*PLASTIC*	Add prop at +10.35 m	-
4	*CONSOLIDATION*	Excavate to +2 m	170
5	*PLASTIC*	Excavate to full depth and activate heave-suppressing slab	-
6	*PLASTIC*	Activate floor slab	-
7	*CONSOLIDATION*	First series of measures	210
8	*CONSOLIDATION*	Second series of measures	60
9	*CONSOLIDATION*	Third series of measures	150

5.3 Choice of model for the cross walls

In the creation of the Verification Model, a choice between two different ways to model the cross walls must be made. In both options the cross walls are modelled with equivalent cross walls according to the Norwegian proposal as described in Chapter 4.2.8.4. The difference between the two models lies in how the connection between the cross walls and the longitudinal diaphragm wall is modelled.

The friction between the longitudinal walls and the cross walls, as well as between the cross walls and the soil, are especially important to model in order to take care of the bottom heave. Therefore, two suggestions are proposed for use in the Verification Model, see Figure 5.2 and Figure 5.3.

Alternative A: NODE TO NODE ANCHOR to diaphragm wall.

Alternative B: Cluster to diaphragm wall.

In Alternative A, it is assumed that the maximum friction value, 1.0, has developed between the diaphragm wall and the cross walls, i.e. the connection between the *NODE TO NODE ANCHORs* and the *PLATE* element has full interaction.

In Alternative B, a friction value between the two concrete elements can be entered by use of *INTERFACE* elements. The limit friction value as prescribed in the Swedish code BRO 2004, is equal to 0.5.

Due to the uncertainty of the magnitude of the friction value between the elements, Alternative B would be preferred. Also, since the cross walls and the diaphragm wall do not have full interaction, Alternative A is less appropriate. Although in reality, even if the cross walls are unreinforced and cannot resist tension forces, tension is not likely to occur.

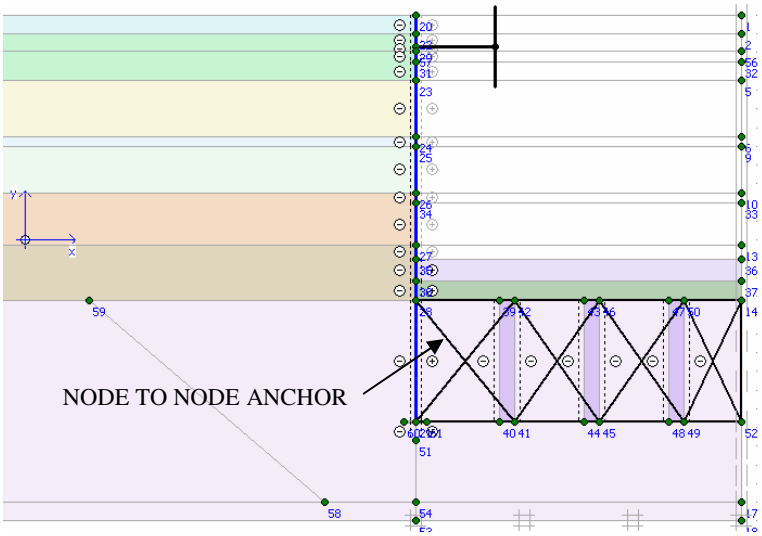

Figure 5.2 Alternative A: NODE TO NODE ANCHOR to diaphragm wall.

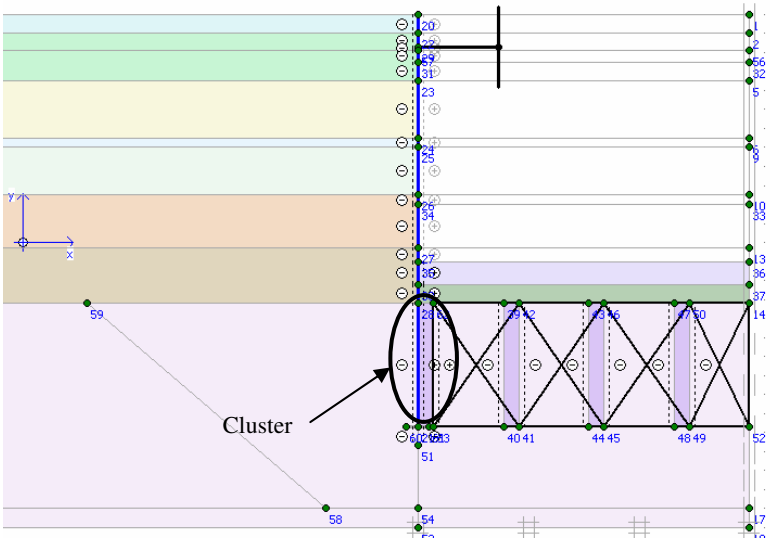

Figure 5.3 Alternative B: Cluster to diaphragm wall.

5.3.1 Alternative A: *NODE TO NODE ANCHOR* to diaphragm wall

In the original Norwegian proposal, the NODE TO NODE ANCHORs in the imaginary steel truss are connected directly to the PLATE element, which represents the longitudinal diaphragm wall. If modelled in this way, the horizontal reaction

forces in the cross walls will be reduced to point loads acting on the diaphragm wall at the two connection locations, see Figure 5.2 and Figure 5.4.

5.3.2 Alternative B: Cluster to diaphragm wall

If an additional equivalent cross wall is placed next to the diaphragm wall with the NODE TO NODE ANCHORs connected to the right corners of the cross wall element, the horizontal reaction forces in the cross wall will distribute over its height in the diaphragm wall, see Figure 5.3 and Figure 5.5.

5.3.3 Results and choice

In Figure 5.4 the shear force acting on the diaphragm wall is shown for Alternative A. Where the upper node is attached to the diaphragm wall, at level –3.2 m, the magnitude of the shear force is $1370\,kN/m$, whereas at level –9.7 m where the lower node is attached, the shear force is approximately 50 kN/m. The difference can possibly be explained by that the upper node attracts all force since the movement at that point is larger than at the bottom of the diaphragm wall. In reality, the force from the cross walls is distributed along a length on the diaphragm wall.

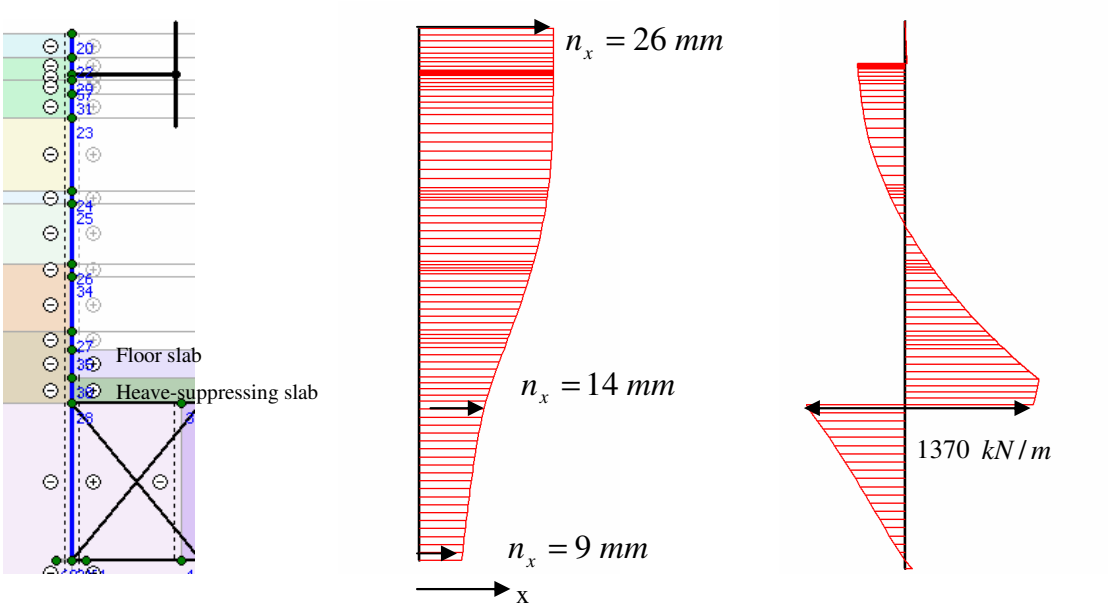

Figure 5.4 *Alternative A: Horizontal deformations and shear force acting on the diaphragm wall. The plots of the displacements and the shear force correspond to the height level in the very left picture.*

The shear forces acting on the diaphragm wall for Alternative B are shown in Figure 5.5. Here it can be seen that the shear force is more evenly distributed than for the previous alternative, which allows for a choice of the second alternative since this represents reality in a better way.

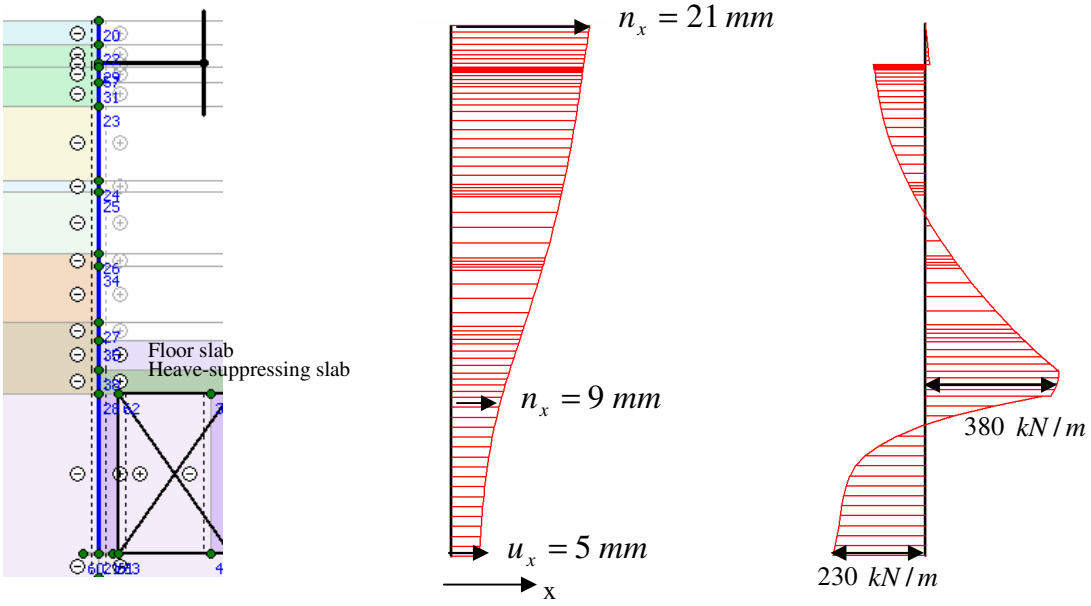

Figure 5.5 *Alternative B: Horizontal deformations and shear force acting on the diaphragm wall. The plots of the displacements and the shear force correspond to the height level in the very left picture.*

5.4 PLAXIS View of Verification Model

Since two plate elements cannot be placed on top of each other as discussed in Chapter 4.2.8.3, two soil layers are created to simulate the concrete slabs: i.e. the heave-suppressing slab and the floor slab. This is a reasonable way to model this, since the floor slab does not interact with the longitudinal diaphragm wall. A view of the elements in the model can be seen in Figure 5.6.

The Verification Model includes a longitudinal diaphragm wall (*PLATE*), a prop (*FIXED END ANCHOR*), a cross wall (clusters and *NODE TO NODE ANCHORs*), a heave-suppressing slab (cluster) and a floor slab (cluster). The vertical brace, which is used during the real construction to support the props, is omitted in the model since the *FIXED END ANCHOR* representing the prop can be given any length without experiencing buckling.

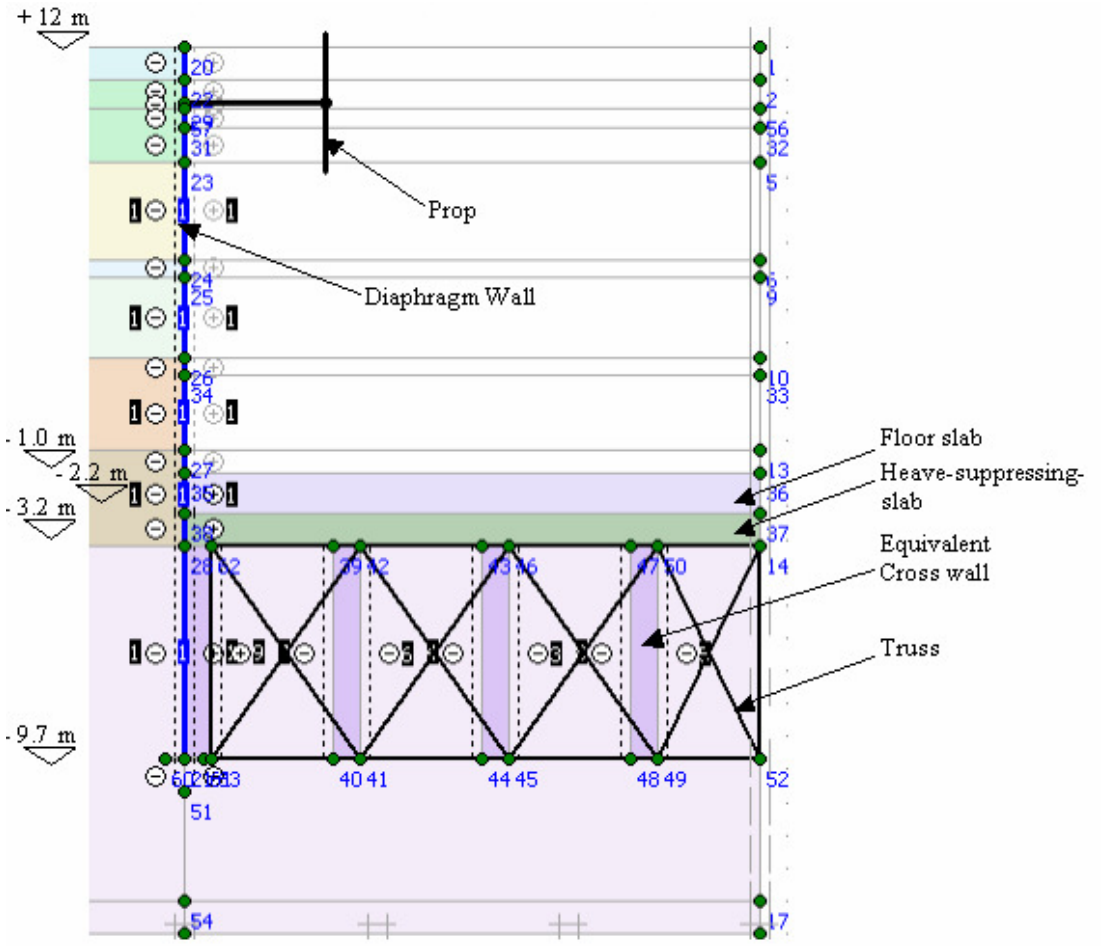

Figure 5.6 Verification Model.

5.5 Sensitivity analysis of soil parameters

Analyses are performed with the soil stiffness based on the earlier mentioned tri-axial tests where $E = 250 \cdot c_{uk}$, as well as with the soil stiffness based on $E = 650 \cdot c_{uk}$ as evaluated by NGI. When the lower value of the stiffness, $E = 250 \cdot c_{uk}$, was used, the analysis became numerically unstable and convergence could not be reached.. Due to that, along with the rather small displacements measured on site, the soil stiffness is instead based on Kjell Karlsrud's experience with soils similar to the Gothenburg clay where $E = 650 \cdot c_{uk}$. [16], [22]

In order to estimate how sensitive the results are to changes in the soil stiffness, analyses with a slightly lower stiffness, $600 \cdot c_{uk}$, are performed. These results can be seen in Table 5.2. It can also be seen in Table 5.2 that there is only a slight difference in the results when choosing $\phi' = 30°$ which is a common value for clay, instead of $\phi' = 35°$ which is to be used together with the evaluated triaxial tests. This can be explained by that the rather small deformations obtained in the soil, lead to stresses located on a safe distance from the strength envelope, see Figure 3.5. For this reason, $\phi' = 35°$ is used in the following analyses.

In the modelling a choice has to be made regarding the size of the friction between the concrete and the soil. To see how the choice of the friction value affects the displacements of the diaphragm wall and the floor and also the load acting on the diaphragm wall, see Table 5.2. and Appendix G.

Table 5.2 Displacements from analyses with $E = 600 \cdot c_{uk}$ *and* $E = 650 \cdot c_{uk}$.

Displacements at +12 m and +0 m as well as in shaft middle.	$+12$ *m*		± 0 *m*		*Shaft middle*	
	n_x [mm]	n_y [mm]	n_x [mm]	n_y [mm]	n_x [mm]	n_y [mm]
E_{650}; $R_{\text{int } er} = 0.4$; $\phi' = 35°$	21	11	12	3	-	4
E_{650}; $R_{\text{int } er} = 0.6$; $\phi' = 35°$	23	12	13	4	-	4
E_{650}; $R_{\text{int } er} = 0.4$; $\phi' = 30°$	23	12	13	4	-	4
E_{600}; $R_{\text{int } er} = 0.4$; $\phi' = 35°$	-	13	13	-	-	4

5.6 Comparison between PLAXIS and IN SITU

When the model yields results that agree with the site measurements, the Verification Model can be expanded to a Evaluation Model.

For analyses of a model with concrete slabs and cross walls according to the evaluations in the earlier chapters, with $E = 650 \cdot c_{uk}$, the Mohr-Coulomb model yields displacements according to Figure 5.7 – Figure 5.9. These figures also include the in situ measurements, which allows for a comparison.

For Figures 5.7 and 5.8, the in situ measurements are obtained with gauges placed directly on the concrete structure, whereas the ones for Figure 5.9 are obtained with an inclinometer placed in the soil next to the diaphragm wall. In Chapter 3, Figure 3.13 and 3.14 show the placement of the measurement equipment. All in situ displacements are measured several times at selected time intervals and compared with results from PLAXIS at corresponding times.

Since the inclinometer was broken some time after its installation, comparable results from PLAXIS are obtained by subtracting the displacements that develop in the first and the second phase (see Table 5.1) from the displacements obtained in the final phase, see Figure 5.9.

Due to the uncertainties of the actual values of the soil properties to be used for the model it is not possible to achieve the exakt same displacements as were measured on

site. As can be seen in the figures, the on site displacements are generally larger than the results from PLAXIS. Though, since the displacements follow a similar pattern, it is verified that an acceptable model is found.

Regarding the differences in the horizontal movements between the model and reality, there are some factors that could influence the results. In the real structure there is a gap between the diaphragm wall and the cross wall, allowing for larger horizontal movement of the diaphragm wall. In the model this is not possible, since the cross wall is placed directly next to the diaphragm wall. The second factor which could influence the results is the magnitude of the modulus, E , where a lower value probably would yield larger deformations.

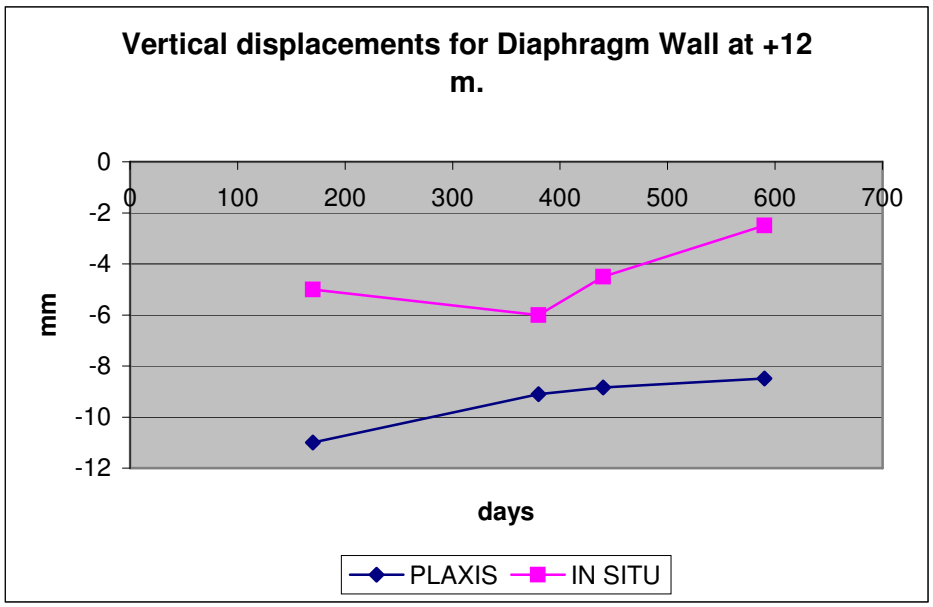

Figure 5.7 *Vertical displacements at the top of the longitudinal diaphragm wall, B-point.* [24]

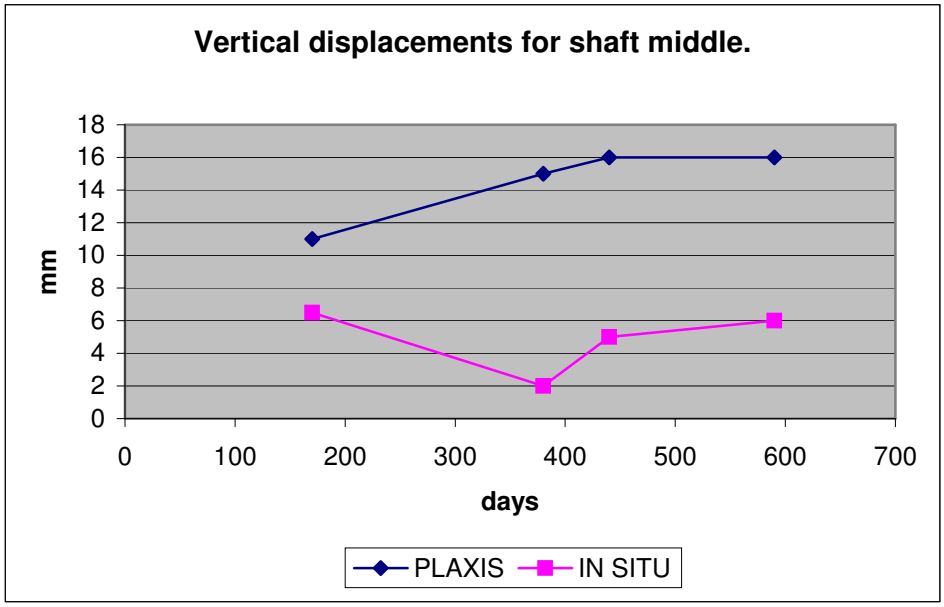

Figure 5.8 *Vertical displacements in shaft middle, right next to the symmetry line, F-point.* [24]

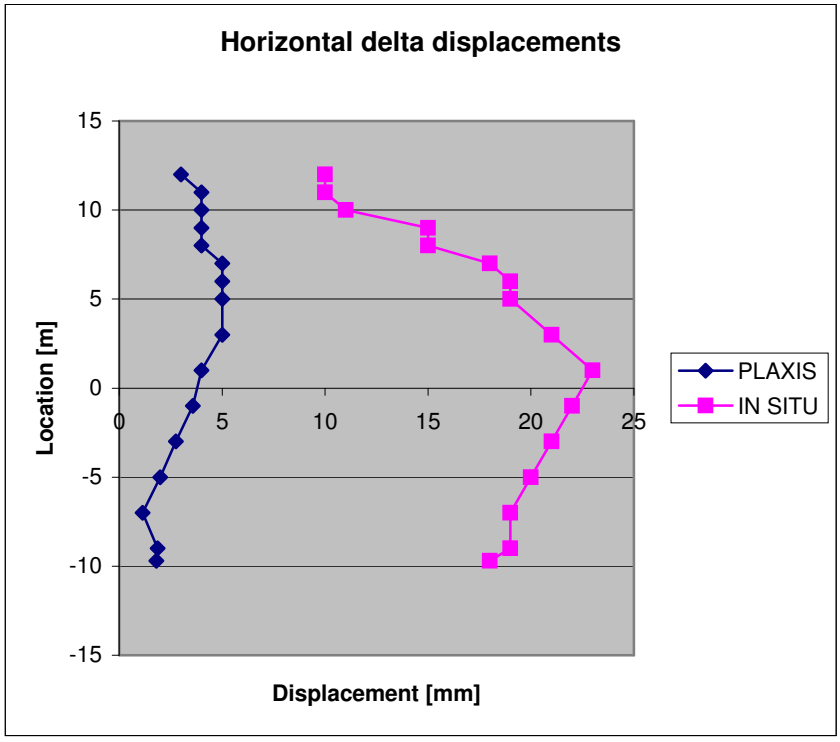

Figure 5.9 *Horizontal displacements along diaphragm wall, inclinometer.* [24]

6 Permanent Stage with Results

In this chapter, an Evaluation Model is created. This model simulates the permanent stage of an imaginary tunnel, where diaphragm walls are used as permanent tunnel walls. The results are evaluated by comparing the FE-analyses with hand calculations. In the search for a reasonable tunnel model, different ways of modelling the floor are investigated. This is due to that in the Evaluation Model the floor slab is attached to the diaphragm walls i.e. the tunnel walls, which is not the case in the Verification Model.

Analyses of varied concrete stiffness are performed where equations according to BBK 2004 are used. Two extreme cases are analysed where all tunnel elements belong to the same state, either State I or State II. Also, a case simulating an estimated real behaviour is analysed, where the concrete stiffness assigned to each structure member depends on whether the critical bending moment is exceeded or not.

Time $t = 0$ corresponds to when the construction of the tunnel is finished, whereas $t = 120$ years correspond to the lifetime of the Göta Tunnel as well as for the imaginary tunnel in the Evaluation model.

6.1 General

The Göta Tunnel gives the dimensions used according to Chapter 3.2, but instead of constructing the tunnel inside the diaphragm walls, the model is created with the diaphragm walls as walls of the tunnel, see Figure 6.1. This is done in order to simulate the behaviour of a diaphragm wall as a permanent part of the tunnel structure. To allow ground water flow above the tunnel, the part of the diaphragm wall that extends above the tunnel roof is cut off before the calculations for the estimated lifetime of the tunnel starts.

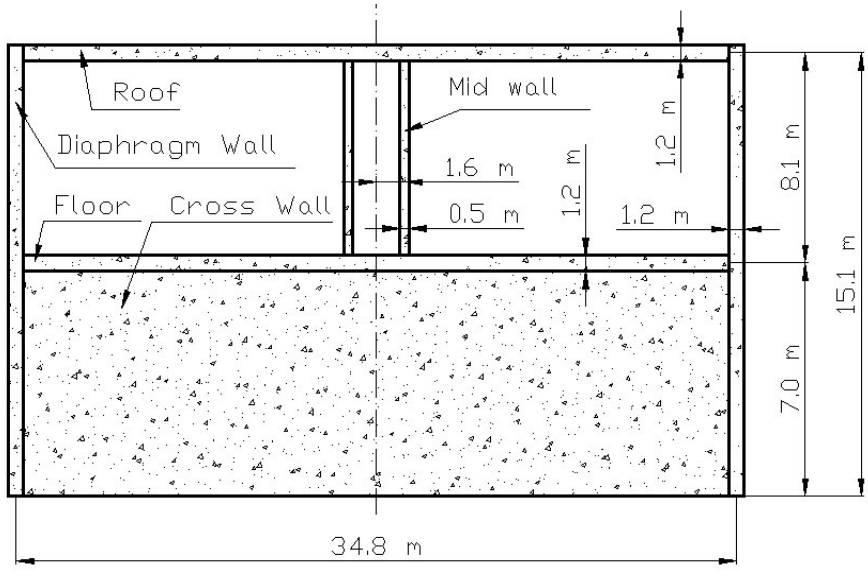

Figure 6.1 Dimensions and layout of the Evaluation Model with cross walls, cc 4.5 m underneath the floor slab. [5]

In the Göta Tunnel the connection between the floor slab and the tunnel wall is to be considered as rigid with full interaction between the two structural members. This is a difference that brings about a change in the way to model the floor slab. In the Verification Model there was no connection between the two, and the floor slab was modelled as soil, which was assigned the geometry and properties for concrete.

6.2 Mesh

A refinement of the element mesh surrounding the shaft is made. The mesh used for the Evaluation Model is seen in Figure 6.2.

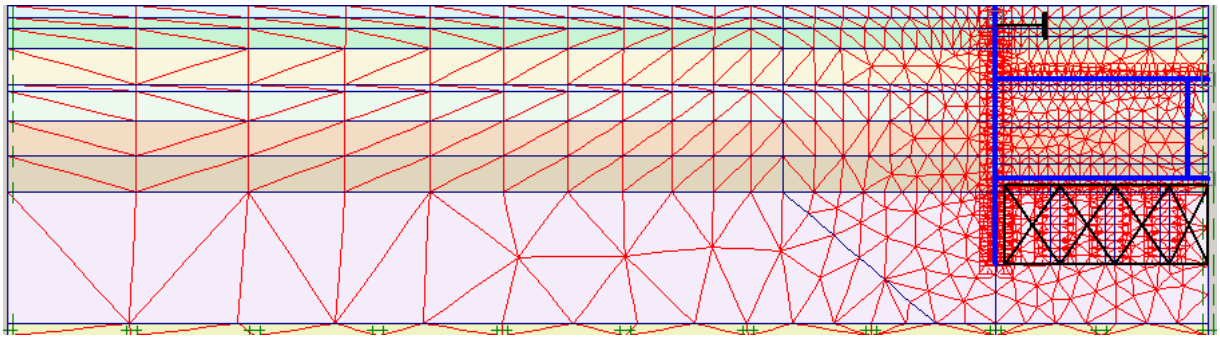

Figure 6.2 Mesh used for Evaluation Model.

6.3 Calculation phases

Some phases from the Verification Model are modified for the analyses with the Evaluation Model, in order to model the diaphragm walls as permanent.

For the excavation, plastic analyses are run where time cannot be entered. Though, to simulate the behaviour of the tunnel after 120 years, *CONSOLIDATION* is used as a last phase, where the time entered represents the expected lifetime of the tunnel.

In the last phase of the excavation, according to Table 6.1, all considered actions have been accounted for in the Calculations program. This table also describes the calculation phases adopted, and what procedures they contain.

Table 6.1 Calculation phases used for Evaluation Model.

Phase no	***Calculation***	***Actions***	***Time [days]***
1	*PLASTIC*	Activate diaphragm wall and crosswall	-
2	*PLASTIC*	Excavate down to prop level, +9.5 m	-
3	*PLASTIC*	Add prop at +10.35 m	-
4	*PLASTIC*	Excavate to +2 m	-
5	*PLASTIC*	Excavate to full depth and activate heave-suppressing slab	-
6	*PLASTIC*	Activate floor slab	-
7	*PLASTIC*	Activate roof slab and mid wall	-
8	*PLASTIC*	Deactivate prop	-
9	*PLASTIC*	Refill soil	-
10	*PLASTIC*	Cut diaphragm wall	-
11	*CONSOLIDATION*	Consolidation over 120 years	43800

6.4 Concrete stiffness

The concrete structure is studied for different flexural rigidities according to the Swedish code BBK 2004, as described earlier in Chapter 2.4.3. For a stiffness corresponding to State I, equation (2.5) is used, whereas for stiffness corresponding to State II, equations (2.7) and (2.8) are used. The two latter equations yield a lower stiffness, which is adopted on the whole structural member, i.e. a simplification is made since the stiffness along a beam is not likely to be the same. In Table 6.2, it is shown which stiffness properties are used in the analyses. In the following chapters, it is closer described when to apply this stiffness.

Table 6.2 Stiffness properties for roof, diaphragm wall and mid wall.

Type	***Diaphragm wall***	***Tunnel roof***	***Mid wall***
State I EA $[kN/m]$	1.54E7	1.54E7	6.4E6
State II EA $[kN/m]$	7.68E6	7.68E6	3.20E6
State I EI $[kNm^2/m]$	1.84E6	1.84E6	1.33E5
State II EI $[kNm^2/m]$	9.22E5	9.22E5	6.67E4

6.5 Floor modelling

In order to achieve full rigidity between the floor slab and the diaphragm wall, as well as to obtain results from the floor slab such as bending moments, shear forces and axial forces in an accessible way, this structural part is modelled with a *PLATE* element. Due to its non-physical thickness, the *PLATE* element must be placed in the middle of the soil layer earlier used for the floor slab in the Verification Model. Thus, in order to keep the distance between the roof and the floor, the *PLATE* element for the roof must be placed at 0.6 m below its origin, see Figure 6.3. Also the thickness of the heave-suppressing slab has to be reduced from 1.0 m to 0.5 m, since otherwise the soil model collapses. This means that the top of the cross walls is moved from –3.2 m to –2.7 m and the bottom of the cross walls is moved from –9.7 m to –9.2 m.

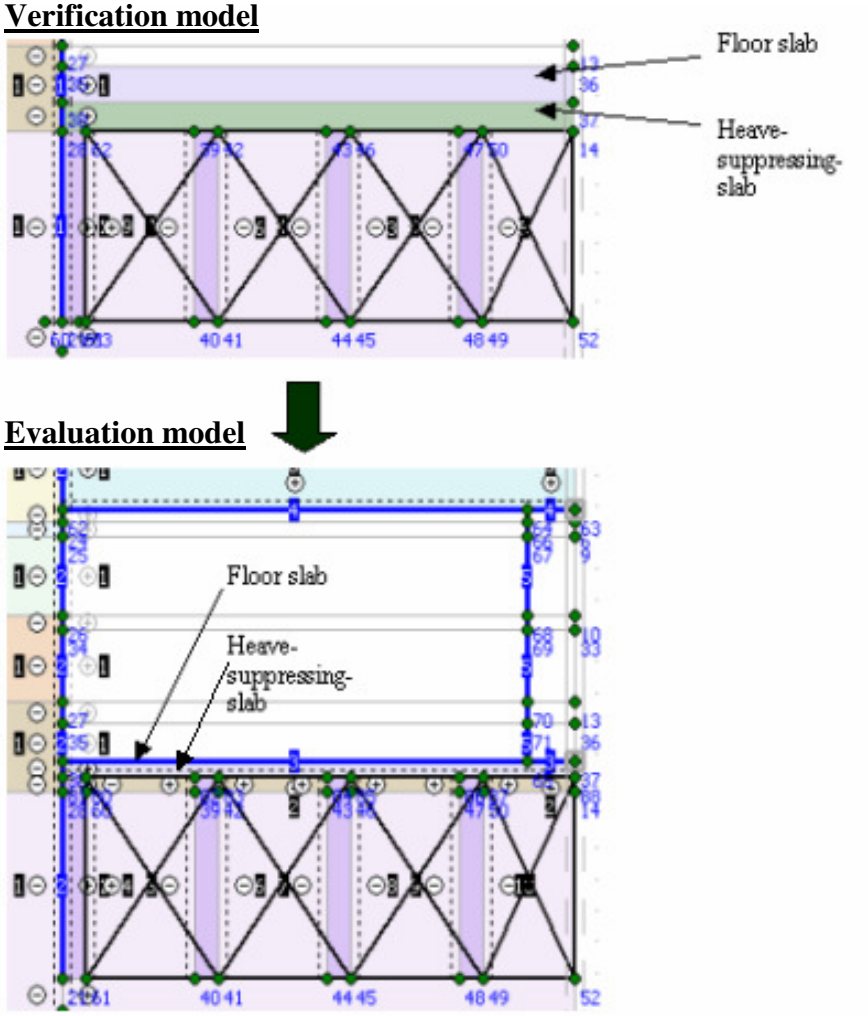

Figure 6.3 Change of floor modelling for Evaluation Model.

Furthermore, the modelling of the heave-suppressing slab must be reconsidered. A change of this into a PLATE element results in an unrealistically small moment distribution in the floor slab. This might be the case in the early phases, but during the consolidation the unreinforced heave-suppressing slab is assumed to be completely cracked so that all moment is attracted to the floor slab. Also, due to the Swedish code BRO 2004 (Chapter 46.15, page 54) it is not acceptable to model the heave-suppressing slab as a concrete slab. Instead, it must be considered as gravel. Due to the non-physical thickness of the PLATE element, the area that surrounds it must be filled up with a material which yields a response close to real behaviour.

Table 6.3 and table 6.4 list soil layers and plates used in the analyses. When only the floor slab is accounted for in the moment of inertia, equation (6.1) is used, whereas when both floor slab and heave-suppressing slab are accounted for, equation (6.2) is used. For the latter moment of inertia, a height of 2.2 m could be used (total height of 1.2 m floor slab and 1.0 m heave-suppressing slab), but then the two slabs are assumed to have full interaction with each other, which is not the case. For a value on the safe side, a moment of inertia according to equation (6.2) is used, which adds the moment of inertia for each member.

$$I_{floor} = \frac{bh^3}{12} = \frac{1 \cdot 1.2^3}{12} = 0.144\, m^4 \tag{6.1}$$

$$I_{floor} + I_{heave\ slab} = 0.144 + \frac{1 \cdot 1^3}{12} = 0.227\, m^4 \tag{6.2}$$

Table 6.3 Names of soil layers with properties.

Properties for soil layers	***Gravel***	***Weightless soil***
Type	Mohr-Coulomb Drained	Mohr-Coulomb Drained
γ $[kN/m^3]$	24	0
k $[m/day]$	0.5	2.9E-5
E_{ref} $[kN/m^3]$	3E4	1.58E4
ν [–]	0.2	0.2
c_{ref} $[kN/m^2]$	0.5	2.37
φ [°]	35	-
ψ [–]	0.5	-
$R_{\text{int}\,er}$ [–]	0.5	0.5

Table 6.4 Names of plate elements with properties.

Properties for plate elements	***Floor***	***Floor and heave-suppressing slab***
Type	Elastic	Elastic
State I: EA $[kN/m]$	1.54E7	2.82E7
State II: EA $[kN/m]$	7.7E6	1.41E7
State I: EI $[kNm^2/m]$	1.84E6	2.91E6
State II: EI $[kNm^2/m]$	9.2E5	1.455E6
w $[kN/m/m]$	24	48
ν $[-]$	0.2	0.2

In the construction phases, a *PLATE* element represents both the floor slab and the heave-suppressing slab with a combined stiffness as well as weight. For the consolidation phase of 120 years, both the weight and the stiffness of the *PLATE* element solely correspond to the floor slab. The area beneath the *PLATE* element, see Figure 6.4, is modelled as weightless soil, which in the consolidation phase is exchanged for gravel with weight, which then represents the totally cracked heave-suppressing slab.

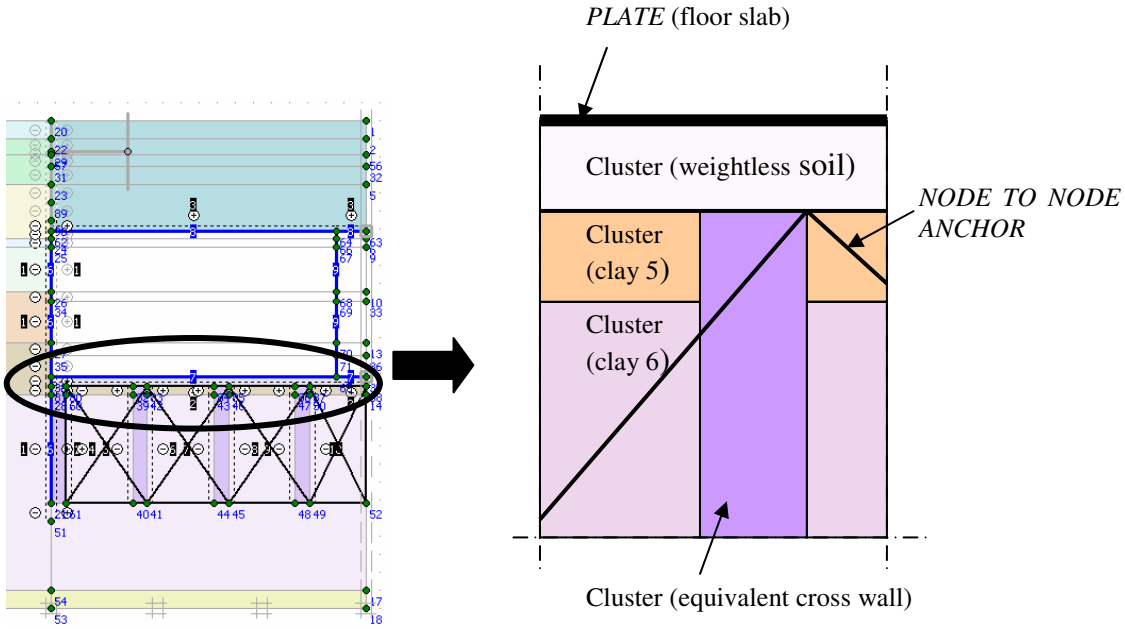

Figure 6.4 Floor modelling.

6.6 PLAXIS View of Evaluation Model

The Evaluation Model includes a diaphragm wall (*PLATE*) a cross wall (clusters and *NODE TO NODE ANCHORs*), a mid wall (*PLATE*), a heave-suppressing slab (cluster) and a floor slab (*PLATE*). The Evaluation Model to be used for further analyses can be seen in Figure 6.5.

After the tunnel construction is finished, the diaphragm wall is cut off to the same level as the tunnel roof.

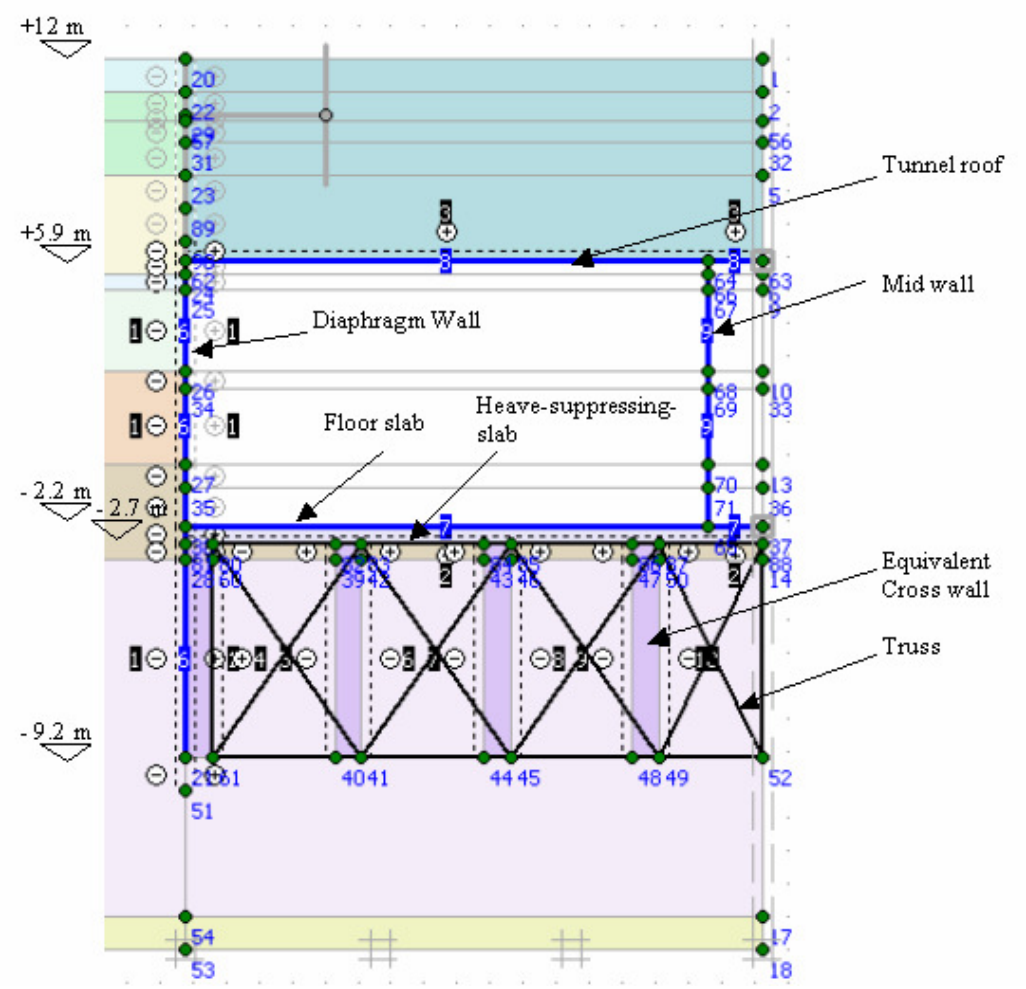

Figure 6.5 Evaluation Model.

6.7 Sensitivity analysis of soil parameters

In order to find out how different values of the soil parameters influence the results, the friction value, R_{inter}, is varied from 0.2 to 0.8, the angle of friction, ϕ', between $30°$ and $35°$, and Poisson's ratio, ν, between 0.1 and 0.2. When analysing what influence each parameter has, only the parameter of interest is changed while the remaining parameters keep their original values. The model used for the sensitivity analysis is Not comparable with the Evaluation Model. Therefore these results can only be compared within the sensitivity analysis.

6.7.1 Friction value

Since the friction value, R_{inter}, equal to 0.4 is used as original input, it is of interest to analyze friction values close to this. Results from analyses with varying friction values, R_{inter}, can be seen in Appendix G. Analyses for friction values of 0.2 and 0.3 are run, but cannot be fully performed. The lowest friction value where the analysis can be completed in combination with $\phi' = 35°$, is $R_{inter} = 0.35$.

6.7.2 Angle of friction

When performing analyses with $\phi' = 30°$ and $\phi' = 35°$, comparisons are made for the moment and the displacements of the diaphragm wall. The results differ only for the vertical displacements, where a constant difference of 20 mm is observed for both $t = 0$ as well as for $t = 120$ *years* for the whole length of the diaphragm wall.

6.7.3 Poisson's ratio

When performing analyses with $\nu = 0.1$ and $\nu = 0.2$ there is no difference in the results for either $t = 0$ or $t = 120$ *years*. Comparisons are made for the moment and the displacements of the diaphragm wall.

6.8 Sensitivity analysis of concrete parameters

To find the most dangerous load case for the diaphragm wall, combinations of tunnel elements belonging to either State I or State II (according to BBK), are used. For the analyses where the whole structure belongs to either State I or State II, the elements are assigned their respective properties in the first PLAXIS phase, and are kept constant throughout the whole analyses; see Table 6.2 and Table 6.4 for input. Also, since it is established through simple analyses that the whole element belongs to one state, only whole elements are varied and not small parts within the element.

The idea is to analyse five different combinations, but since the analyses for the combination of most interest, combination II, cannot be completed in the Calculation program in PLAXIS, this idea is discarded. For a description of the intended combinations, see Table 6.5.

Table 6.5 Stiffness combination of tunnel elements.

Name	***Diaphragm wall***	***Floor slab***	***Wall***	***Roof***	***Analysis completed for t = 120 years?***
I	State II	State I	State I	State I	Yes
II	State I	State II	State II	State II	No
III	State I	State II	State I	State II	No
IV	State II	State I	State II	State II	Yes
V	State I	State II	State I	State I	No

After reconsideration, a choice is made of analysing the two extreme cases, where the whole concrete structure belongs to either State I or State II throughout the analyses. Further on, a third combination is considered, which is intended to simulate the true behaviour. The combinations used are seen in Table 6.6, and are described in the following sub-chapters.

Table 6.6 Stiffness combination of tunnel elements.

Combination name	***Diaphragm wall***	***Floor***	***Tunnel wall***	***Roof***
Tunnel I	State I	State I	State I	State I
Tunnel II	State II	State II	State II	State II
Tunnel III	Change of element stiffness according to M_{cr} (See Table 6.10)			

By a simple hand calculation using the pore pressure underneath the floor slab as an uplifting force and assuming the floor slab as rigidly connected at both sides, it is estimated what magnitude of moment the floor slab should have in the PLAXIS model to be close to reality. Also, the moment in the diaphragm wall is investigated in a similar way. The calculations and the comparisons can be seen in Appendix F.

6.9 Analysis of Evaluation Model; Tunnel I

When assigning stiffness corresponding to State I for all tunnel elements, the excess pore pressures at $t = 0$ are shown in Figure 6.6. Displacements, moment distributions and loads are obtained according to Figure 6.7 – Figure 6.9. See Figure 4.8 for the sign rule for the bending moment.

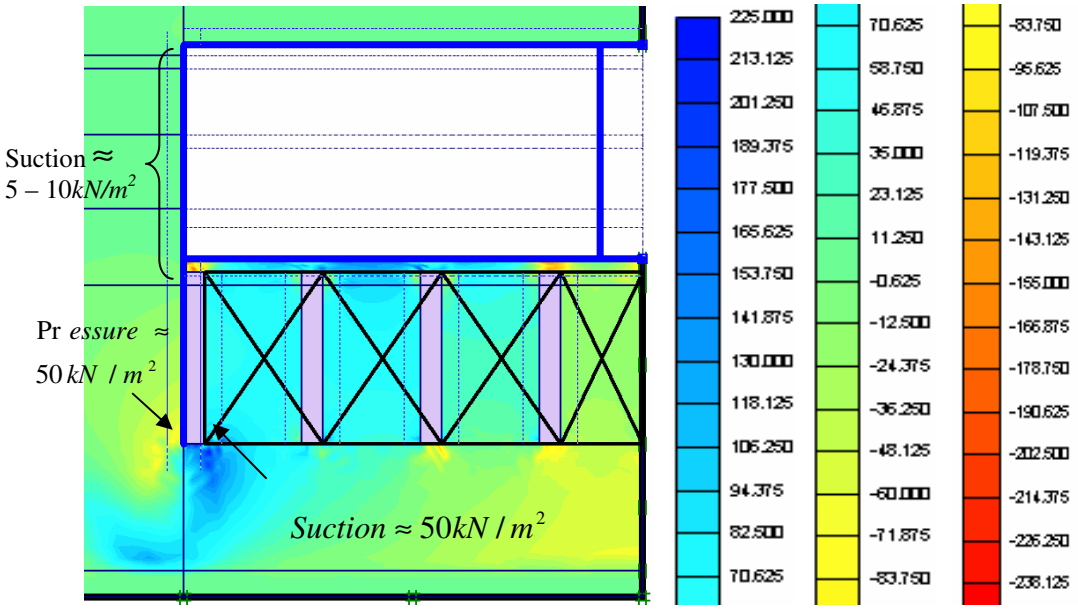

Figure 6.6 Excess pore pressures at t = 0, Tunnel I (negative indicates pressure).

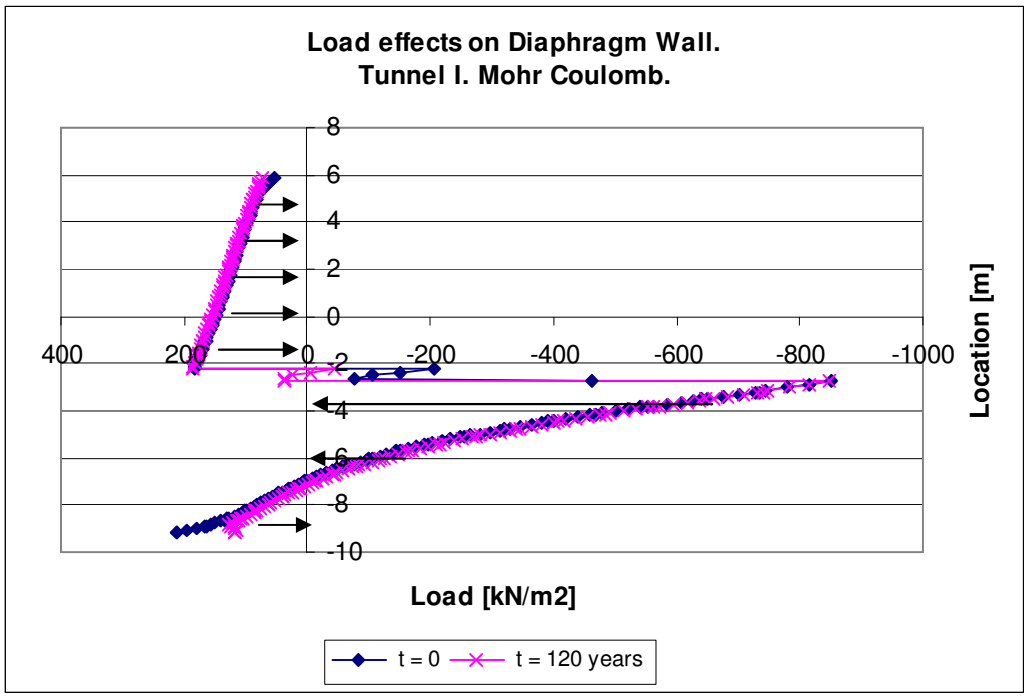

Figure 6.7 Load effects on the diaphragm wall, Tunnel I.

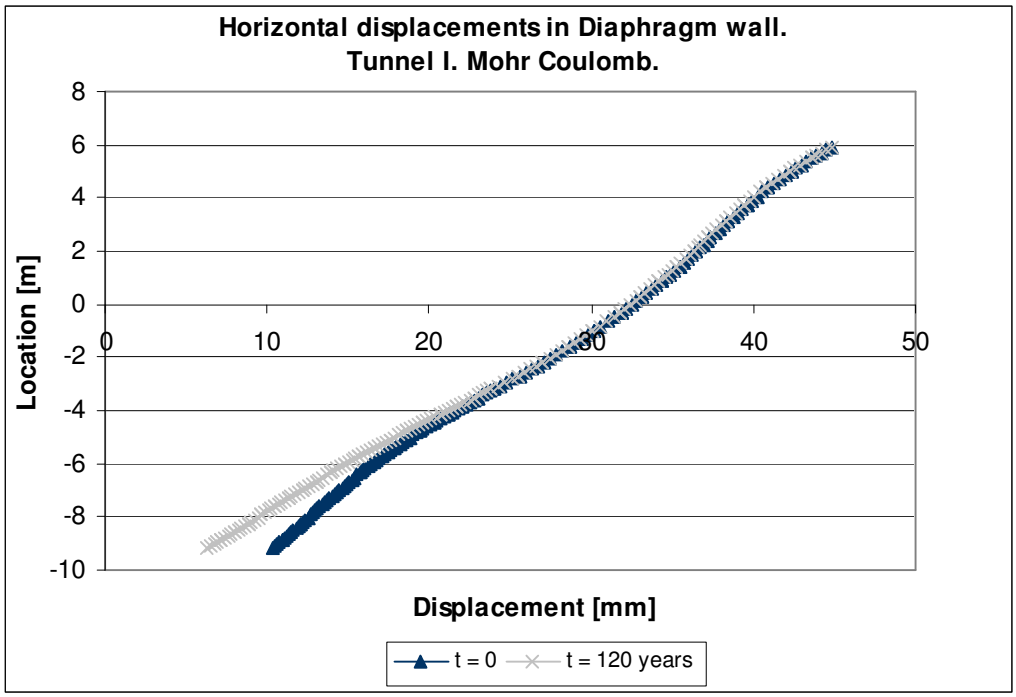

Figure 6.8 Horizontal displacements in the diaphragm wall, Tunnel I.

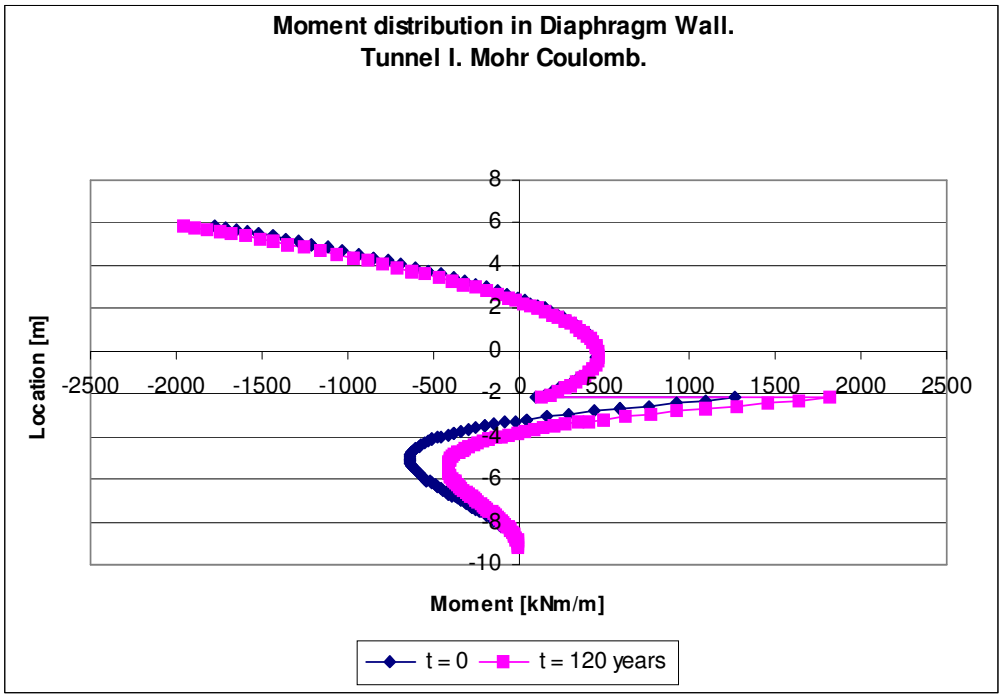

Figure 6.9 Moment distribution in the diaphragm wall, Tunnel I.

When studying the results in Figure 6.6 - Figure 6.9 it can be seen that the differences between $t = 0$ and $t = 120$ *years* are small in the area for the tunnel wall. Excess pore pressures caused by loading contribute to an increase or decrease of the loads after long time. For Tunnel I the excess pore pressures are about 5 to 10 kN/m^2 along the tunnel wall, which corresponds to the load increase of the same magnitude from $t = 0$ to $t = 120$ *years*. Below the level of the floor, at -2.2 m, it is difficult to estimate the exact reactions the excess pore pressures will give rise to after $t = 120$ *years*. But at the bottom of the diaphragm wall, around level –9.2 m on the active side, they create a pressure of about 50 *kN/m*^{2}. On the passive side at the latter level, they create a negative pressure (suction) of about 50 *kN/m*^{2}. With time these pressures even out and since they both work in the active direction at *t = 0*, the load at *t = 120 years* is reduced accordingly. The moment redistribution and the decrease of the horizontal displacement are due to the load change at the bottom of the diaphragm wall.

6.10 Analysis of Evaluation Model; Tunnel II

When assigning stiffness corresponding to State II for all tunnel elements, the excess pore pressures at *t = 0* are shown in Figure 6.10. Displacements, moment distributions and loads are obtained according to Figure 6.11 - Figure 6.13. See Figure 4.8 for the sign rule.

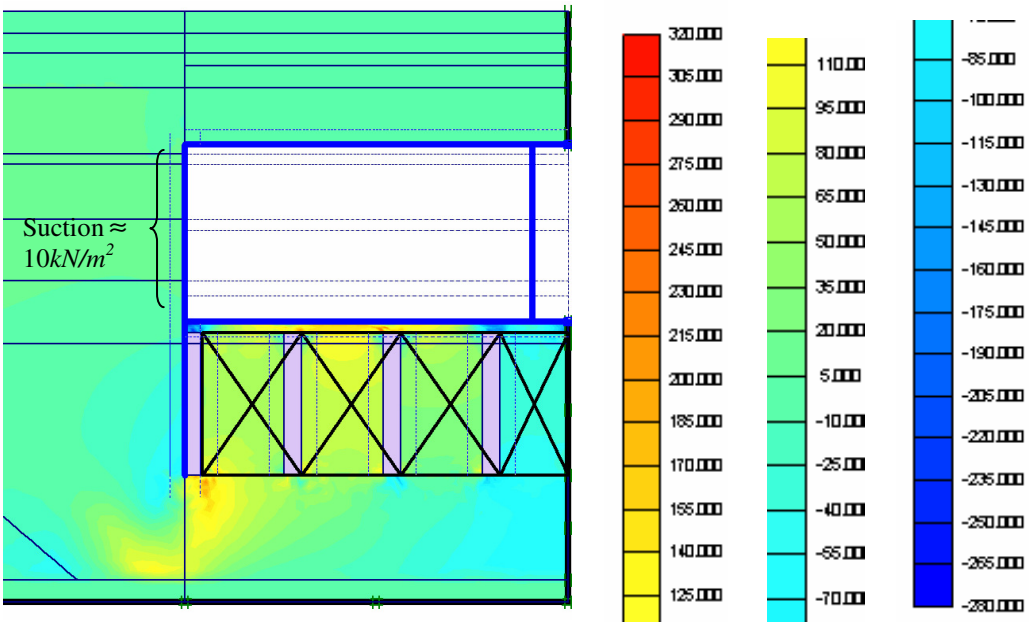

Figure 6.10 Excess pore pressures at t = 0, Tunnel II (negative indicates pressure).

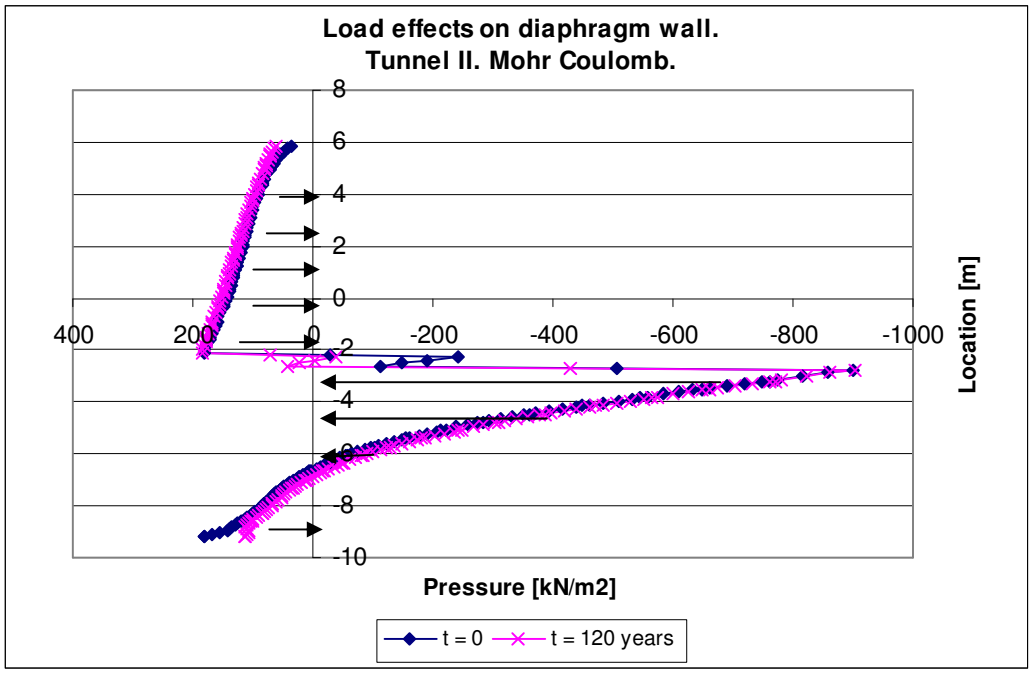

Figure 6.11 Loads acting on the diaphragm wall, Tunnel II.

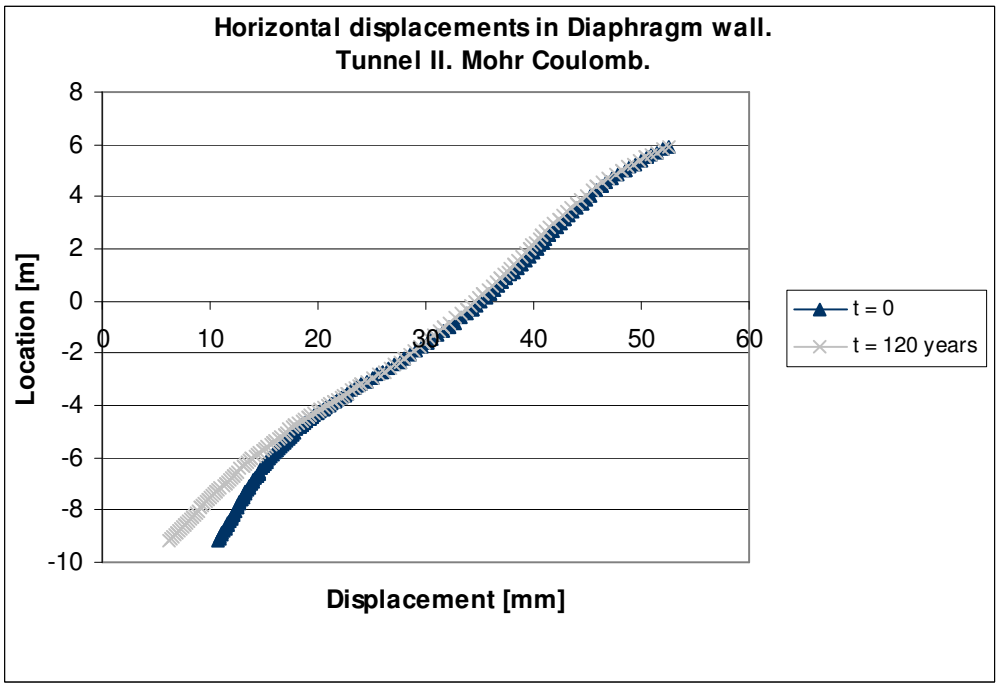

Figure 6.12 Horizontal displacements in the diaphragm wall, Tunnel II.

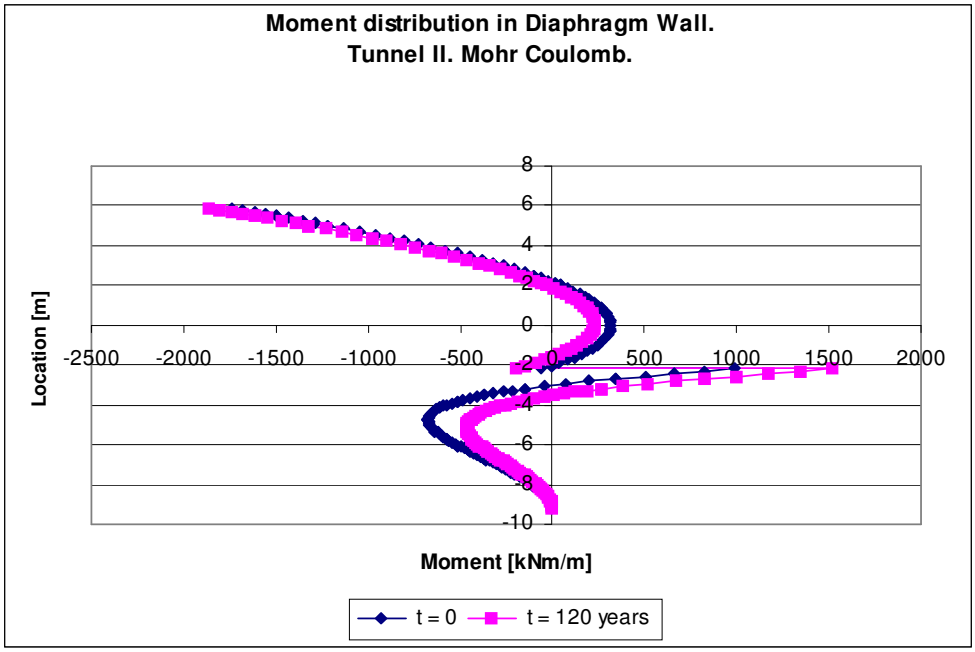

Figure 6.13 Moment distribution in the diaphragm wall, Tunnel II.

When observing these figures, a similar response as for Tunnel I is recognised. In Figure 6.11 – Figure 6.13 the resulting displacements and loads are approximately the same for $t = 0$ and $t = 120$ *years*, with a slightly larger change in the moment distribution compared to Tunnel I. Figure 6.10 shows the excess pore pressures at $t = 0$ and it can be seen that there is negative pressure (suction) with a mean magnitude of about 10 *k*N/m^2, along the tunnel wall, which corresponds to the load increase of the same magnitude. The suction along the tunnel wall will cause a load increase in this area (+5.9 m to –2.2 m), ranging from 5 *kN/m*^{2} to 25 *kN/m*^{2} at *t = 120 years*, as can be seen in Figure 6.11. Below the level of the floor, at -2.2 m, it is difficult to estimate the exact reactions the excess pore pressures will give rise to.

6.11 Comparison; Tunnel I and Tunnel II

A comparison is made between results from Tunnel I and Tunnel II and it can be seen in Figure 6.14 that the load differences between them are small. Due to the stiffer concrete in Tunnel I compared to the concrete stiffness in Tunnel II, the latter analysis allows for larger displacements of the diaphragm wall in the area of the excavated shaft as can be seen in Figure 6.15. Consequently, the bending moment in Tunnel I reaches a higher magnitude in this area, compared to the moment in Tunnel II, see Figure 6.16.

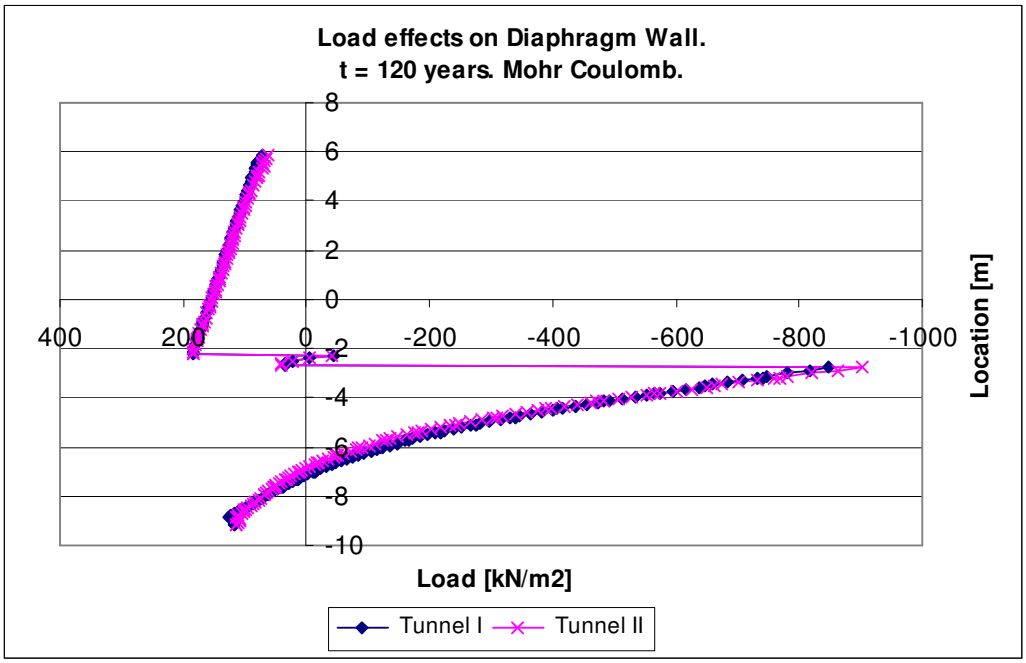

Figure 6.14 Comparison of load distribution on the diaphragm wall.

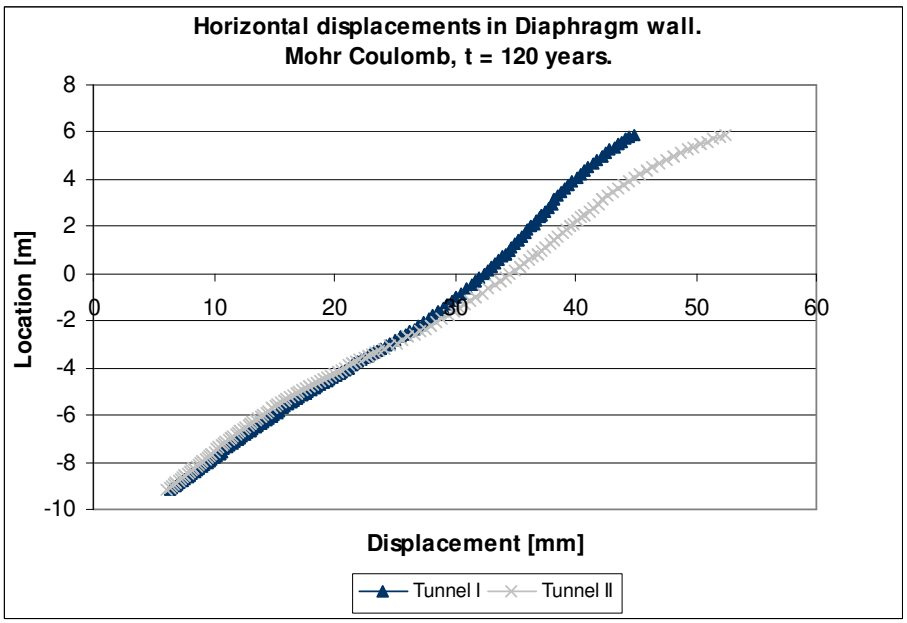

Figure 6.15 Comparison of horizontal displacements of the diaphragm wall.

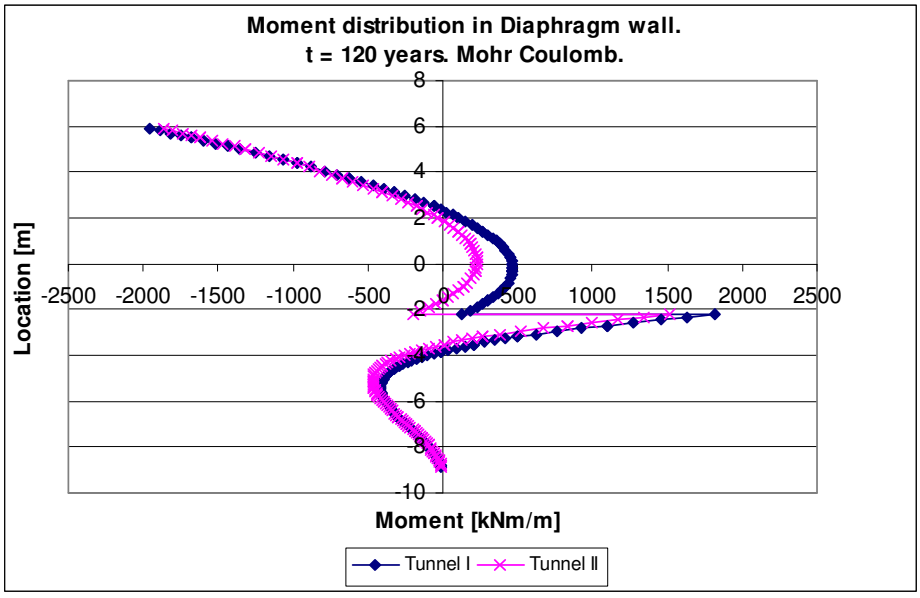

Figure 6.16 Comparison of moment distribution in the diaphragm wall.

6.12 Analysis of Evaluation Model; Tunnel III

For a behaviour of the diaphragm wall as close to reality as possible, analyses with focus on the critical moment, M_{cr}, are performed. The procedure is to analyse all tunnel elements separately for each PLAXIS' phase and to investigate whether the moment in any point of the structural element exceeds the cracking moment, M_{cr}, or not. Since it is already concluded that the bending moments in every point of each element exceeds the cracking moment at the same time, as discussed earlier in Chapter 4.3 the whole element is given a stiffness corresponding to State II, see Table 6.7 The excess pore pressures at $t = 0$ are shown in Figure 6.18. Obtained displacements, loads and moment distributions are shown in Figure 6.19 – Figure 6.21. See Figure 4.8 for the sign rule.

Since it is difficult to perform a complete analysis in a similar way for Tunnel III with the phases adopted for analyses with State I and State II, some small modifications are done in order for the model to work. Compare Table 6.1 with Figure 6.17, where it can be seen that phase 2,4 and 9 are changed from *PLASTIC* to *CONSOLIDATION*. Further on, in the last phase the earlier used *CONSOLIDATION* phase is traded for *MINIMUM PORE PRESSURE.* By doing this, the analysis can be fully performed and results from the last phase can be obtained. When using *MINIMUM PORE PRESSURE* the calculations continue until the chosen condition of excess pore pressures equal to $1\ kN/m^2$ is reached. In Figure 6.17 it is seen that full consolidation is achieved after approximately three years.

Initial phase	0	0	N/A	N/A	0,00 day	0
Activate diaphragm wall	1	0	Plastic	Staged construction	0,00 day	1
Excavate to +9,5	2	1	Consolidation	Staged Construction	60,00 day	2
Activate prop	3	2	Plastic	Staged construction	0,00 day	2
Excavate to +2m	4	3	Consolidation	Staged Construction	14,00 day	4
Excavate to full depth and add cookie	5	4	Plastic	Staged construction	14,00 day	5
Activate floor plate	6	5	Plastic	Staged construction	14,00 day	6
Add roof and mid wall	7	6	Plastic	Staged construction	14,00 day	7
Deactivate prop	8	7	Plastic	Staged construction	14,00 day	8
Refill soil	9	8	Consolidation	Staged Construction	14,00 day	9
Cut DW t=0	10	9	Plastic	Staged construction	0,00 day	10
<Phase 11>	11	10	Consolidation	Minimum pore pressure	1088,50 day	10

Figure 6.17 Phases adopted for Tunnel III. [7]

Table 6.7 Element stiffness combination for Tunnel III.

Phase	***Diaphragm wall***	***Floor***	***Tunnel wall***	***Roof***
Activate DW and CW	State I	-	-	-
Excavate to +9.5 m	State I	-	-	-
Activate prop	State I	-	-	-
Excavate to +2 m	State II	-	-	-
Excavate full, add heave suppress. slab	State II	-	-	-
Activate floor plate	State II	State I	-	-
Activate roof and mid wall	State II	State II	State I	State I
Deactivate prop	State II	State II	State I	State II
Refill soil	State II	State II	State I	State II
Cut diaphragm wall, $t = 0$	State II	State II	State I	State II
Consolidation, $t = 120$ *years*	State II	State II	State I	State II

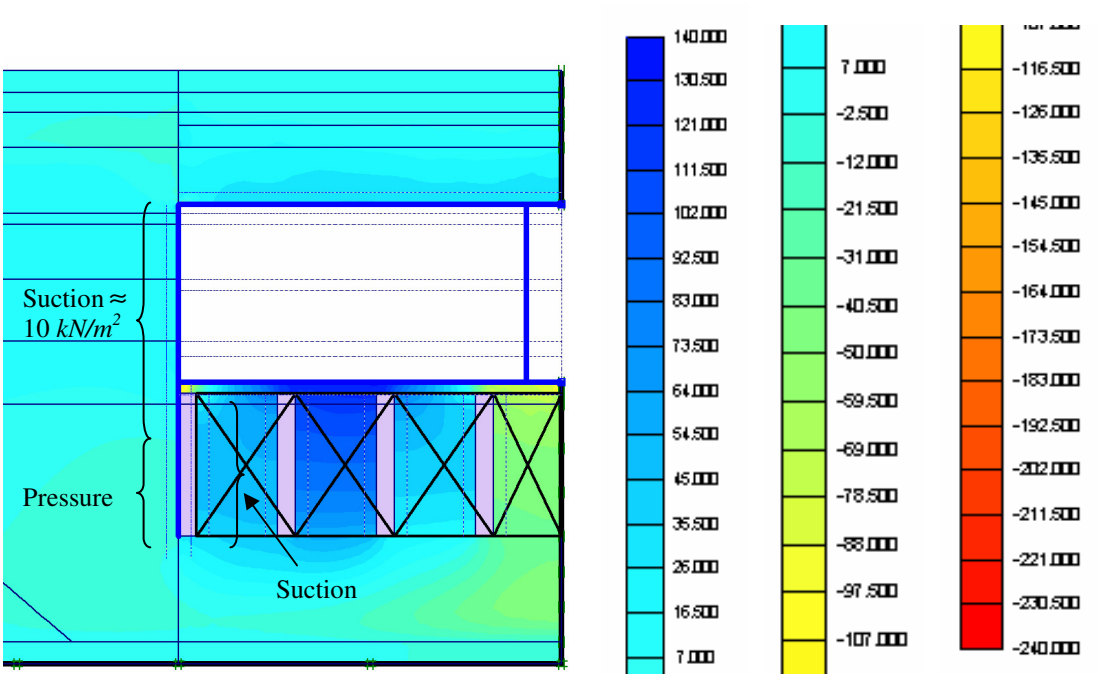

Figure 6.18 Excessive pore pressures at t = 0, Tunnel III at t = 0 (negative indicates pressure).

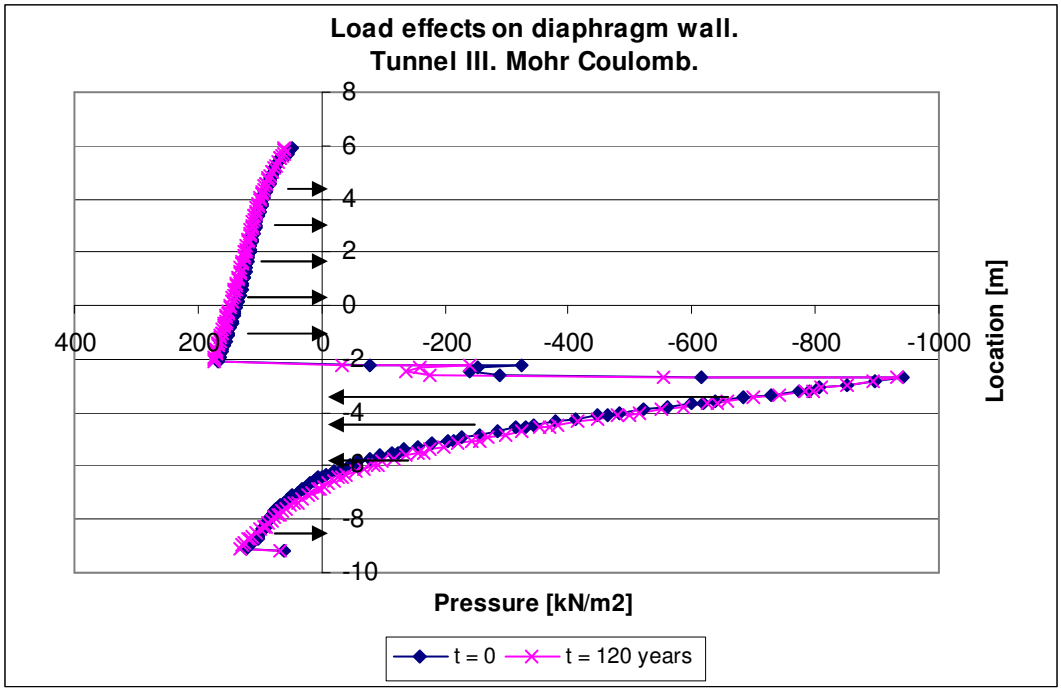

Figure 6.19 Load effects on the diaphragm wall, Tunnel III.

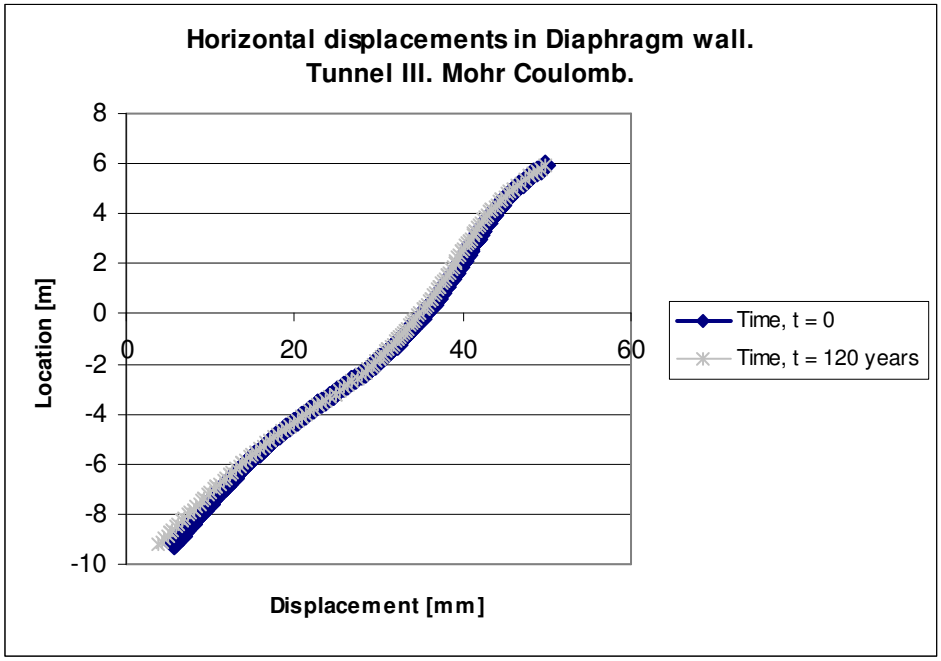

Figure 6.20 Horizontal displacements in the diaphragm wall, Tunnel III.

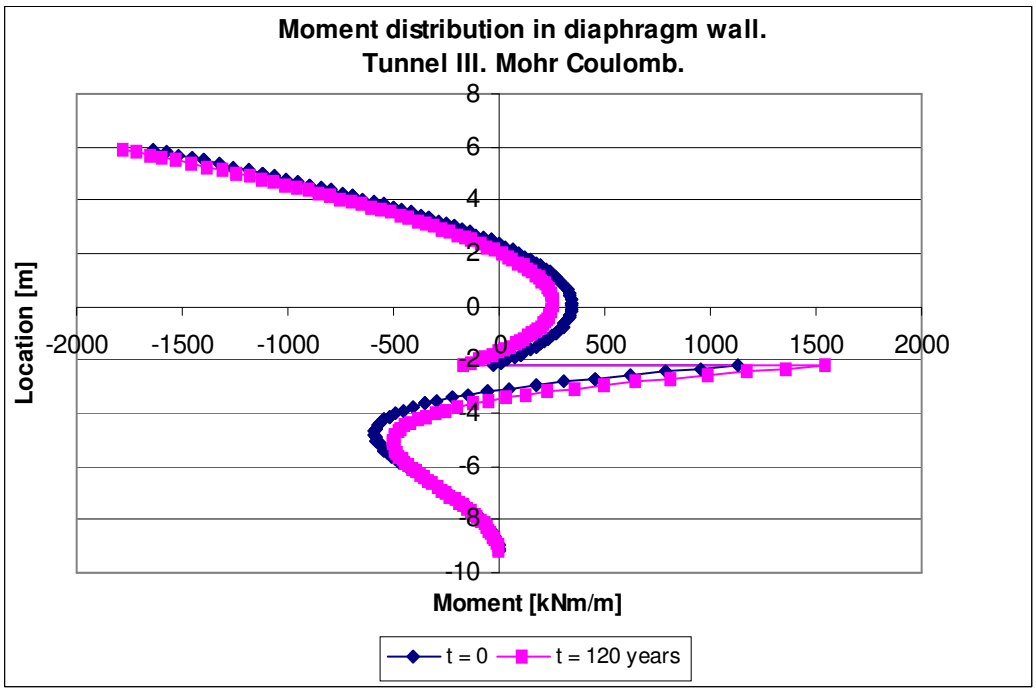

Figure 6 .21 Moment distribution in the diaphragm wall, Tunnel III.

The negative excess pore pressure (suction) along the tunnel wall causes a small load increment after *120 years,* whereas below the level of the floor the suction on the passive side work in the same direction as the excess water pressure on the active side, thus reducing the active earth pressure after *120 years,* see Figures 6.18 and 6.19.

When studying the results for Tunnel III, as for the two earlier analyses of Tunnel I and Tunnel II, also here the differences between $t = 0$ and $t = 120$ *years*, are small. The excess pore pressures, shown in Figure 6.18, are small with a magnitude of about 10 kN/m^2 along the tunnel wall, which agrees with the load increment of about 5 - 7 % (about 8 kN/m^2) over time when observing Figure 6.19.

6.13 Cross Wall influence on Results

All loads, previously presented in this thesis, are obtained by the derivative of the shear force in the diaphragm wall, and are comparable to pressures in vertical sections right next to the diaphragm wall. On the active side the comparable section runs through actual soil, whereas on the passive side the section runs through the equivalent cross wall, see the continuous line in Figure 6.22.

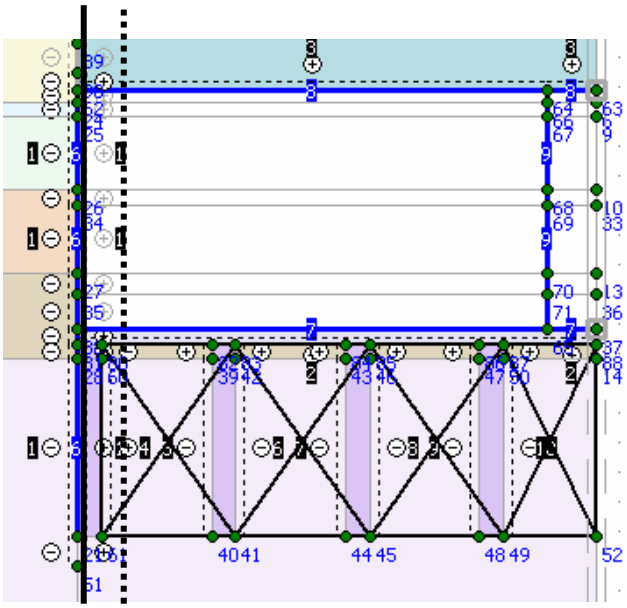

Figure 6.22 Soil sections in Evaluation Model. Continuous line corresponds to section through cross wall whereas dotted line corresponds to section through soil.

If instead choosing to analyze a section drawn vertically outside the cross wall, in the soil (dotted line), the obtained loads acting on the diaphragm wall are seen in Figure 6.23. The figure shows that there is a significant difference between the two soil sections on the passive side, which can be explained by the truss in the cross wall; when analyzing one section in PLAXIS that intersects with a *NODE TO NODE ANCHOR*, the forces through this element are not included in the Output program for

earth pressures, and have to be investigated individually. Thus, if choosing to model the cross walls the way it is proposed in this thesis, it is important to keep this in mind when attempting to achieve the desired earth pressures acting on the diaphragm wall.

Resulting earth pressures from the two earth sections as marked in Figure 6.22, are seen in Figure 6.23 and Figure 6.24, where earth pressures from Tunnel III at $t = 120$ *years* are presented. The pressures obtained from the section through the cross wall, correspond to pressures in the sections where the cross walls are located in the Göta Tunnel, whereas the pressures obtained from the section outside the cross wall roughly corresponds to the sections in between the cross walls in the Göta Tunnel.

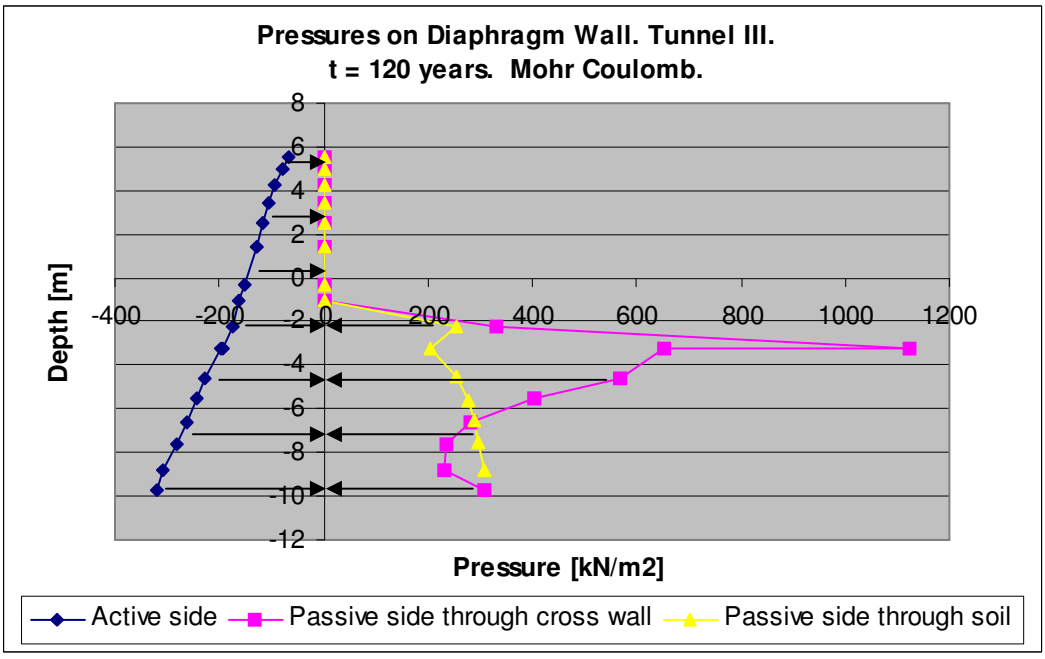

Figure 6.23 Pressures on the diaphragm wall, Tunnel III. "Passive side through cross wall" corresponds to the continuous line and "Passive side through soil" corresponds to the dotted line in Figure 6.22.

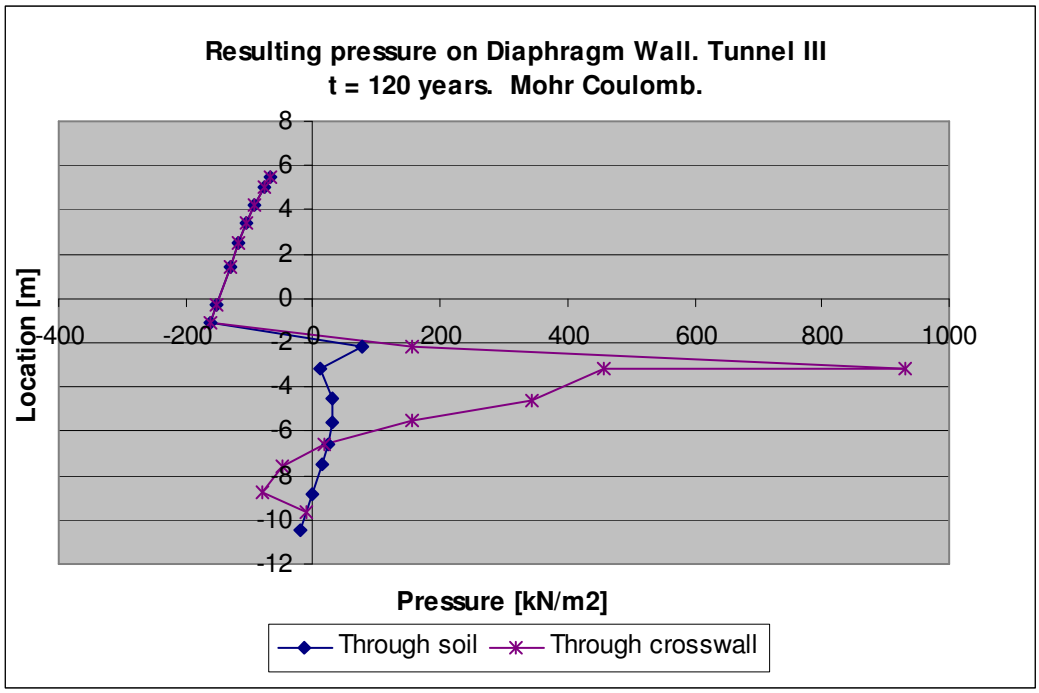

Figure 6.24 Resulting pressure (acive minus passive, and pressure directions according to Figure 6.23) on the diaphragm wall, Tunnel III.

6.14 Tunnel wall reactions; Tunnel I, Tunnel II, Tunnel III

When only observing the part of the diaphragm wall that acts as tunnel wall in the structure, i.e between +5.9 m (roof location) and –2.2 m (floor slab location), comparisons between results obtained from PLAXIS and hand calculations are made. The hand calculations include the design load for underground structures, the earth pressure "at rest", according to BRO 2004, as well active undrained/drained earth pressures, (see Appendix C). Figure 6.25 shows resulting earth pressures as total pressures. [23], [11]

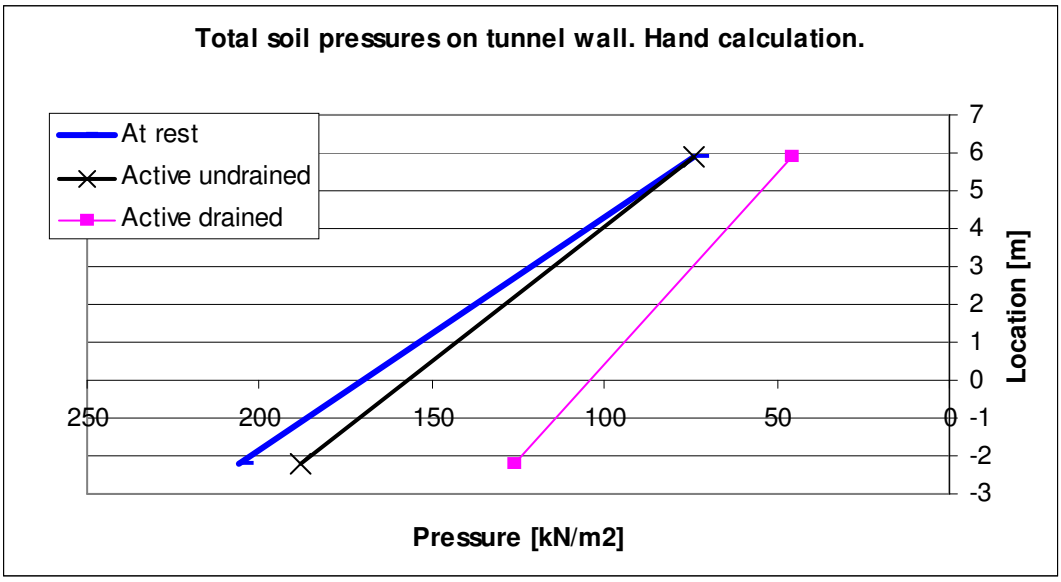

Figure 6.25 Total resulting loads on tunnel wall, hand calculation.

When including loads achieved from PLAXIS for $t = 0$ and $t = 120$ *years* for Tunnel I, Tunnel II and Tunnel III, it can be seen in Figure 6.26 and Figure 6.27 that Tunnel I and Tunnel II yield the largest loads. The horizontal displacements of the tunnel wall are shown in Figures 6.28 and 6.29. Moment distributions in the tunnel wall for all three analyses are shown in Figure 6.30 and Figure 6.31.

When observing the loads achieved from Tunnel III, it can be seen in Figure 6.26 and Figure 6.27 that they do not exceed the earth pressures "at rest" at any point of time. The moment distributions for Tunnel III, see Figure 6.30 and Figure 6.31, show that the field moment at $t = 120$ *years* is about 75 % of the field moment at $t = 0$, whereas the moments at the supports (roof and floor) increase with about 9 %.

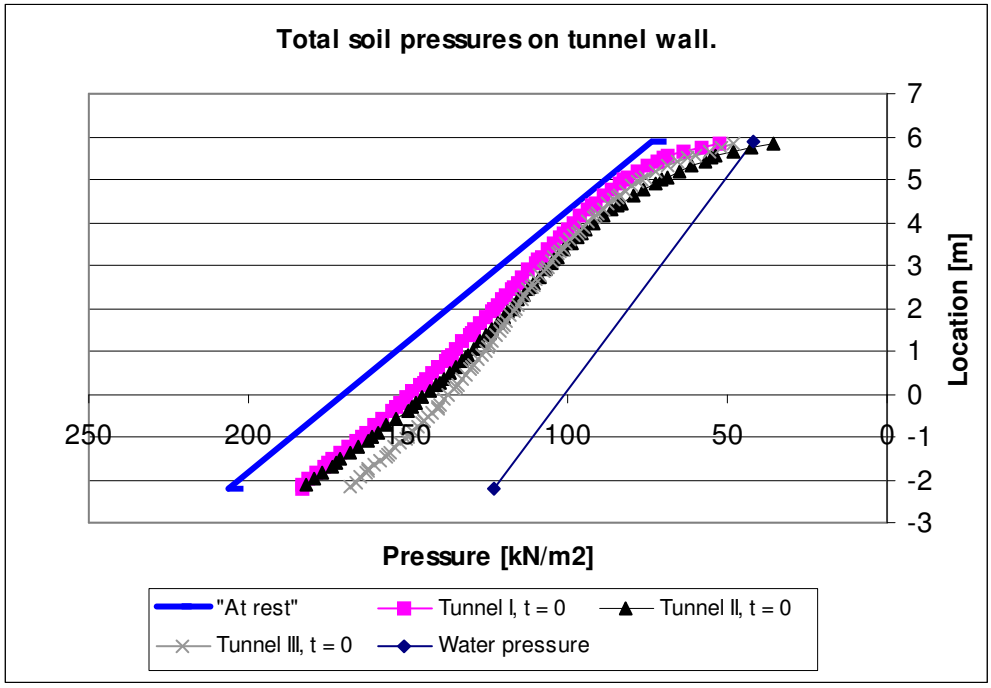

Figure 6.26 Total resulting loads on tunnel wall, PLAXIS $t = 0$ and hand calculation ("at rest" and water pressure).

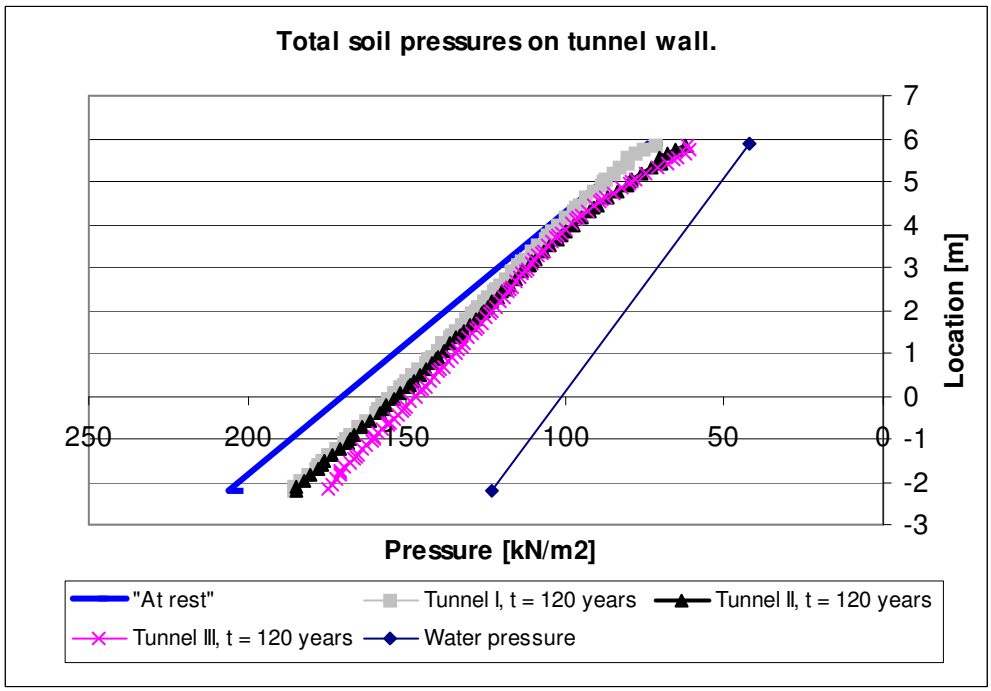

Figure 6.27 Total resulting loads on tunnel wall, PLAXIS for $t = 120$ years and hand calculation ("at rest" and water pressure).

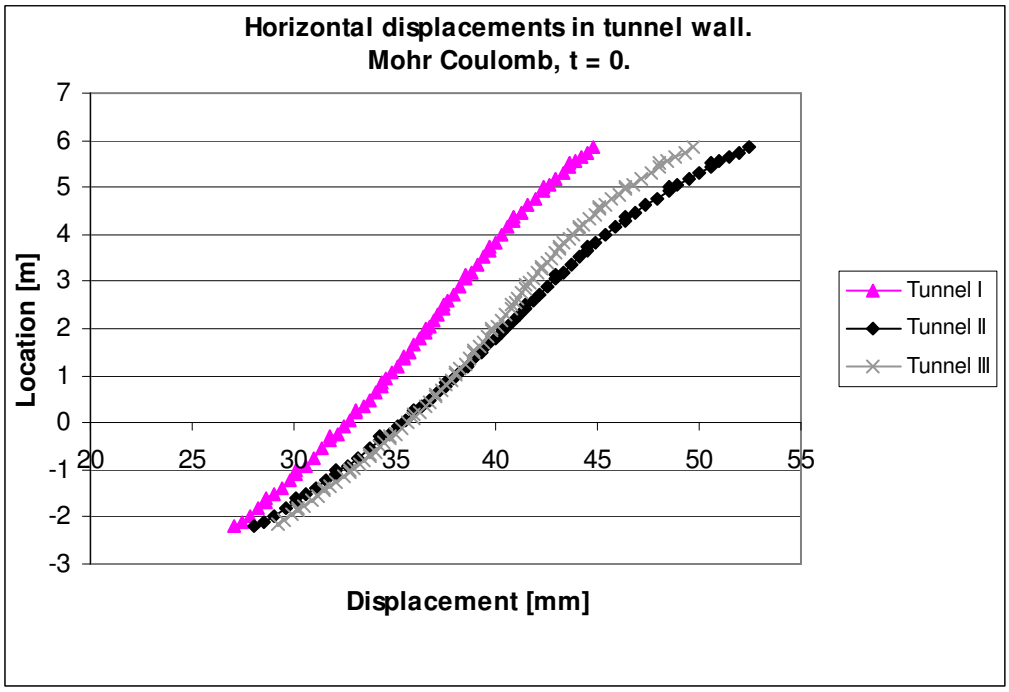

Figure 6 .28 Horizontal displacements in tunnel wall, t = 0.

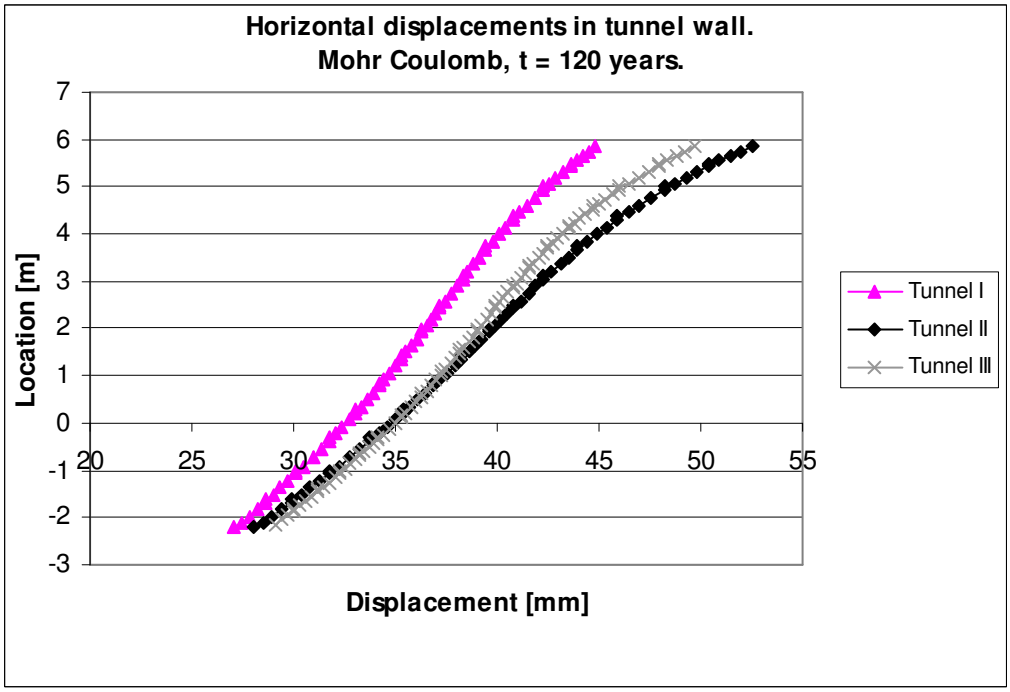

Figure 6 .29 Horizontal displacements in tunnel wall, $t = 120$ years.

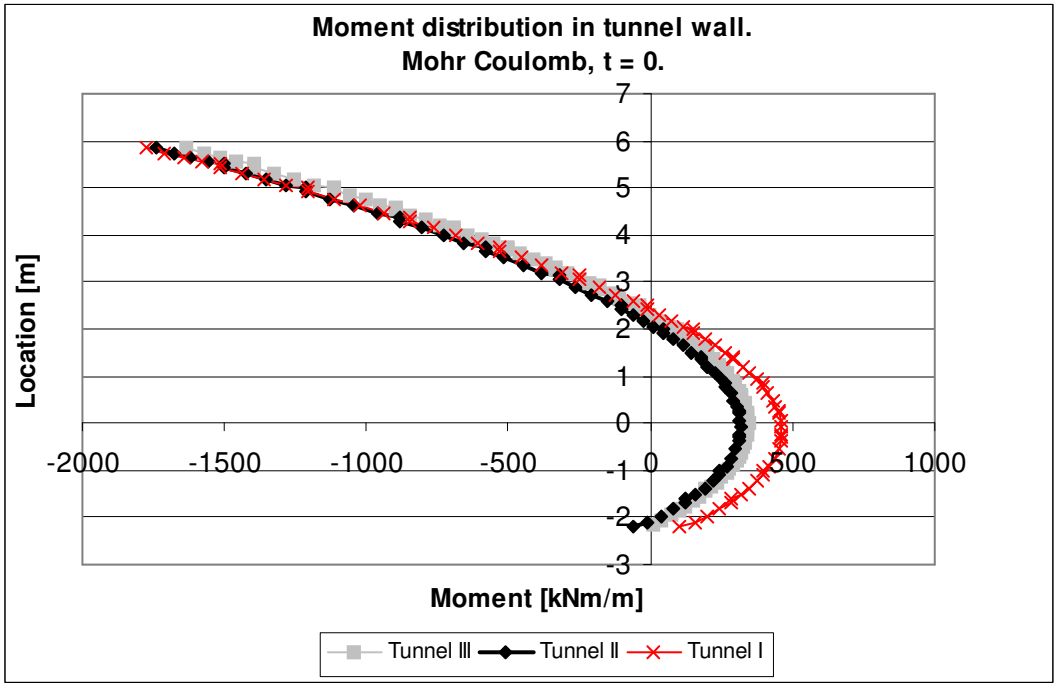

Figure 6 .30 Moment distribution in tunnel wall, $t = 0$.

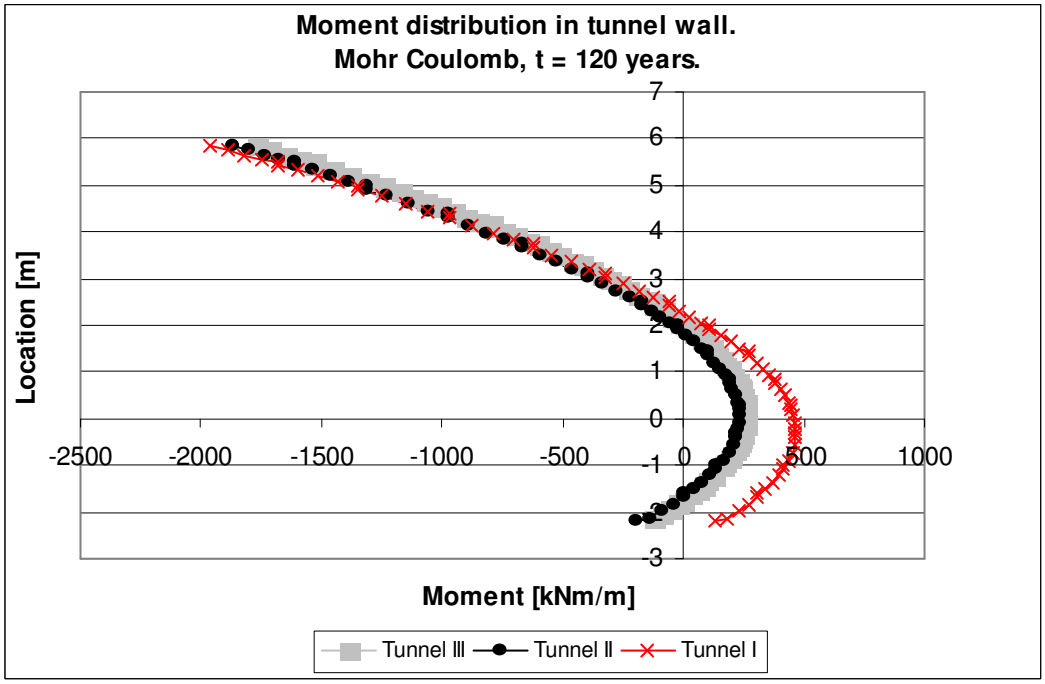

Figure 6 .31 Moment distribution in tunnel wall, $t = 120$ years.

In Figure 6.26 and Figure 6.27 it can be seen that all three analyses yield a load increment with time. In the upper part of the tunnel wall, the load for Tunnel I coincides with the soil pressure "at rest", while the loads obtained for Tunnel II and Tunnel III do not exceed the soil pressure "at rest" at any time. Figure 6.28 and Figure 6.29 show that the stiffer structure of Tunnel I yields a smaller horizontal

displacement than for Tunnel II and III. The smaller displacement yields a bending moment in field which is about 33 % larger at $t = 0$ and about 80% larger at $t = 120$ *years* than for Tunnel II and III. Moreover, the field moments in Tunnel II and III decrease with time, while the field moment in Tunnel I slightly increases. At the level of the floor (-2.2 m), the support moment for Tunnel III actually changes sign. At the same level the support moments for both Tunnel I and II increase, although in different directions, see Figure 6.30 and Figure 6.31 as well as Table 6.8.

Table 6.8 Moment magnitudes in three locations at $t = 0$ *and* $t = 120$ *years*.

Max moment in tunnel wall PLAXIS [*kNm / m*]		$t = 0$	$t = 120$ *years*
Tunnel I:	+5.9 m	-1776	-1958
	field	+460	+465
	-2.2 m	+104	+132
Tunnel II:	+5.9 m	-1738	-1868
	field	+316	+229
	-2.2 m	-61	-201
Tunnel III:	+5.9 m	-1634	-1774
	field	+344	+256
	-2.2 m	+8	-129

It should be noted that the concrete was modelled as an elastic material, thus allowing for unlimited stress magnitudes in the concrete members. During the time for the project the size of these stresses should have been investigated and compared with the capacity of the concrete which was used, but unfortunately this was not done

6.14.1 Lateral earth coefficient "at rest",K_0

The lateral earth coefficient "ar rest", K_0, after 120 years for analyses with the Mohr-Coulomb theory is shown in Figure 6.32. This coefficient is obtained by dividing the effective horizontal earth pressure with the effective vertical earth pressure, as described earlier by equation 3.10. The vertical earth pressure should be the same for all three analyses of the Evaluation Model. Since the horizontal load obtained for Tunnel I is larger than for Tunnel II and Tunnel III, this explains why K_0 for Tunnel I is slightly larger. The loads in the lower part of the tunnel wall differ between Tunnel II and Tunnel III, thereby explaining the differences in K_0. The redistribution of load

resistance in Tunnel III during the ongoing analysis could possibly explain some differences in the K_0 distribution when comparing to the other two analyses.

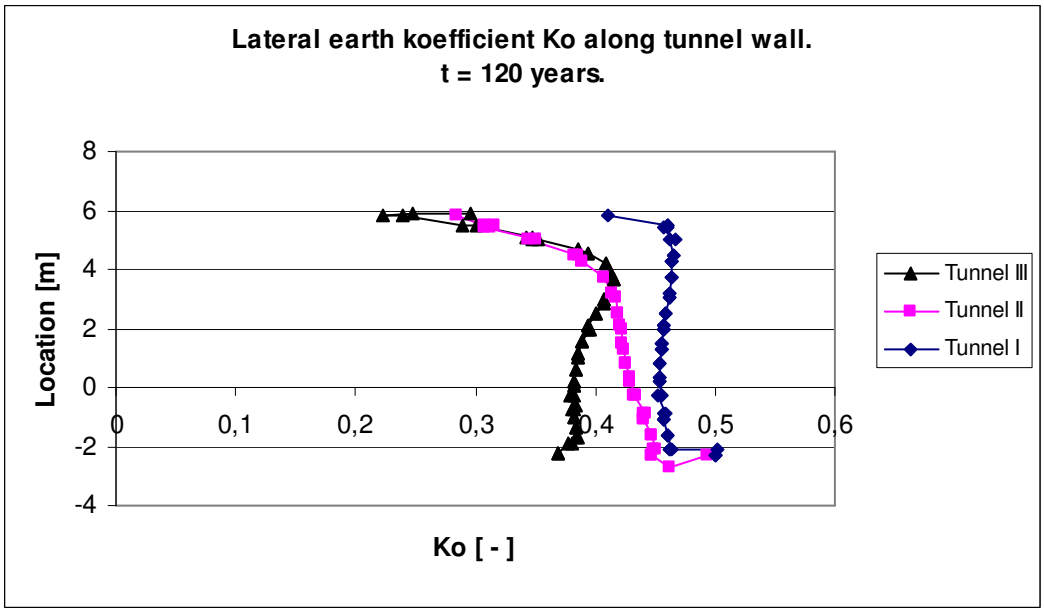

Figure 6.32 Lateral earth coefficient, K_0, along tunnel wall at $t = 120$ years.

6.15 Comparison; Mohr Coulomb and elastic analyses

In this chapter results from Mohr Coulomb analyses are compared with results from elastic analyses. Figure 6.33 – Figure 6.35 show the resulting loads on the tunnel wall.

If disregarding the upper part of the tunnel wall where the largest displacements occur, Figure 6.33 - Figure 6.35 show that the elastic analyses yield approximately the same loads as the Mohr Coulomb analyses. In the major part of the tunnel wall the difference between the results varies between 2% and 4%. However, in the upper part of the wall the results differ with about 9% for Tunnel I, 13% for Tunnel II, while for Tunnel III the elastic load is 24% larger than the load obtained with Mohr Coulomb. For Tunnel I and II the Mohr Coulomb analysis yields the largest load in this area after *120 years*, whereas for Tunnel III the elastic load is the largest. At the top of the tunnel wall the soil pressure "at rest" is equal to 74 kN/m^2, which is only exceeded by the results obtained from the elastic analysis of Tunnel III, although the load from Tunnel I reaches the same magnitude as the design load at the surroundings of level +5 m.

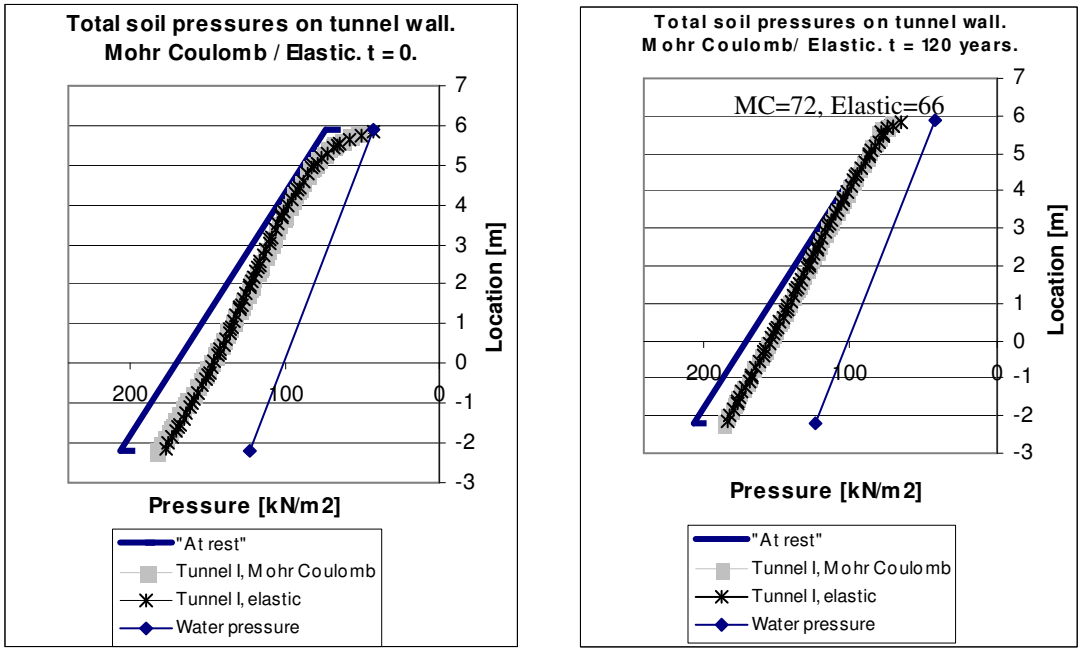

Figure 6.33 Comparison Mohr Coulomb and elastic analysis, Tunnel I. The magnitudes 72 and 66 refer to the pressure at the top of the tunnel wall.

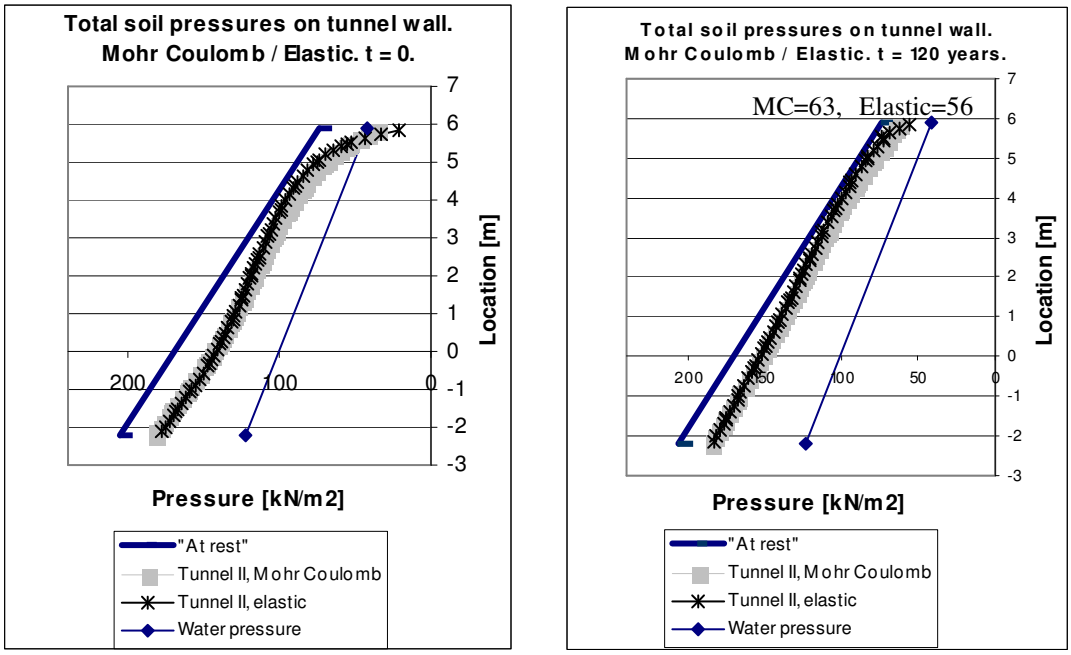

Figure 6.34 Comparison Mohr Coulomb and elastic analysis, Tunnel II. The magnitudes 63 and 56 refer to the pressure at the top of the tunnel wall.

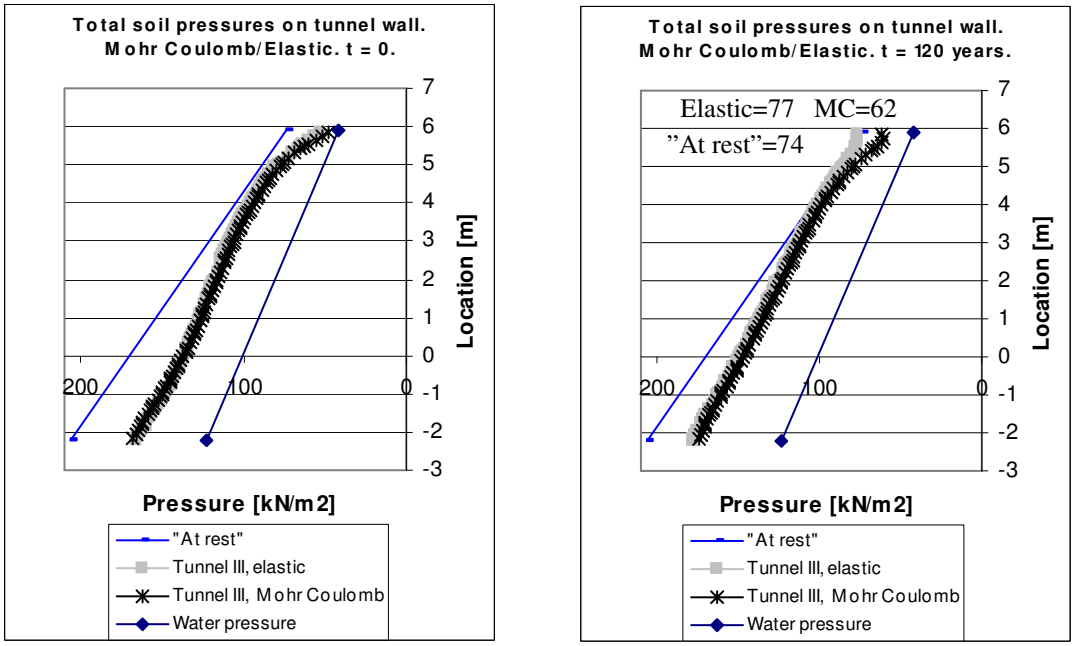

Figure 6.35 Comparison Mohr Coulomb and elastic analysis, Tunnel III. The magnitudes 77 and 62 refer to the pressure at the top of the tunnel wall.

7 Comments and discussion

In this chapter some general difficulties when modelling with PLAXIS is discussed, as well as the particular problem of modelling the, cross walls. Also, a discussion regarding the models and the results from the analyses is held.

PLAXIS issues

There are several difficulties to overcome when modelling with PLAXIS depending on what type of problem to be studied. As discussed earlier in this thesis, the cross walls were particularly difficult to model. The Norwegian model with equivalent cross walls, as proposed by Karlsrud et al [22], was adopted without any closer investigation but should yield acceptable results for the diaphragm wall since both the heave effect and the horizontal movements are accounted for.

Another difficulty is that in PLAXIS sometimes numerical problems will arise if the stiffness difference between, either two adjacent soil clusters, or one soil cluster replacing a previous one, is large. This can probably be overcome by experimenting with *INTERFACE* elements and friction values.

Soil parameters

For this thesis, due to difficulties in achieving complete analyses for low soil stiffness, the influence of varying soil stiffness was not investigated closely. The results though indicate that when choosing parameters for the PLAXIS input, the stiffness of the soil is important to evaluate since it seems to affect the displacements the most. The differences in the results for the remaining properties are small and commonly used values should be sufficient to use. Although the performed analyses with varying soil parameters were based on water conditions different from the analyses of Tunnel I – Tunnel III, the results still provide usable data.

Verification Model

The first analysed model represents the temporary stage, i.e. the open shaft before the tunnel is constructed. When comparing the on site displacements with the ones obtained with PLAXIS, there is a difference in the magnitudes, see Chapter 5.6. To find the exact same material parameters as in reality is difficult, but the disagreements between the displacements could possibly be improved by changes in the soil stiffness. Though, since the results from the analyses showed the same pattern as the on site displacements, it was concluded that the model was acceptable and could be developed into the Evaluation Model.

Evaluation Model

As can be seen in the results for the Evaluation Model, the differences between $t = 0$ and $t = 120$ *years* are very small in all analyses. This is partly due to that most of the swelling occurs in the beginning and is therefore fully developed and taken care of during the excavation phase. Another reason is that the excess pore pressures, caused by excavating and loading, are small. Hence, the additional soil pressures after consolidation are small as well. This is true for all three tunnel analyses using both Mohr Coulomb and elastic theory.

The loads obtained with PLAXIS for all analyses are lower than the design value according to BRO 2004, the soil pressure "at rest", for both $t = 0$ and $t = 120$ *years*, the lowest loads are obtained from the Tunnel III analysis. The aim with Tunnel III was to resemble real behaviour and extra care was taken when applying the concrete stiffness. At level –2.2 m Tunnel III yields a load which is about 85 % of the design load, whereas at level 5.9 m the load is approximately 95 % of the design load. Considering the load differences between the design load and the PLAXIS results, FE-modelling seems to yield refined design criteria provided that the user is well informed and critical to input as well as output. Due to the 33 % larger field bending moment in Tunnel I compared to the other two tunnel analyses, there seems to be reasons to regard the stiffness of the concrete structure in a thorough way. Since space is limited, especially when casting diaphragm walls, and less reinforcement will allow for easier pouring of concrete as well as for the construction work to be more cost as well as labour efficient, the possibility to decrease the required amount of reinforcement should be of interest.

It should be noted that the concrete was modelled as an elastic material throughout all analyses, thus allowing for unlimited stress magnitudes in the concrete members. During the time for the project the size of these stresses should have been investigated and compared with the capacity of the used concrete. Unfortunately this was not done. Large stresses occur for large displacements, especially in stiff structures. The place with the largest displacement in the model is found at the level of the roof and this is thereby the area with the highest risk of developing stresses larger than the capacity.

Mohr Coulomb / Elastic

The load curves from the elastic analyses correspond well to the ones from the Mohr Coulomb analyses, with a difference ranging from 0 to 4%. At the top of the tunnel wall though, a rather large difference can be noted. In this area, despite the support from the roof, the largest horizontal displacements occur and the two different theories yield quite different results, with a difference ranging from 9 to 24%. A comparison of the results from elastic analyses with results from Mohr Coulomb analyses of Tunnel I, Tunnel II and Tunnel III still indicate that, for stiff structures such as diaphragm walls, the elastic approach should be sufficient if combined with extra care in areas with expected large deformations and when designing structural connections.

8 Conclusion

When attempting to simulate the behaviour of soil interacting with concrete, there are several aspects to consider:

- Due to difficulties in finding the exact same material properties for the model as in reality, and also due to the error tolerance for displacements measured on site (the true measured value lies within a certain range), it is difficult to achieve the exact same displacements with the FE-analyses.

- Investigate the modulus of elasticity closely for both soil and concrete. For soil it is important especially if the displacement magnitudes are of interest, and for concrete the stiffness affects the sectional forces, such as distribution and magnitudes of the bending moment. Thus, it is of importance to simulate behaviour as close as possible to reality, in terms of correct concrete stiffness as well as investigations of at what point the structural members, or parts of them, are likely to enter state II.

- If using friction values for the interface surfaces within the range allowed by the Swedish code, the difference in the results is small.

- For stiff structures like diaphragm walls, Mohr Coulomb analyses is to prefer although in case of time shortage or if a Mohr Coulomb model is not available, elastic analysis should be sufficient if combined with extra consideration of connections.

The results from analyzing Tunnel III indicate that careful and accurate modelling of the concrete affects the resulting loads and load effects in a positive manner. Thus, there should be economic interest in considering the concrete stiffness more carefully. However, not having enough knowledge about the used FE software might lead to unrealistic results with undesirable consequences if used, which should also be kept in mind.

9 Future research

This thesis has been written with focus on the soil, and a FE-program developed for soil has been used for modelling of both soil and concrete. It is apparent that PLAXIS does not consider the concrete in a profound way, i.e. there are not enough concrete parameters for input and therefore the concrete behaviour is not correctly described. In order to analyse the concrete more correctly, a FE-program for modelling of the concrete can be used where the soil is modelled as springs. Furthermore, analyses with both a FE-program for soil as well as with a FE-program for concrete allows for a comparison to be able to see the accuracy in the results.

To be able to use PLAXIS for modelling of both soil and concrete, it is desirable that some changes in the software are made. Advisable is to add input for moment/curvature distribution for concrete.

References

Web pages

[1] *Welcome to Diaphragm Wall.com* http://www.diaphragmwall.com 2005-08-30

[10] *Basic mechanics of soils.* http://fbe.uwe.ac.uk/public/geocal/SoilMech/basic/soilbasi.htm 2005-09-19

[30] Hermansson K (2002): *Götaleden – tunnelbygge i centrala Göteborg.* http://www.vv.se/filer/publikationer/KH[Skrivskyddad].pdf . 2005-09-22

[20] *Stadskartan.* http://www.stadskartan.se/start/kartor/index.asp?page=europa 2005-09-22

Publications

[2] Kennedy H (2003): *Deformationer till följd av djup schakt I lös lera – jämförelse av beräknade och uppmätta rörelser*. Master's thesis. Department of Geotechnical Engineering, Chalmers University of Technology, publication no. 2003:6, Göteborg, Sweden, 2003.

[3] Alte B, Olsson T, Sällfors G, Bergsten H (1989): *Djupdykning I Göteborgsleran.* Report. Alte AB and Chalmers University of Technology, Göteborg, Sweden, 1989.

[4] *Väg 45, Götatunneln*. Obj.429011. Tender document, handling 05.11.1138. Göteborg, Sweden, 2000.

[6] R. B. J. Brinkgreve (2002): *PLAXIS 2D Version 8*. User manual. A.A. Balkema Publiskers, Netherlands, 2002.

[8] Persson J (2004): *The unloading modulus of soft clay: a field and laboratory study*. Göteborg, Sweden, 2004.

[9] Larsson R (1994): *Deformationsegenskaper i jord.* Rapport B 1994:6. Department of Geotechnical Engineering, Chalmers University of Technology, publication no. 1994:6, Göteborg, Sweden, 1994.

[11] Sällfors G (1995). *Geoteknik Jordmateriallära Jordmekanik*. Vasastadens Bokbinderi AB.

[12] Brinkgreve R B J (1999): *Beyond 2000 in Computational Geotechnics- 10 years of PLAXIS International* ©. Balkema, Rotterdam, 1999. ISBN 90 5809 040X

[13] Potts D M, Zdravković L (2001): *Finite element analysis in geotechnical engineering*. Great Britain, MPG Books, Bodmin, Cornwall, 2001.

[15] Engström B (1994): *Beräkning av betong- och murverkskonstruktioner*. Concrete structures, Chalmers University of Technology, kompendium nr 94:2B, Göteborg, Sweden, 2001.

[17] Yan, W. M. (1999): *Three-dimensional Modelling of Diaphragm Wall Installation.* MPhil Thesis, Hong Kong University of Science and Technology.

[21] Harryson P, Laninge M (2005): *Slitsmurstekniken permanentas*. Väg och vattenbyggaren nr 4 2005, article, Göteborg, Sweden, 2005.

[22] Karlsrud K, Engelstad Ø, Wunsch R, Svärd D (2005): *Diaphragm Walls with cross walls used to prevent bottom heave.*

[23] Vägverket RAP 1997:0288

[25] BRO 2004. VV Publ 2004:56

[26] Oskarsson R, Thorén T (2004): *Studie av 3-dimensionella sidoeffekter vid etappvis schaktning i Götatunneln, J2.* Department of Geotechnical Engineering, Chalmers University of Technology, publication no. 2004:8, Göteborg, Sweden, 2004.

[27] Diaphragm wall seminar, Gothenburg: *"Diaphragm Walls as permanent structures"*. 2005-05-19.

[28] Larsson R (1977): *Basic behaviour of Scandinavian soft clays*. Swedish geotechnical institute, report no 4, Linköping, 1977.

[29] Boverkets handbok om byggkonstruktioner, Band 1, Konstruktion. Boverket, Byggavdleningen. AB svensk Byggtjänst. Tryckeri Balder AB, Stockholm 1994. Diarienummer: B645-1021/94.

Personal communication

[5] Laninge M. Vägverket. 2005-09-13.

[7] Kullingsjö A. Skanska Sweden, and Chalmers University of Technology. 2005-09-14.

[14] Lundgren. K. Chalmers University of Technology. 2005-11-01.

[16] Sandberg M. WSP, Edmark C. Skanska. 2005-09-26.

[18] Wood T. NCC Teknik. 2005-09-29

[19] Andresen L. NGI. 2005-10-25

[24] Davidsson N. LBT. 2005-10-25

Appendix A – PLAXIS input

A1: Mohr Coulomb

Table A.1 Input in PLAXIS for Mohr-Coulomb analyses.

Mohr-Coulomb	γ_{unsat} kN/m^3	γ_{sat} kN/m^3	c_{ref} kN/m^2	c_{incr} kN/m^2	ν	ϕ °	ψ °	$k_x = k_y$ 10^{-5} m/day
Fill 1 (drained)	19	21	0.5	0	0.2	34	0.5	1E5
Fill (drained)	19	21	0.5	0	0.2	34	0.5	1E5
Clay 1 (undrained)	16	16	1.6	0	0.2	35	0	4.8
Clay 2 (undrained)	16	16	1.6	0	0.2	35	0	5.2
Clay 3 (undrained)	17	17	1.6	0.14	0.2	35	0	14
Clay 4 (undrained)	17	17	1.95	0.14	0.2	35	0	5.5
Clay 5 (undrained)	17	17	2.37	0.14	0.2	35	0	2.9
Clay 6 (undrained)	17	17	2.79	0.14	0.2	35	0	5.8
Friction soil (drained)	19	21	0.5	0	0.2	34	0.5	1E5
Refill (drained)	19	21	0.5	0	0.33	34	0.5	1E5
Gravel (drained)	24	24	0.5	0	0.2	34	0.5	0.5E5
Weight-less soil (undrained)	0	0	2.37	0	0.2	35	0	2.9

Cross wall concrete set as Linear Elastic, Non-Porous with $\gamma_{unsat} = \gamma_{sat} = 24\ kN/m^3$, $\nu = 0.2$ *and* $k_x = k_y = 0$.

A2: Elastic

Table A.2 Input in PLAXIS for Elastic analyses.

Elastic	γ_{unsat} kN/m^3	γ_{sat} kN/m^3	ν	$k_x = k_y$ 10^{-5} m/day
Fill 1 (drained)	19	21	0.2	1E5
Fill 2 (drained)	19	21	0.2	1E5
Clay 1 (undrained)	16	16	0.2	4.8
Clay 2 (undrained)	16	16	0.2	5.2
Clay 3 (undrained)	17	17	0.2	14
Clay 4 (undrained)	17	17	0.2	5.5
Clay 5 (undrained)	17	17	0.2	2.9
Clay 6 (undrained)	17	17	0.2	5.8
Friction soil (drained)	19	21	0.2	1E5
Refill (undrained)	19	21	0.33	1E5
Gravel (drained)	24	24	0.2	0.5E5
Weight-less soil (undrained)	0	0	0.2	1.58E4

Cross wall concrete set as Linear Elastic, Non-Porous with $\gamma_{unsat} = \gamma_{sat} = 24\ kN/m^3$, $\nu = 0.2$ *and* $k_x = k_y = 0$.

A3: Modulus of elasticity

Table A.3 Modulus with depth.

Mohr-Coulomb and Elastic	E_{ref} kN/m^2	E_{incr} kN/m^2	y_{ref} m
Fill 1	4E4	0	0
Fill 2	4E4	0	0
Clay 1	1.04E4	0	0
Clay 2	1.04E4	0	0
Clay 3	1.08E4	910	+5
Clay 4	1.31E4	910	+2.5
Clay 5	1.58E4	910	-0.5
Clay 6	1.86E4	910	-3.5
Friction soil	4E4	0	0
Refill	4E4	0	0
Gravel	3E4	0	0
Weightless soil	1.58E4	0	0
Cross wall concrete	3.2E7	0	0

Appendix B – In situ measurements

B1: Inclinometer

Date: 11/23/2004
Page: 1
Enclosure:

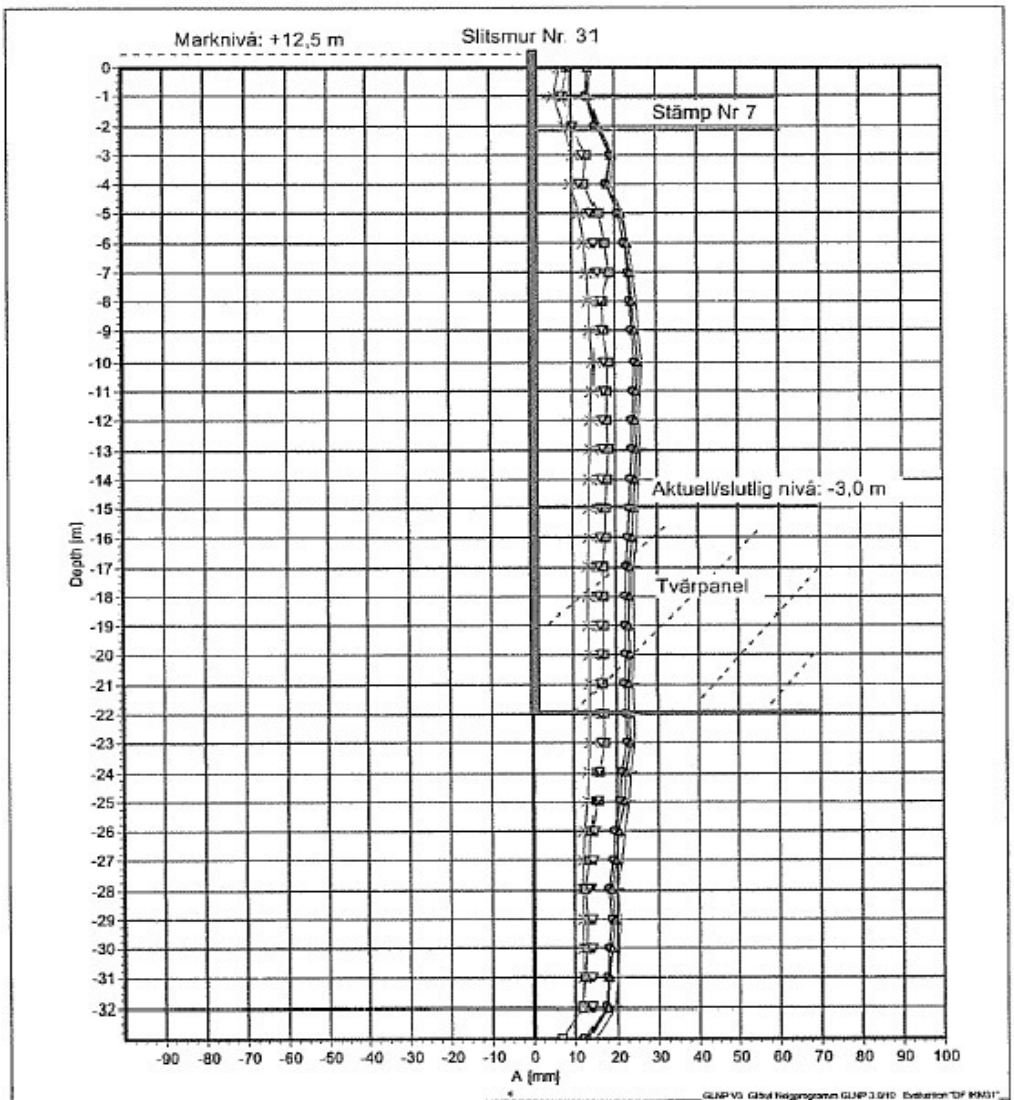

Curve	Measuring level	Measuring series	Date	Diff.days	Depth [m]	Deformation
	IKM31 - 32	LBT-31-39-LBT-31n-11	11/19/2004-10/23/2003	393	33	
	IKM31 - 32	LBT-31-38-LBT-31n-11	11/18/2004-10/23/2003	392	33	
	IKM31 - 32	LBT-31-37-LBT-31n-11	9/30/2004-10/23/2003	343	33	
	IKM31 - 32	LBT-31-36-LBT-31n-11	9/2/2004-10/23/2003	315	33	
	IKM31 - 32	LBT-31-34-LBT-31n-11	4/22/2004-10/23/2003	182	32	
	IKM31 - 32	LBT-31-33-LBT-31n-11	4/15/2004-10/23/2003	175	32	

Figure F.1 Horizontal displacements along the diaphragm wall measured at different points of time, 10/23/2003 is date for reference measuring.

B1: Inclinometer

Date: 1/24/2005
Page: 1
Enclosure:

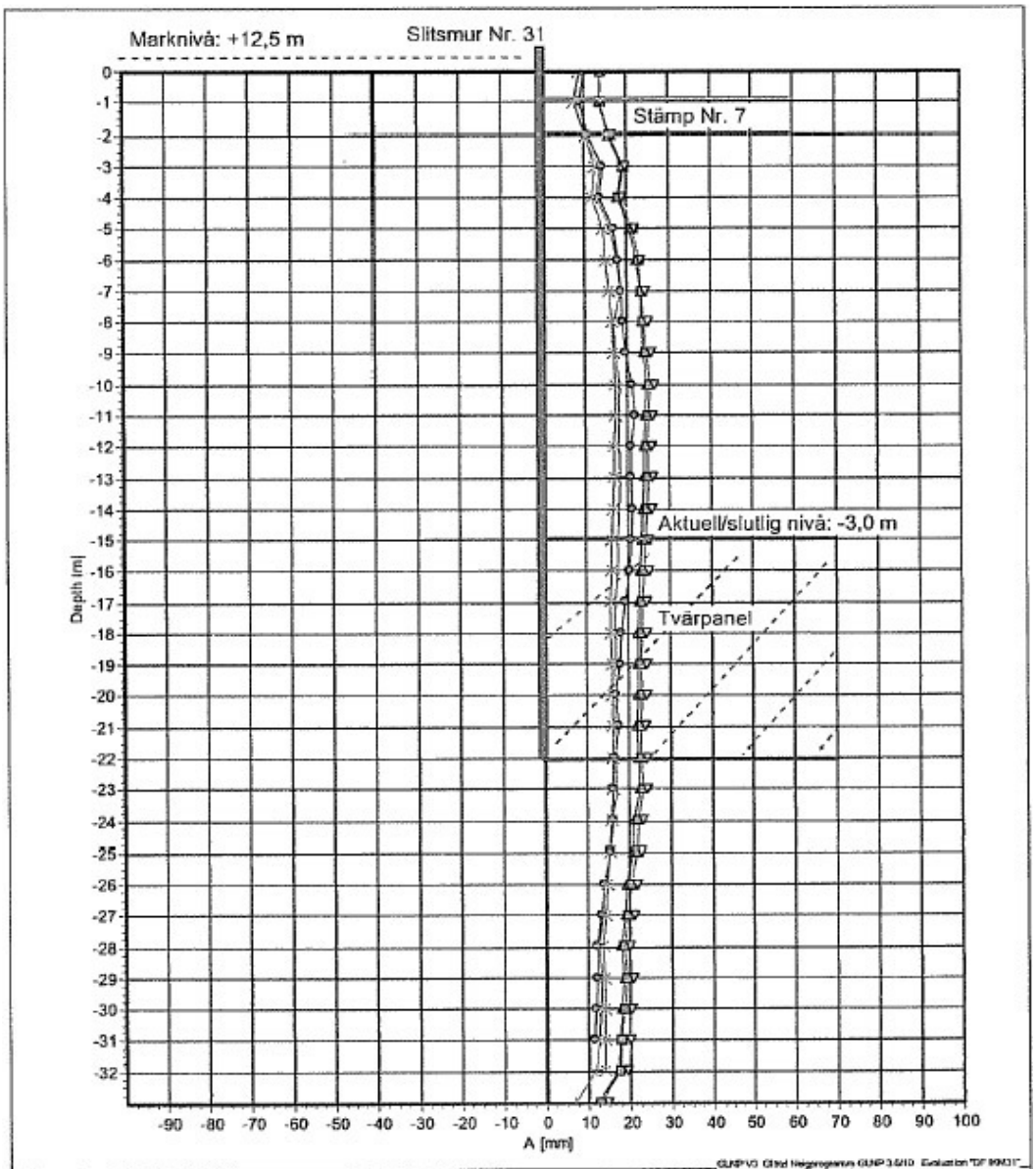

Curve	Measuring level	Measuring series	Date	Diff.days	Depth [m]	Deformation
—◎—	IKM31 - 32	LBT-31-40-LBT-31n-11	1/21/2005-10/23/2003	456	31	
—△—	IKM31 - 32	LBT-31-39-LBT-31n-11	11/19/2004-10/23/2003	393	33	
—□—	IKM31 - 32	LBT-31-38-LBT-31n-11	11/18/2004-10/23/2003	392	33	
—+—	IKM31 - 32	LBT-31-37-LBT-31n-11	9/30/2004-10/23/2003	343	33	
	IKM31 - 32	LBT-31-36-LBT-31n-11	9/2/2004-10/23/2003	315	33	
—×—	IKM31 - 32	LBT-31-34-LBT-31n-11	4/22/2004-10/23/2003	182	32	

Figure F.2 Horizontal displacements along the diaphragm wall measured at different points of time, 10/23/2003 is date for reference measuring.

B2: Point gauge, B point (top of diaphragm wall).

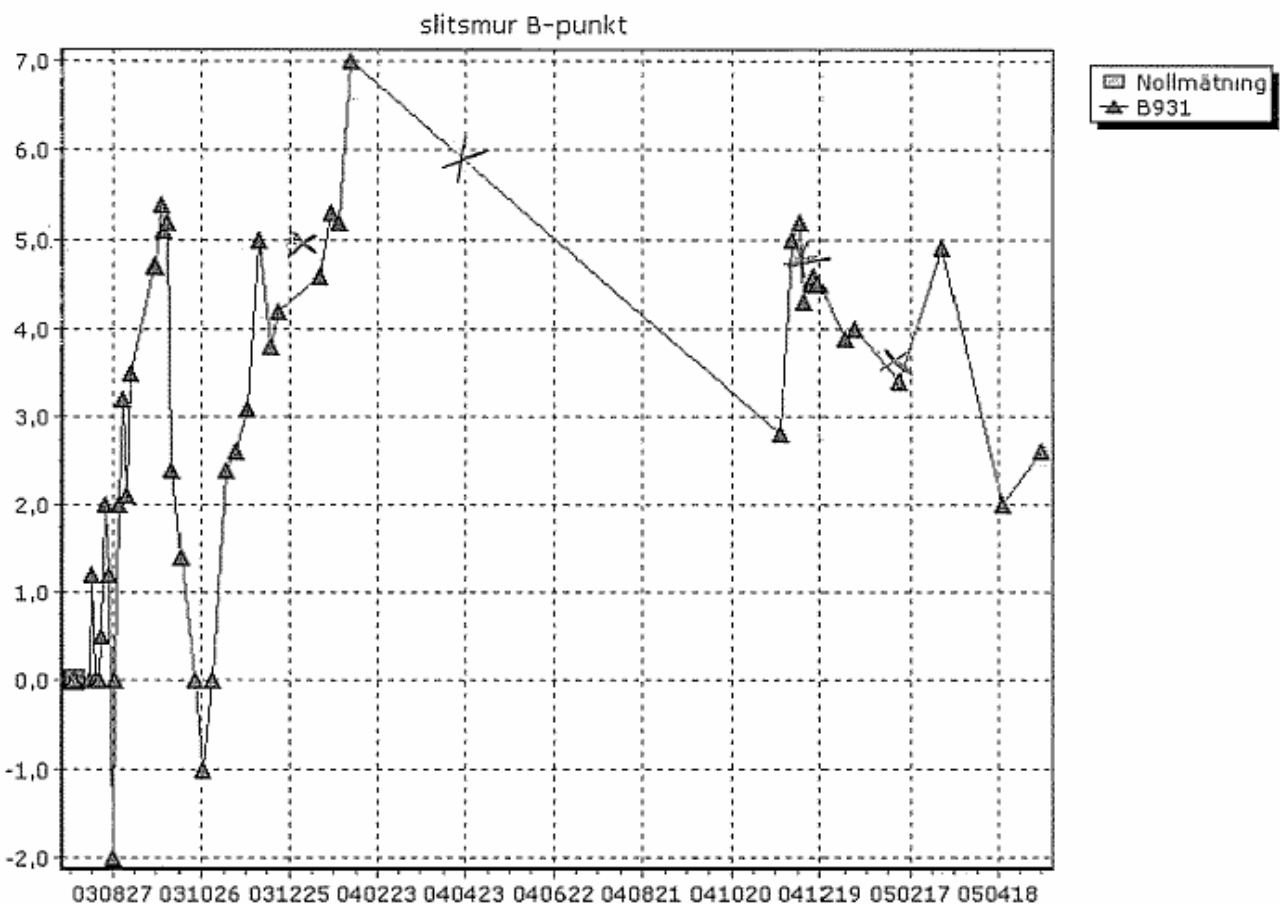

Figure F.3 Vertical displacements in the top of the diaphragm wall measured at different points of time.

B3: Point gauge, F point (middle of shaft).

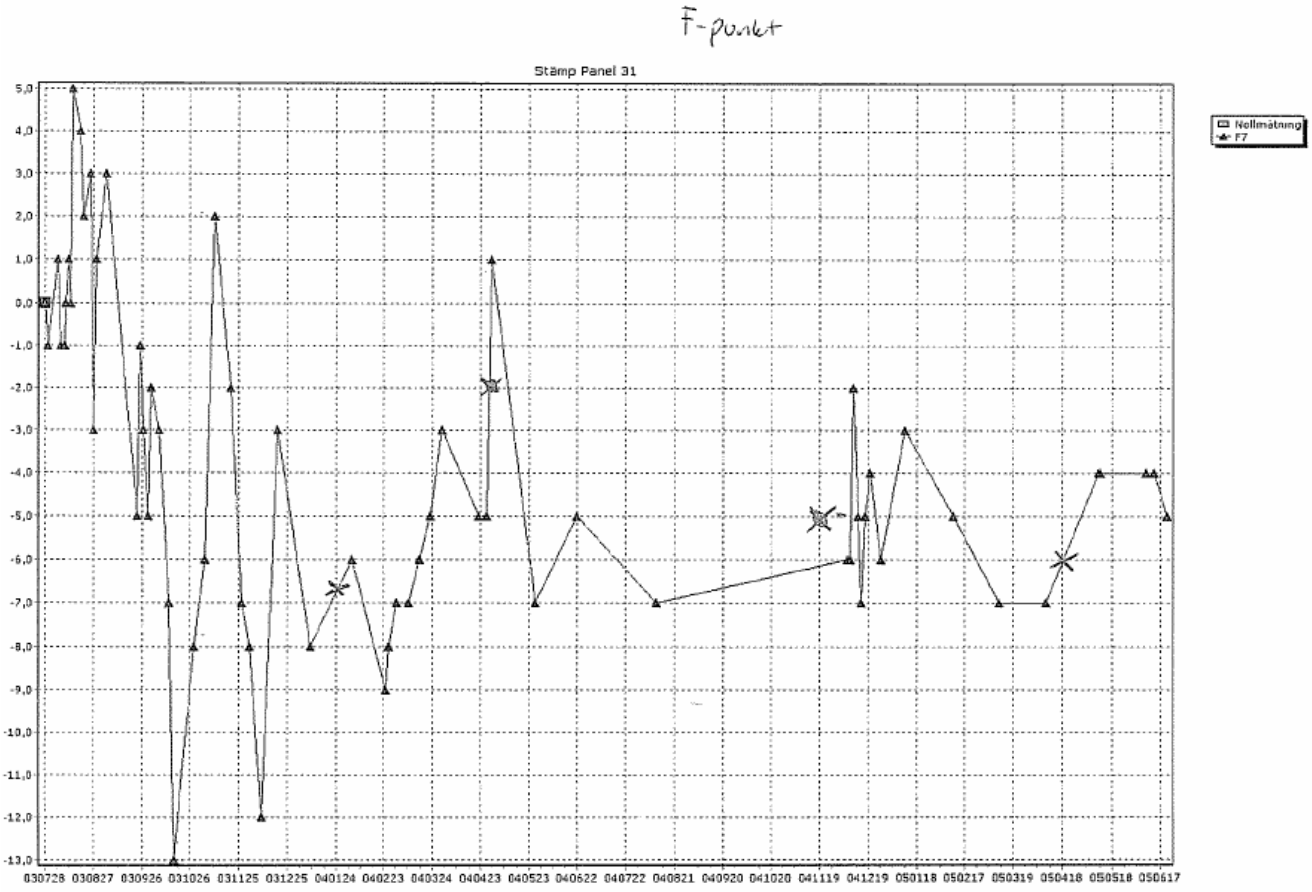

Figure F.4 Vertical displacements in the middle of the shaft measured at different points of time.

Appendix C - Hand calculation of earth pressures

C1: Equations

$$\sigma_v = \gamma \cdot z \, [kN/m^2] \tag{C.1}$$

$$\sigma_v' = \sigma_v - u \, [kN/m^2] \tag{C.2}$$

$$\sigma_h = k_0 \cdot \sigma_v' + u \, [kN/m^2] \tag{C.3}$$

$$\sigma_A = \sigma_v' \cdot K_A - \tau \cdot K_{AC} + u \, [kN/m^2] \tag{C.4}$$

$$\sigma_P = \sigma_v' \cdot K_P + \tau \cdot K_{PC} + u \, [kN/m^2] \tag{C.5}$$

$$K_A = \tan^2(45 - \frac{\phi'}{2}) \tag{C.6}$$

$$K_{AC} = 2\tan(45 - \frac{\phi'}{2}) \tag{C.7}$$

$$K_P = \tan^2(45 + \frac{\phi'}{2}) \tag{C.8}$$

$$K_{PC} = 2\tan(45 + \frac{\phi'}{2}) \tag{C.9}$$

To obtain the earth pressure "at rest", which is the design load for underground structures according to BRO 2004, equation C.3 is used. Regarding the active earth pressures, which are obtained for comparison reasons, equation C.4 is used. In order to achieve the drained and/or undrained earth pressure, the shear strength, τ, and the angle of friction, ϕ, are assigned values corresponding to either drained or undrained conditions.

Equation (C.6) – equation (C.9) are the earth coefficients to be used to calculate active and passive earth pressures when the friction value, *r*, is equal to zero. Otherwise, the earth coefficients are obtained from the diagrams in Figure C.1. In Figure C.2 the locations for the calculations are shown.

C1: Earth coefficients when $r \neq 0$

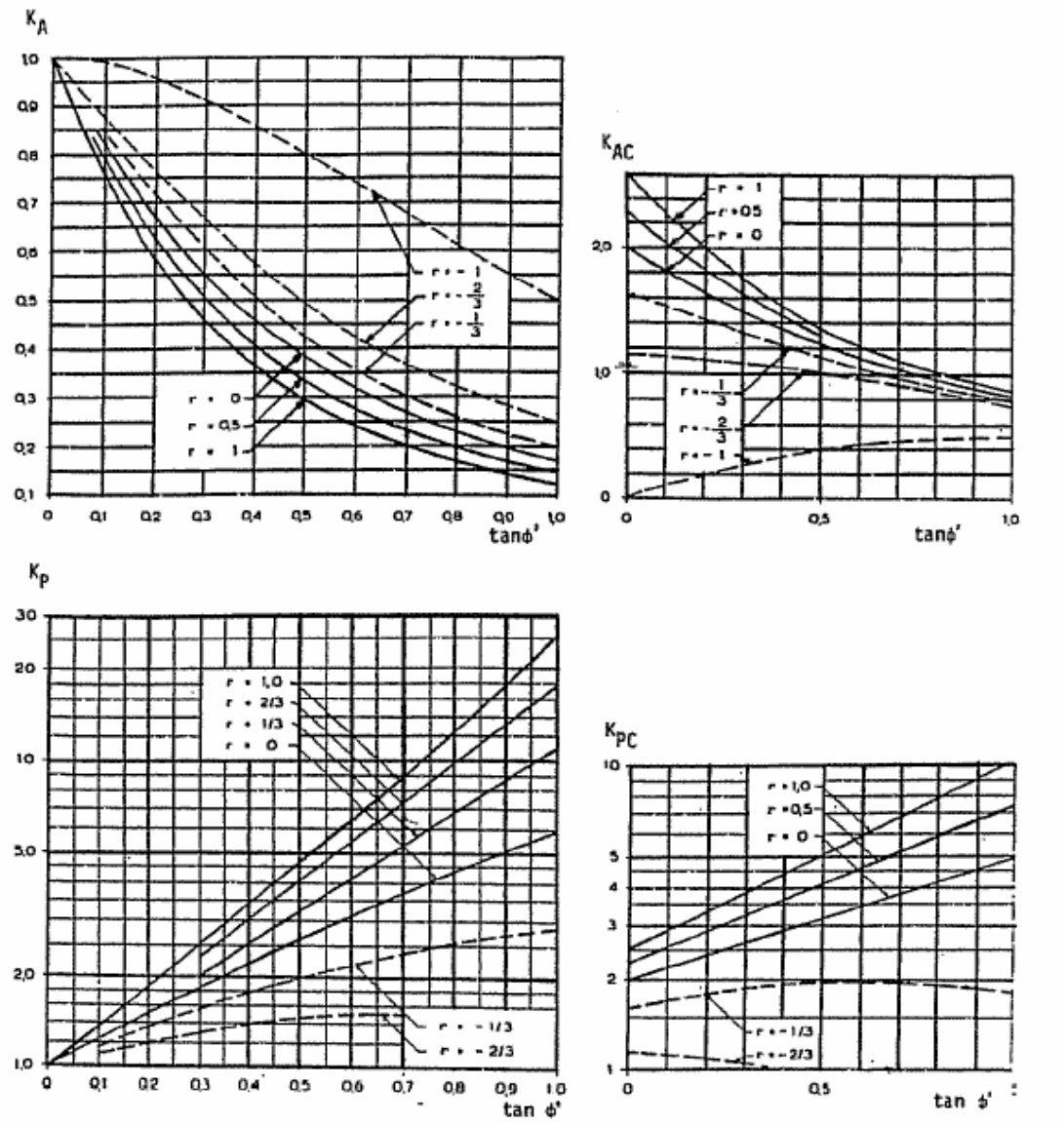

Figure C.1 Earth coefficients to use when considering friction between soil and structure. [11]

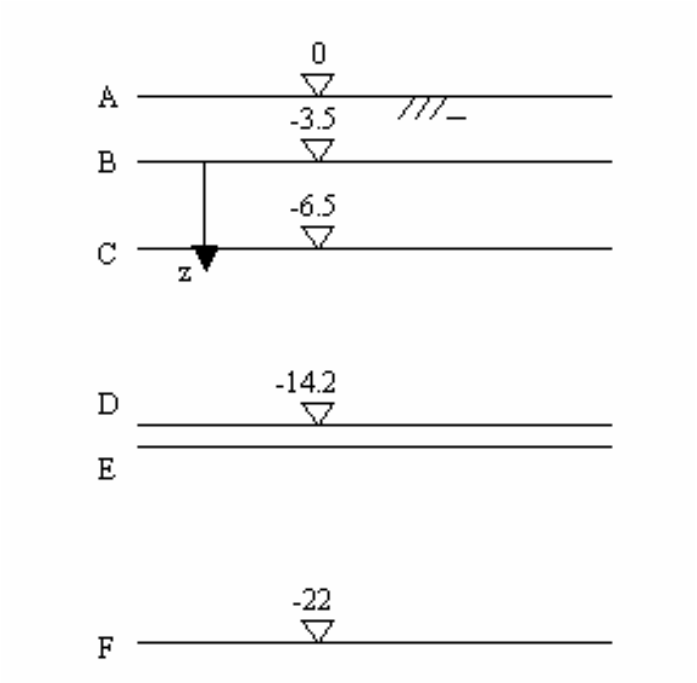

Figure C.2 Locations for hand calculation of earth pressure.

C2: Earth pressure “at rest”, active side.

The horizontal earth pressure is calculated for location A – E (see Figure C.2) according to equation (C.1) – equation (C.3).

$$K_0^{Fill} = 0.5$$
$$K_0^{Clay} = 0.66$$

Unit weight fill material

$$\gamma_{k,dry} = 19\ kN/m^3$$

$$\gamma_{k,sat} = 21\ kN/m^3$$

Unit weight clay

$$\gamma_k = 16\ kN/m^3 \quad \text{(clay 1)}$$

$$\gamma_k = 17 kN/m^3 \quad \text{(clay 2)}$$

Location		Vertical earth pressure	
A	$z_A = 1.9$	$\sigma_A = 1.9 \cdot 9$	$\sigma_A = 36$
B^+	$z_B = 3.5$	$\sigma_{B^+} = \sigma_A + 1.6 \cdot 21$	$\sigma_{B^+} = 70$
B^-	$z_B = 3.5$	$\sigma_{B^-} = \sigma_{B^+} + 0 \cdot 16$	$\sigma_{B^-} = 70$
C	$z_C = 6.5$	$\sigma_C = \sigma_{B^-} + 3 \cdot 16$	$\sigma_C = 118$
D	$z_D = 14.2$	$\sigma_D = \sigma_C + 7 \cdot 17$	$\sigma_D = 249$
E	$z_E = 14.7$	$\sigma_E = \sigma_D + 0.5 \cdot 17$	$\sigma_E = 257$
F	$z_F = 22$	$\sigma_F = \sigma_E + 7.3 \cdot 17$	$\sigma_F = 381$

Location		Horizontal earth pressure at rest	
A	$z_A = 1.9$	$\sigma_{A,h} = 0.5 \cdot \sigma_{A,v}$	$\sigma_{A,h} = 18$
B^+	$z_B = 3.5$	$\sigma_{B^+,h} = 0.5 \cdot (\sigma_{B^+,v} - u_1) + u_1$	$\sigma_{B^+,h} = 43$
B^-	$z_B = 3.5$	$\sigma_{B^-h} = 0.66 \cdot (\sigma_{B^-,v} - u_2) + u_2$	$\sigma_{B^-,h} = 52$
C	$z_C = 6.5$	$\sigma_{C,h} = 0.66 \cdot (\sigma_{C,v} - u_3) + u_3$	$\sigma_{C,h} = 94$
D	$z_D = 14.2$	$\sigma_{D,h} = 0.66 \cdot (\sigma_{D,v} - u_4) + u_4$	$\sigma_{D,h} = 206$
E	$z_E = 14.7$	$\sigma_{E,h} = 0.66 \cdot (\sigma_{D,v} - u_5) + u_5$	$\sigma_{E,h} = 213$
F	$z_F = 22$	$\sigma_{F,h} = 0.66 \cdot (\sigma_{E,v} - u_6) + u_6$	$\sigma_{F,h} = 320$

C3: Drained active earth pressure, r = 0.4.

The total active horizontal earth pressure is calculated according to equation (C.10) and equation (C.11), at locations A – F, see Figure C.2. The shear strengths used in the calculations are obtained with equation (C.12).

Fill material

Active earth pressure:

$$P_A = K_{AF} \cdot \sigma_0^{'} + u \qquad (K_{AF} = 0.271) \tag{C.10}$$

Unit weight

$$\gamma_{k,dry} = 19\ kN/m^3$$

$$\gamma_{k,sat} = 21\ kN/m^3$$

$$\gamma_k^{'} = 11\ kN/m^3$$

Clay

Active soil pressure:

$$P_A = K_{AL} \cdot \sigma_0^{'} - K_{AC} \cdot t + u \qquad (K_{AL} = 0.24,\ K_{AC} = 1.01) \tag{C.11}$$

Unit weight; clay 1

$$\gamma_k = 16\ kN/m^3$$

$$\gamma_k^{'} = 6\ kN/m^3$$

Unit weight; clay 2

$$\gamma_k = 17 kN/m^3$$

$$\gamma_k^{'} = 7\ kN/m^3$$

Drained shear strength

$$\tau' = t = c' + \frac{\sigma_v' + \sigma_h'}{2} \cdot \tan(35^\circ) \qquad \text{(C.12)}$$

$$t = 3 + \frac{53.7 + 35.4}{2} \cdot \tan(35^\circ) = 34.2$$
$$t_2 = 3 + \frac{71.7 + 47.3}{2} \cdot \tan(35^\circ) = 44.7$$
$$t_3 = 3 + \frac{122.6 + 79.9}{2} \cdot \tan(35^\circ) = 73.9$$
$$t_4 = 3 + \frac{126.1 + 82.2}{2} \cdot \tan(35^\circ) = 75.9$$
$$t_5 = 3 + \frac{177.2 + 115.9}{2} \cdot \tan(35^\circ) = 105.6$$

Location		Water pressure	Active earth pressure
A	$z_A = 1.9$	$u_1 = 0$	$P_a = K_{aF} \cdot 19 \cdot 1.9 + u_1$
B^+	$z_B^+ = 3.5$	$u_2 = 16$	$P_B^+ = K_{AF}(19 \cdot 1.9 + 11 \cdot 1.6) + u_2$
B^-	$z_B^- = 3.5$	$u_2 = 16$	$P_B^- = K_{AL}(19 \cdot 1.9 + 11 \cdot 1.6) - t \cdot K_{AC} + u_2$
C	$z_C = 6.5$	$u_3 = 46$	$P_C = K_{AL}(19 \cdot 1.9 + 11 \cdot 1.6 + 6 \cdot 3) - t_2 \cdot K_{AC} + u_3$
D	$z_D = 14.2$	$u_4 = 126$	$P_D = K_{AL}(19 \cdot 1.9 + 11 \cdot 1.6 + 6 \cdot 3 + 7 \cdot 7.7 - t_3 \cdot K_{AC} + u_4$
E	$z_E = 14.7$	$u_5 = 131$	$P_E = K_{AL}(19 \cdot 1.9 + 11 \cdot 1.6 + 6 \cdot 3 + 7 \cdot 8.2 - t_4 \cdot K_{AC} + u_5$
F	$z_F = 22.0$	$u_6 = 201$	$P_D = K_{AL}(19 \cdot 1.9 + 11 \cdot 1.6 + 6 \cdot 3 + 7 \cdot 15.5 - t_5 \cdot K_{AC} + u_6$

Active earth pressure [kN/m^2]

$$P_A = 10$$
$$P_B^+ = 35$$
$$P_B^- = -6$$
$$P_C = 18$$
$$P_D = 81.5$$
$$P_E = 92$$
$$P_F = 144.4$$

C4: Undrained active earth pressure, r = 0.4

Earth pressure for the fill material is obtained with equation (C.13), while equation (C.14) yield earth pressures for the clay. The undrained shear strengths used in the calculations are obtained with equation (C.15).

Fill material

Active earth pressure:

$$P_A = K_{AF} \cdot \sigma_0^{'} + u\,, \quad (K_{AF} = 1) \tag{C.13}$$

Unit weight

$$\gamma_{k,dry} = 19\ kN/m^3$$

$$\gamma_{k,sat} = 21\ kN/m^3$$

$$\gamma_k^{'} = 11\ kN/m^3$$

Clay

Active soil pressure:

$$P_A = \sigma_0 - 2c\sqrt{1+\frac{2}{3}r}\,, \quad \text{r} = 0.4 \tag{C.14}$$

Unit weight; clay 1

$$\gamma_k = 16\ kN/m^3$$

$$\gamma_k^{'} = 6\ kN/m^3$$

Unit weight; clay 2

$$\gamma_k = 17 kN/m^3$$

$$\gamma_k^{'} = 7\ kN/m^3$$

Undrained shear strength [kN/m^3]

$$\tau = t = 16 + 1.4 \cdot (z' - 6.5) \qquad \text{(C.15)}$$

$$t_1 = 16$$

$$t_2 = 16$$

$$t_3 = 16 + 1.4 \cdot (14.2 - 6.5) = 26.8$$

$$t_4 = 16 + 1.4 \cdot (14.7 - 6.5) = 27.5$$

$$t_5 = 16 + 1.4 \cdot (22 - 6.5) = 27.7$$

Location Water pressure Active earth pressure

$A \quad z_A = 1.9 \quad u_1 = 0 \quad P_A = K_{AF} \cdot 19 \cdot 1.9 + u_1$

$B^+ \quad z_B^+ = 3.5 \quad u_2 = 16 \quad P_B^+ = K_{AF}(19 \cdot 1.9 + 11 \cdot 1.6) + u_2$

$B^- \quad z_B^- = 3.5 \quad u_2 = 16 \quad P_B^- = 19 \cdot 1.9 + 11 \cdot 1.6) - 2t_1\sqrt{1 + \frac{2}{3}r} + u_2$

$C \quad z_C = 6.5 \quad u_3 = 46 \quad P_C = 19 \cdot 1.9 + 11 \cdot 1.6 + 6 \cdot 3) - 2t_2\sqrt{1 + \frac{2}{3}r} + u_3$

$D \quad z_D = 14.2 \quad u_4 = 126 \quad P_D = 19 \cdot 1.9 + 11 \cdot 1.6 + 6 \cdot 3 + 7 \cdot 7.7 - 2t_3\sqrt{1 + \frac{2}{3}r} + u_4$

$E \quad z_E = 14.7 \quad u_5 = 131 \quad P_E = 19 \cdot 1.9 + 11 \cdot 1.6 + 6 \cdot 3 + 7 \cdot 8.2 - 2t_4\sqrt{1 + \frac{2}{3}r} + u_5$

$F \quad z_F = 22.0 \quad u_6 = 201 \quad P_D = 19 \cdot 1.9 + 11 \cdot 1.6 + 6 \cdot 3 + 7 \cdot 15.5 - 2t_5\sqrt{1 + \frac{2}{3}r} + u_6$

Active earth pressure [kN/m^2]

$$P_A = 35$$

$$P_B^+ = 70$$

$$P_B^- = 34$$

$$P_C = 80$$

$$P_D = 188$$

$$P_E = 195$$

$$P_F = 296$$

Appendix F - Verification of Evaluation Model

F1: Forces

A first verification of the Evaluation Model is performed in State I for $t = 120$ *years*.

The Axial force, N, and the Shear force, Q, is looked upon in four connections of a simple tunnel geometry, see Figure F.1. The verification is seen in Table F.1, and the values are obtained from the Output program in PLAXIS. Table F.1 shows that equilibrium is obtained for all connections.

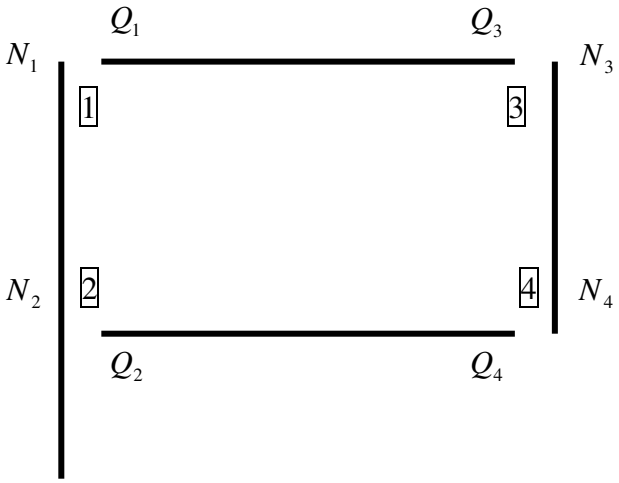

Figure F.1 Simple model of tunnel geometry with defined connection numbers, 1-4.

Table F.1 Verification of forces for Evaluation Model, absolute values for Axial force, N, and Shear force, Q, in connections 1-4.

Connection Number	***Axial force, N*** *kN / m*	***Shear force, Q*** *kN / m*
1	1135	1135
2	1025	1016
3	1425	1424
4	1620	1611

F2: Water pressure on tunnel floor

A second verification of the Evaluation Model is performed for the floor in Tunnel I, Tunnel II and Tunnel III, where.

The water pressure, acting as an uplifting force under the floor plate, is estimated according to equation (F.1) for the field moment, and equation (F.2) for the moment at the support. The comparison between the calculated moments and the moments obtained from PLAXIS is seen in Table F.2 – Table F.4.

$$M_{field} = \frac{q \cdot L^2}{24} = \frac{123 \cdot 18.2^2}{24} = 1660\,kNm \tag{F.1}$$

$$M_B = \frac{q \cdot L^2}{12} = \frac{123 \cdot 18.2^2}{12} = 3395\,kNm \tag{F.2}$$

Table F.2 Field moment in tunnel floor.

M_{field} $[kNm]$	***Tunnel I***	***Tunnel II***	***Tunnel III***	***Hand calculation***
$t = 120$ *years*	1860	1720	1830	1660

Table F.3 Support moment in tunnel floor.

M_B $[kNm]$	***Tunnel I***	***Tunnel II***	***Tunnel III***	***Hand calculation***
$t = 120$ *years*	2650	2500	2520	3395

Table F.4 Summation of field moment and support moment.

$\frac{qL^2}{8} = M_{field} + M_B$ $[kNm]$	***Tunnel I***	***Tunnel II***	***Tunnel III***	***Hand calculation***
$t = 120$ *years*	4510	4220	4350	5055

The summation of the hand calculated moments in the floor, obtained by the water pressure, yields 5055 kNm. Table F.4 shows that the summated moments obtained by PLAXIS yield 4510 kNm for Tunnel I, 4220 kNm for Tunnel II and 4350 kNm for Tunnel III. Since the cross walls interfere with the earth pressures on the floor, as well as since the hand calculation is approximate, it is not possible to achieve the exact same results.

F3: Water pressure on tunnel wall

The load acting on the tunnel wall is shown in Figure F.2. It is calculated with equation (F.3) – equation (F.8) where the load is divided in one triangular load and one rectangular load. Equation (F.3) – equation (F.5) represent the triangular load, and equation (F.6) – equation (F.8) represent the rectangular load.

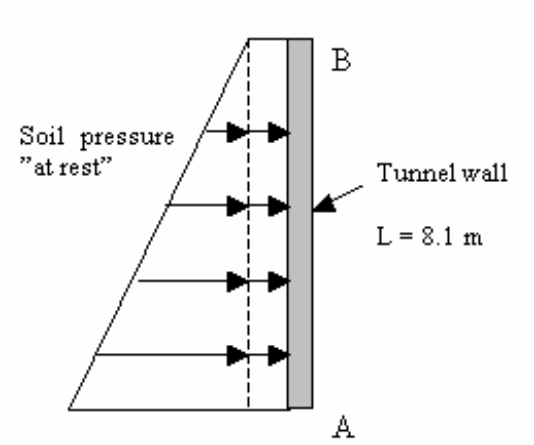

Figure F.2: Load on tunnel wall divided in two parts.

$$M_A^{Triang} = q\frac{l^2}{30} = \frac{246 \cdot 8.1^2}{30} = 538\ kNm \tag{F.3}$$

$$M_B^{Triang} = q\frac{l^2}{20} = \frac{246 \cdot 8.1^2}{20} = 807\ kNm \tag{F.4}$$

$$M_{field,\max}^{Triang} = q\frac{l^2}{46.6} = \frac{246 \cdot 8.1^2}{46.6} = 346\ kNm \tag{F.5}$$

$$M_A^{Rect} = M_B^{Rect} = q\frac{l^2}{12} = \frac{74 \cdot 8.1^2}{12} = 405\ kNm \tag{F.6}$$

$$M_{field,\max}^{Rect} = q\frac{l^2}{24} = \frac{74 \cdot 8.1^2}{24} = 202\ kNm \tag{F.7}$$

$$M_{field}(x) = \frac{q}{2}(l \cdot x - x^2 - \frac{l^2}{6}) = (x = 4.44) = 198\ kNm \tag{F.8}$$

The summation of the calculated moments according to the equations above is shown in equation (F.9).

$$\sum M_{hand} = \frac{M_A^{Triang} + M_A^{Rect} + M_B^{Triang} + M_B^{Rect}}{2} + M_{field,\max}^{Triang} + M_{field}(x) = 1620\ kNm \tag{F.9}$$

The summation of the moments from PLAXIS is shown in equation (F.10). Table F.5 - Table F.7 show comparisons between the hand calculation and the PLAXIS results.

$$\left.\begin{aligned} M_A &= 165 \\ M_B &= 1774 \\ M_{field} &= 256 \end{aligned}\right\} \sum M_{Plaxis} = \frac{165 + 1774}{2} + 256 = 1226\ kNm \tag{F.10}$$

Table F.5 Field moment in tunnel wall.

M_{mid} [kNm]	***Tunnel III***	***Hand calculation***
$t = 120$ *years*	256	548

Table F.6 Support moment in tunnel wall.

M_B [kNm]	***Tunnel III***	***Hand calculation***
$t = 120$ *years*	970	1078

Table F.7 Summation of field moment and support moment.

$\frac{qL^2}{8} = M_{mid} + M_f$ [kNm]	***Tunnel III***	***Hand calculation***
$t = 120$ *years*	1226	1626

When comparing the hand calculated moments for the tunnel wall with moments obtained from PLAXIS, the latter values exceed the hand calculated values. Since the hand calculation is based on earth pressure "at rest" and the PLAXIS load for 120 years is lower than the earth pressure "at rest", this is reasonable.

Appendix G –

Sensitivity analysis of soil parameters

Analyses are performed for different friction values, as well as for two different angles of friction, $\phi' = 30°$ and $\phi' = 35°$. This is done in order to investigate the influence they might have on the resulting loads. The reader should be aware that the material properties and the geometry correspond to the Evaluation model, but the excavation shaft was not set to *CLUSTER DRY*, which was the case for Tunnel I – Tunnel III, therefore the results are not comparable with these analyses. Comparisons between the analyses with varying friction value are still applicable though. The results of most interest for this thesis are the loads acting on the tunnel wall, i.e. the loads between + 5.9 m and – 2.2 m, which correspond to – 6.1 m and – 14.2 m in the figures below.

In Figure G.1 loads obtained with different friction values are shown, and as can be seen the largest friction value yield the largest horizontal load, although the difference is not large.

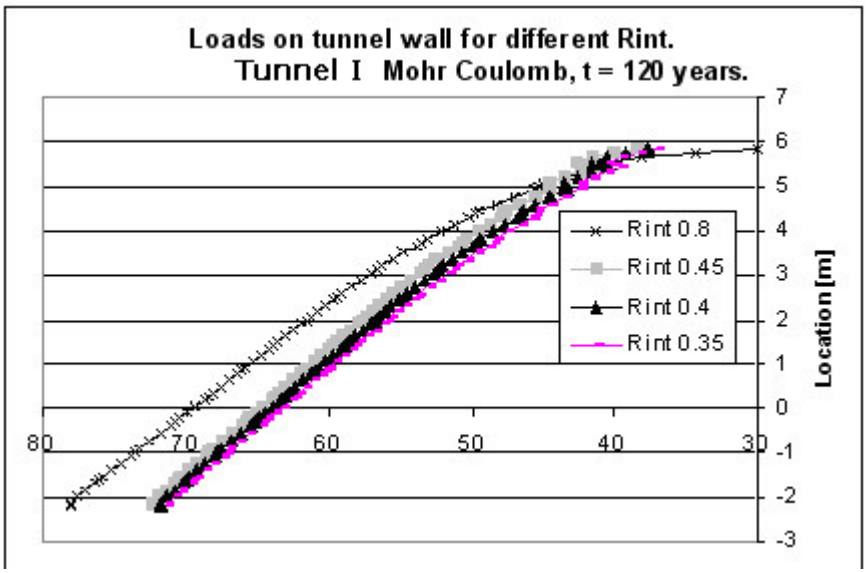

Figure G.1 Horizontal earth pressures on the tunnel wall, for different friction values.

Depending on the choice of the friction value, $R_{\text{int }er}$, the interaction between concrete and soil can be varied. For the analyses performed for this thesis, a lower value than 0.35 was not possible to use, since the calculations became numerically unstable and could not be completed. The choice of $R_{\text{int }er}$ mainly affects the vertical movements of the diaphragm wall, with a difference of 60 mm between and $R_{\text{int }er} = 0.35$ and $R_{\text{int }er} = 0.8$, see Figure G.2.

Friction values from 0.35 to 0.5 yield almost the same moment distribution in the diaphragm wall. If instead choosing $R_{\text{int}\,er} = 0.8$, the moment distribution above the floor agrees with the ones from the smaller friction values, whereas the peak of the moment below the floor moves upwards and this magnitude increases, see Figure G.3 and Figure G.4.

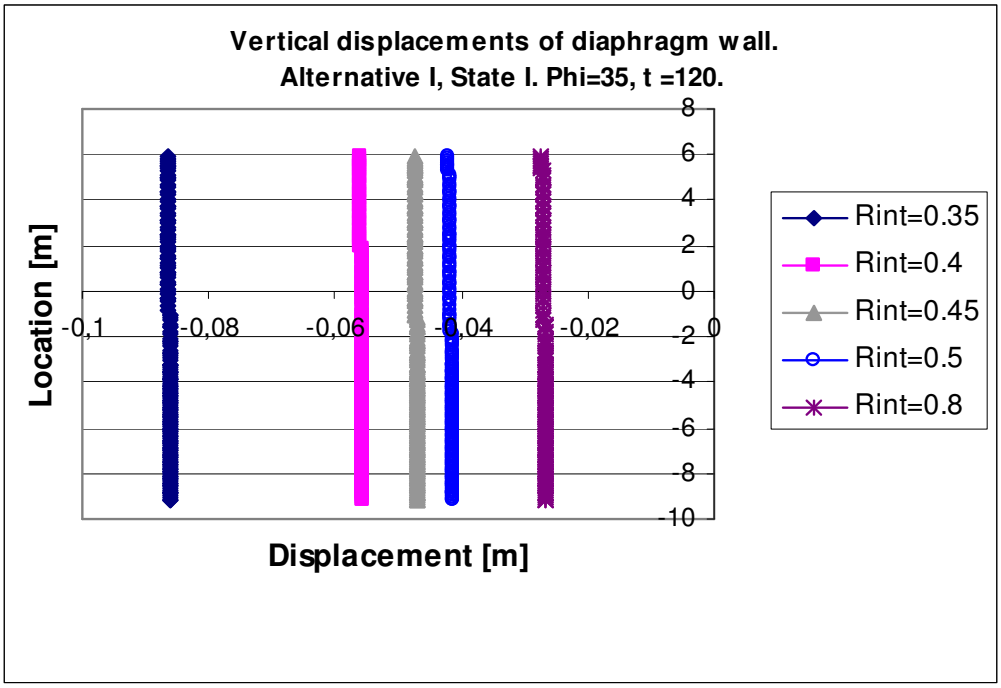

Figure G.2 Vertical (downward) movement of the diaphragm wall.

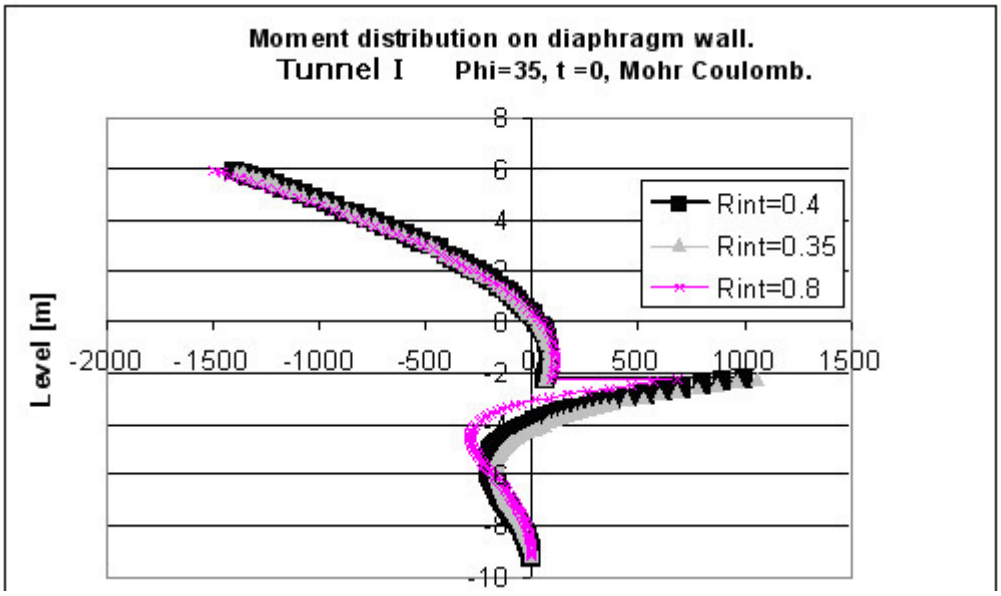

Figure G.3 Comparison of moment distributions at $t = 0$ for different friction values.

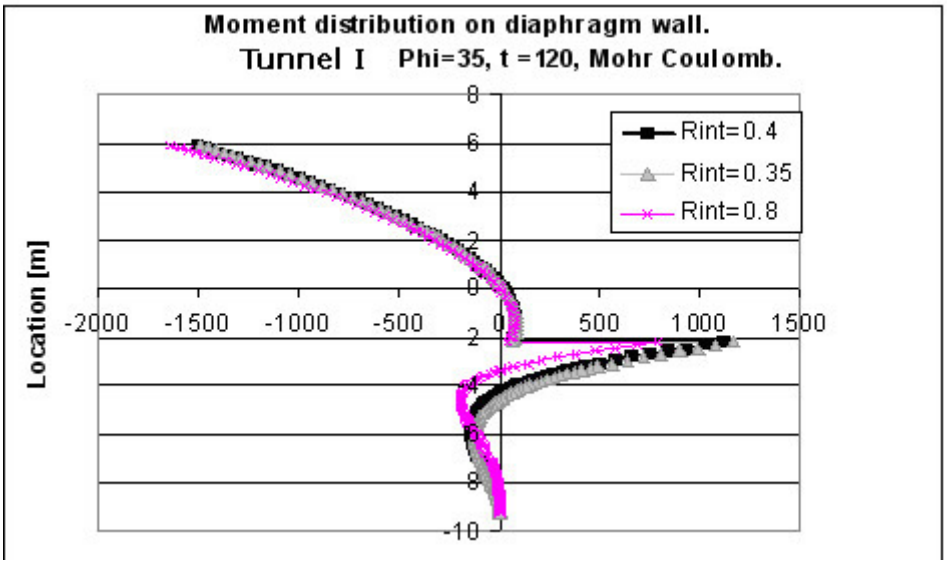

Figure G.4 Comparison of moment distributions at $t = 120$ years for different friction values.

In the floor the largest difference between the vertical displacements, obtained for the different friction values, is 5 mm. In the horizontal direction the difference is barely measurable. The peak of the moment is largest for $R_{\text{int}\,er} = 0.35$, see Figure G.5 and Figure G.6.

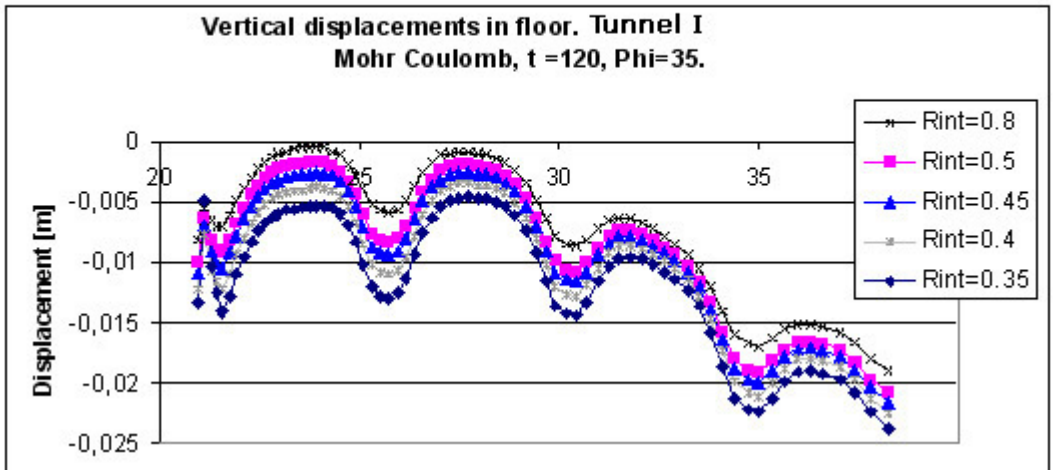

Figure G.5 Comparison of vertical displacements at $t = 120$ years for different friction values.

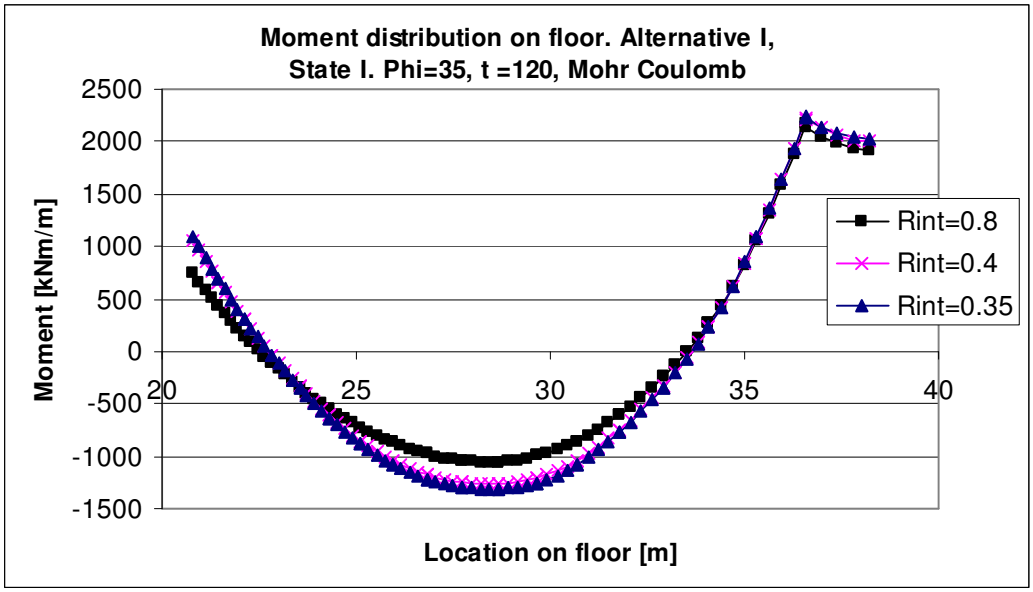

Figure G.6 Comparison of moment distributions at $t = 120$ years for different friction values.

In Figure G.7 the vertical displacement of the diaphragm wall obtained for different friction values are plotted against the friction values. It can be seen that the response is fairly proportionate to the variation in the friction value.

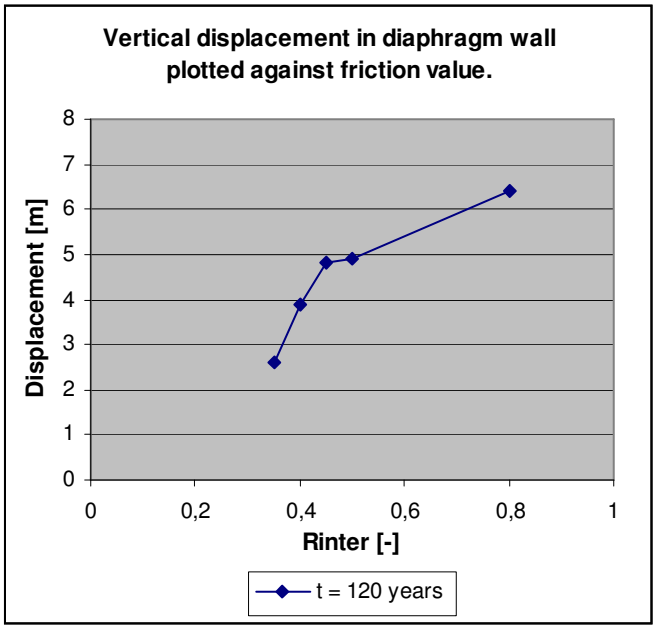

Figure G.7 Vertical displacement in the diaphragm wall for different friction values between 0.35 and 0.8. (Compare with Figure G.2).

Appendix H - Shear strength

When trying to estimate the earth pressures for the structure, different shear strengths are considered. As the excess pore pressures disappear from the clay the soil stresses increase or decrease. Since the effective shear strengths depend on the stresses, they also increase with time, and the soil will be more stable. Equation (H.1) and Equation (H.2) are used to obtain the shear strengths in Figure H.1.

$$\tau_{fu,k} = c_{uk} \tag{H.1}$$

$$\tau' = 0.1 \cdot c_{uk} + \frac{\sigma_v' + \sigma_h'}{2} \cdot \tan(35^\circ) \tag{H.2}$$

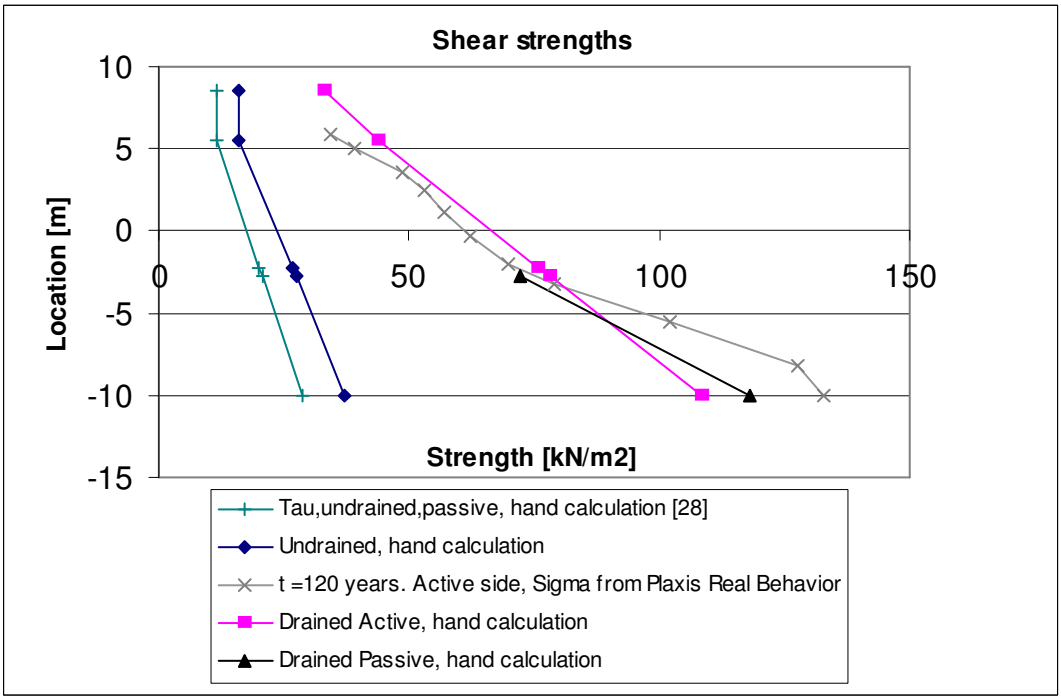

Figure H.1 *The Shear Strengths for t = 120 years are calculated using soil stresses obtained with PLAXIS, whereas the remaining values are based on hand calculated soil stresses.*